

## STATUS OF THESIS

Title of thesis

Active Vibration Cancellation of a Free-Piston Linear Generator Engine

I **YEE HONG HOE** hereby allow my thesis to be placed at the Information Resource Center (IRC) of Universiti Teknologi PETRONAS (UTP) with the following conditions:

1. The thesis becomes the properties of UTP.
2. The IRC of UTP may make copies of the thesis for academic purposes only.
3. This thesis is classified as

Confidential

Non-confidential

If this thesis is confidential, please state the reason:

Patents pending

---

---

The contents of the thesis will remain confidential for 3 years.

Remarks on disclosure:

-

Endorsed by

\_\_\_\_\_  
Signature of Author

32, Lorong BDK 1/11,  
Bandar Damansara Kuantan  
26100 Kuantan.  
Pahang

Date:

\_\_\_\_\_  
Signature of Supervisor

Universiti Teknologi  
PETRONAS

Date:

# APPROVAL PAGE

UNIVERSITI TEKNOLOGI PETRONAS

Approval by Supervisor (s)

The undersigned certify that they have read, and recommend to The Postgraduate Studies Program for acceptance, a thesis entitled “**Active Vibration Cancellation of a Free-Piston Linear Generator Engine**” submitted by (Yee Hong Hoe) for the fulfillment of the requirements for the degree of Master of Science in Mechanical Engineering.

Signature : \_\_\_\_\_

Main supervisor : A. P. Dr. Abdul Rashid Abdul Aziz

Date : \_\_\_\_\_

**TITLE PAGE**

UNIVERSITI TEKNOLOGI PETRONAS

**Active Vibration Cancellation of a Free-Piston Linear Generator Engine**

By  
Yee Hong Hoe

A THESIS  
SUBMITTED TO THE POSTGRADUATE STUDIES PROGRAMME AS A  
REQUIREMENT FOR THE  
DEGREE OF MASTER OF SCIENCE  
MECHANICAL ENGINEERING  
BANDAR SERI ISKANDAR,  
PERAK

JUNE 2009

## DECLARATION

I hereby declare that the thesis is based on my original work except for quotations and citations which have been duly acknowledged. I also declare that it has not been previously or concurrently submitted for any degree at Universiti Teknologi PETRONAS or other institutions.

Signature : \_\_\_\_\_

Name : Yee Hong Hoe

Date : \_\_\_\_\_

## **DEDICATION**

To my parents

## **ACKNOWLEDGEMENT**

My first gratitude is to my supervisor A.P. Dr. Abdul Rashid, who giving me the opportunity to involve in the LG project. His guides throughout the project are much valuable to me in this research. Truly grateful to former UTP LG Project manager, Mr. Razali for his patient, assistant and being informative whenever I faced difficulties. Lastly, to those who helped me for succeeding this thesis and research indirectly.

## ABSTRACT

A free-piston linear generator engine (LG) is a device that couples a free-piston combustion engine with a linear electric generator. The engine is consisted with a part called piston-rod assembly (PRA), where two pistons are connected by a rod attached with permanent magnet. During the operation of LG, PRA will linearly reciprocate between two internal combustion chambers on the opposite sides. However, when the PRA is on one side of the engine, an unbalanced impact force is created. The unbalanced forces provide an undesirable impact force acting on the engine block, causing the engine to vibrate. The control of vibration for the LG becomes crucial, because proper vibration controls maintain a consistent electricity output and maximize the efficiency of the engine. Current work proposed using a linear motor (LM) to create an anti-phase momentum into the system to counter the impact forces created by PRA. The works are based on analytical modeling with MATLAB used for simulation. Simulation shows the system instability characteristics, the time and frequency responses for LG. The results showed the existence of a real pole at the right hand side of complex plane which contribute to the system instability. The non-proportional damped time response obtained using state-space approach shows the overall interaction between mass forcer and PRA decreased with respect to time. The frequency responses showed that with the application of active vibration cancellation, the resonance can be delayed and the magnitude of the resonance can be reduced. A lumped-mass quarter car suspension model is used for validation. Case study is carried out to decide the best available driven forces that drive the LG. The conclusion of current study showed that with proper vibration control for the LG, the vibration level of LG can be reduced to a desirable level while maintaining the optimum operating conditions.

## ABSTRAK

Enjin-penjana lurus bebas-omboh (LG) merupakan satu peranti yang menggabungkan sebuah enjin pembakaran bebas-omboh dengan sebuah motor penjanaan elektrik lurus. Enjin tersebut mempunyai satu bahagian, di mana dua omboh digabungkan oleh satu rod yang dipanggil PRA. Bahagian PRA bergerak antara dua kebuk pembakaran dalaman menyebabkan masalah ketidakseimbang berat pada enjin. Ketidakseimbang berat inilah yang menyebabkan masalah gegaran kepada LG. Oleh itu, pengawalan gegaran pada LG menjadi penting kerana dapat meningkatkan lagi efisiensi dan prestasi enjin. Kerja penyelidikan yang dijalankan mengemukakan satu alternatif dengan menggunakan sebuah motor lurus (LM) beroperasi sekali dengan LG untuk mengawal tahap gegaran pada LG. LM bertujuan untuk menjanakan fasa bertentangan dengan pergerakan PRA dari LG. Simulasi digunakan kerana dapat menunjukkan hubungan antara LM dengan LG dengan lebih tepat melalui aspek ketidakseimbangan system, reaksi masa antara LM dengan LG, dan reaksi frekuensi. Hasil simulasi menunjukkan terdapatnya 'poles' benar yang merupakan faktor utama ketidakseimbang sistem. Selain itu, reaksi masa antara LM dengan LG juga menunjukkan pengurangan dalam jumlah ayunan dengan kaedah 'state-space'. Reaksi frekuensi pula menunjukkan terdapatnya pengurangan nilai pada salunan diikuti dengan penundaan. Sistem penggantungan roda kenderaan telah dipilih untuk tujuan pengesahan penggunaan dan ketepatan simulasi. Dua kes pembelajaran telah diadakan dengan menggunakan data daripada ujikaji supaya dapat menonjolkan lagi pentingnya pengawalan gegaran. Kesimpulannya, dengan adanya pengawalan gegaran pada LG, tahap gegaran dapat dikurangkan kepada tahap yang lebih memuaskan, pada masa yang sama meningkatkan lagi prestasi enjin tersebut.



## TABLE OF CONTENTS

STATUS OF THESIS.....	i
APPROVAL PAGE.....	ii
TITLE PAGE.....	iii
DECLARATION.....	iv
DEDICATION.....	v
ACKNOWLEDGEMENT.....	vi
ABSTRACT.....	vii
ABSTRAK.....	viii
TABLE OF CONTENTS.....	ix
LIST OF FIGURES.....	xiii
LIST OF TABLES.....	xiv
LIST OF ABBREVIATIONS.....	xv
CHAPTER I INTRODUCTION.....	1
1.1 Background.....	1
1.2 Research Focus.....	2
1.3 Dissertation Organization.....	4
CHAPTER II LITERATURE REVIEW.....	6
2.2 Free-piston linear generator engine.....	6
2.3 Active Vibration Control.....	9
2.4 Pole-zero Plots and Root Locus Plots.....	11
2.5 Time Response.....	12
2.6 Frequency Response.....	13
2.7 Validation: Quarter Car Suspension System.....	15
2.8 Damping Properties.....	15
2.9 Conclusion.....	16
CHAPTER III RESEARCH METHODOLOGY.....	17
3.1 Introduction.....	17
3.2 LG Mechanical Forces.....	19
3.3 LG Dynamic Equations.....	21

3.4 Analytical Analysis.....	24
3.4.1 Mathematical Modeling.....	24
3.4.2 Transfer Function Approach.....	25
3.4.2.1 Poles.....	25
3.4.2.2 Zeros.....	25
3.4.2.3 Pole-zero plots.....	25
3.4.2.4 Root Locus Plots.....	26
3.4.3 State-space Modeling.....	26
3.4.3.1 State-space equation.....	26
3.4.3.2 Non-proportional Damped Time Response.....	27
3.4.4 Modal State-space approach.....	28
3.4.4.1 Modal Analysis.....	28
3.4.4.2 Modal Analysis: State-space form.....	30
3.4.4.3 Proportional Damped Time Response.....	30
3.4.5 Frequency Response (Bode Plots).....	31
CHAPTER IV MODELING AND SIMULATION.....	32
4.1 Mathematical Modeling.....	32
4.1.1 Modeling of AVC.....	32
4.1.2 Free Body Diagram.....	32
4.1.3 Equations of Motion (EOM).....	33
4.1.4 Simulation parameters.....	33
4.2 Transfer Function Approach.....	34
4.2.1 Denominator.....	34
4.2.2 Poles and Zeros.....	35
4.2.3 Pole-zero Plots.....	36
4.2.3.1 Pole-zero plots: 3BM and 3BC.....	36
4.2.3.2 Pole-zero plots: 5BM.....	37
4.2.4 Root Locus Plots.....	38
4.2.5 Frequency Response – Transfer Function Approach.....	39
4.2.5.1 Before the application of AVC.....	39
4.2.5.2 After the application of AVC.....	40
4.3 State-space Modeling Approach.....	42
4.3.1 State-space equation.....	42

4.3.2 Complex Eigenvalue and Eigenvector – State-space form.....	44
4.3.3 Complex Eigenvalue combining to give real motion .....	45
4.3.4 Non-proportional damped time response.....	46
4.3.5 Frequency Response – State-space modeling approach .....	48
4.4 Modal State-space Approach .....	50
4.4.1 Eigenvalues .....	50
4.4.2 Eigenvectors.....	50
4.4.3 Normalizing Eigenvectors .....	51
4.4.4 Writing Homogeneous EOM.....	52
4.4.5 EOM – Physical Coordinates.....	52
4.4.6 EOM – Principal Coordinates.....	53
4.4.7 Proportional damped time response.....	54
4.4.8 Frequency Response – Modal state-space approach.....	57
4.5 Results Comparison .....	58
CHAPTER V SIMULATION RESULTS VALIDATION .....	59
5.1 Development and control of an automotive smart suspension system .....	60
5.1.1 Passive suspension system.....	60
5.1.2 Semi-active suspension system.....	61
5.1.3 Smart suspension system .....	62
5.1.4 Time Response.....	64
5.1.5 Frequency Response .....	65
5.2 Active suspension simulation through software interface .....	68
5.2.1 Time Response.....	70
5.2.2 Frequency Response .....	71
5.3 Aspect of achievable performance for quarter car active suspension.....	74
5.3.1 Frequency Response .....	75
CHAPTER VI CASE STUDY.....	78
6.1 Before the application of AVC .....	79
6.2 After the application of AVC.....	80

CHAPTER VII CONCLUSION.....	82
7.1 Introduction.....	82
7.2 Objective of the research .....	82
7.3 Summary of finding and conclusions .....	82
7.4 Recommendations for future work .....	83
7.5 Limitation and potential problem.....	83
7.6 Contribution to Knowledge.....	83
REFERENCES .....	84
APPENDIX A.....	89
APPENDIX B.....	93
APPENDIX C.....	94
APPENDIX D.....	96
APPENDIX E.....	97
APPENDIX F.....	99

## LIST OF FIGURES

- Figure 1.1: Free-piston Linear Generator Engine  
Figure 1.2: Possible impact forces distribution  
Figure 1.3: Proposed AVC mechanism for LG
- Figure 2.1: Single piston and dual piston free-piston engine  
Figure 2.2: Schematic of vibration control system  
Figure 2.3: Responses of disc A  
Figure 2.4: Bode diagram
- Figure 3.1: The research methodology of active vibration cancellation for LG  
Figure 3.2: LG free-body diagram  
Figure 3.3: Force generated by 3BM (complete cycle = 0.22s)  
Figure 3.4: Force generated by 5BM (complete cycle = 0.14s)  
Figure 3.5: Force generated by 3BC (complete cycle = 0.22s)  
Figure 3.6: Mass-spring-damper models  
Figure 3.7: Typical state-space model  
Figure 3.8: Modal analysis model flow chart
- Figure 4.1: AVC Mathematical Modeling  
Figure 4.2: FBD of the mathematical model  
Figure 4.3: Pole-zero plots of 3BM and 3BC  
Figure 4.4: Pole-zero plots of 5BM  
Figure 4.5: Root locus for LG after the application of AVC  
Figure 4.6: Bode plot before the application of AVC  
Figure 4.7: Magnitude plots after the application of AVC – transfer function  
Figure 4.8: Magnitude plots after the application of AVC – transfer function  
Figure 4.9: Non-prop damped time response for 3BM and 3BC  
Figure 4.10: Non-prop damped time response for 5BM  
Figure 4.11: Magnitude plots after application of AVC – state-space approach  
Figure 4.12: Phase plots after the application of AVC – state-space approach  
Figure 4.13: Proportional damped time responses for 3BM and 3BC  
Figure 4.14: Proportional damped time responses for 5BM  
Figure 4.15: Magnitude plots after application of AVC – Modal state-space approach  
Figure 4.16: Phase plots after the application of AVC – Modal state-space approach
- Figure 5.1:  $\frac{1}{4}$  car models with passive suspension system  
Figure 5.2:  $\frac{1}{4}$  car models with semi-active suspension system  
Figure 5.3:  $\frac{1}{4}$  car models with smart suspension system  
Figure 5.4: Time response of suspension deflection  
Figure 5.5: Verified time response for passive, semi-active and smart suspension system  
Figure 5.6: Frequency response of suspension deflection

- Figure 5.7: Verified frequency response for passive, semi-active and smart suspension system
- Figure 5.8: Block diagram of a  $\frac{1}{4}$  car model equipped with a semi-active suspension system using optimal control law
- Figure 5.9:  $\frac{1}{4}$  car models with active suspension system
- Figure 5.10: Time response of suspension displacement for a  $\frac{1}{4}$  car model active suspension system
- Figure 5.11: Verified time response for active suspension system
- Figure 5.12: Frequency response of suspension displacement for a  $\frac{1}{4}$  car model active suspension system
- Figure 5.13: Verified Frequency response for active suspension system
- Figure 5.14: Closed-loop optimal control (LQR)
- Figure 5.15: The  $\frac{1}{4}$  car model of the vehicle suspension system
- Figure 5.16: Frequency response of suspension travel using coprime factorization
- Figure 5.17: Verified frequency response using state-space approach
- 
- Figure 6.1: Bode plots of LG before the application of AVC
- Figure 6.2: Bode plots of LG after the application of AVC

### **LIST OF TABLES**

- Table 2.1: The values of the damping ratios obtained from the well defined vibration responses
- 
- Table 4.1: Simulation Parameters
- 
- Table 5.1: Parameters defined in simulation for passive, semi-active and smart quarter car model suspension system
- Table 5.2: Parameters defined for simulation for  $\frac{1}{4}$  car active suspension system using LQR
- Table 5.3: Parameters defined for simulation for  $\frac{1}{4}$  car active suspension system using Coprime Factorization
- 
- Table 6.1: Magnitudes of 'Poles' before the application of AVC
- Table 6.2: Magnitudes for 'poles' and 'zeros' after the application of AVC

## LIST OF ABBREVIATIONS

3BC	three batteries motoring force with combustion
3BM	three batteries motoring force
5BM	five batteries motoring force
ADAM	Automatic Dynamic Analysis of Mechanical System
AVC	Active Vibration Cancellation
CRL	Complementary Root Locus
Den	Denominator
DOF	Degree of Freedom
EMF	Electromagnetic Force
EOM	Equation of Motion
Er-MCSI	Error-Driven Minimal Controller Synthesis
$z_1/F_1$	Displacement of LM due to inertia force generated by ‘forcer’
$z_2/F_1$	Displacement of LG due to inertia force generated by ‘forcer’
$z_1/F_1$	Displacement of LM due to inertia force generated by PRA
$z_2/F_2$	Displacement of LM due to inertia force generated by PRA
FXLMS	Filtered-X Least-Mean-Square
HEV	Hybrid-Electric Vehicle
IP	Imaginary Poles
LG	Free-piston Linear Generator Engine
LM	Linear Motor
LPV	Linear Parameter Varying
LQG	Linear Quadratic Gaussian
LQR	Linear Quadratic Regulator
LTI	Linear Time-invariant
MATLAB	Matrix Laboratory
MDOF	Multiple Degree-of-freedom
MIMO	Multi-input Multi-Output
PPF	Positive Position Feedback
PRA	Piston-rod Assembly
RHP	Real Poles
RL	Root Locus
SISO	Single-Input Single-Output
VIS	Vibration Isolation System

## CHAPTER I INTRODUCTION

### 1.1 Background

Ever-tightening environmental legislation drives a significant research effort to reduce the environmental impacts of hydrocarbon fuel combustion in internal combustion engines. Within the automotive industry, the hybrid-electric vehicle (HEV) has gained much attention in recent years and such technology is becoming commercially available from an increasing number of manufacturers [1].

The hybrid vehicle concept is environmentally friendly, highly efficient, and is gaining popularity by the day. This drives most vehicle manufacturer to have a share in the emerging hybrid vehicles market. The resulting competition among vehicle manufacturers in turn stresses the engineers and researchers working with alternative vehicles to find even newer and better propulsion solutions. Common demands are high specific performance, increase system efficiency and reduce number of system components, etc. The free-piston generator concept is one of the relatively new (and still emerging) hybrid vehicle concepts that could offer good solutions to some of these demands [2].

A free-piston linear generator engine (LG) is a device that couples a free-piston combustion engine with a linear electric generator [2, 3, 4, 5]. A general schematic of LG is shown in Figure 1.1. (See *Appendix A* for more details about LG)

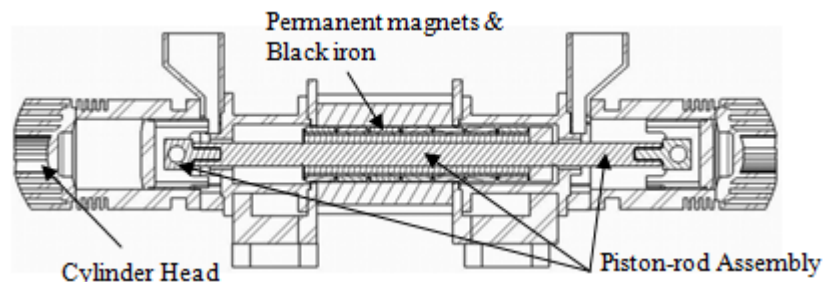


Figure 1.1: Free-piston Linear Generator Engine



The engine is consisted with a part called piston-rod assembly (PRA), where two pistons are connected by a rod attached with permanent magnet. The motion of the PRA is not mechanically prescribed but rather a result of the balance of in-cylinder pressures, inertia forces, friction forces and the applied load. The linearly reciprocating, ignition and compression processes, in the two linear combustion chambers cause the PRA to have an oscillating motion. Now, if this rod is placed in a magnetic field (containing coils), and if the movement of the rod causes a disturbance of the field, an electromagnetic force (EMF) will be induced in the coils (See *Appendix B* for further detailed descriptions). Hence, the output of LG is direct electricity rather mechanical torques.

Due to the changed of engine output, the crankshaft, which is normally presence in conventional hybrid concepts, is therefore eliminated. The disappearance of the crankshaft has beneficial aspects. The friction losses associated with the crankshaft, the conventional connecting rod, and their accessories are eliminated. Piston friction is reduced, as it is no longer under the influence of an angular loading. The system also becomes more robust, as the number of moving parts is reduced to one. As the engine compression ratio is now no longer fixed, theoretically, multi-fuel operation is enabled due to combustion optimization flexibility [2, 6].

## 1.2 Research Focus

For the engine to generate a consistent electricity output, a low vibration level is desirable. However, if PRA is at one side of the engine, an impact force which resulted from PRA oscillations (internal forces reaction) will deliver additional excitations on the engine block. Figure 1.2 shows the possible impact forces which causes additional excitation on the engine block.

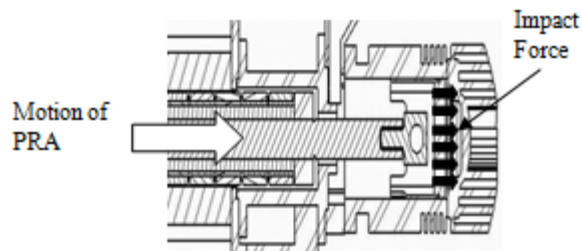


Figure 1.2: Possible impact forces distribution

The presence of additional excitations or vibration is undesirable, wasting energy and creating unwanted noise [7]. The control of vibration for the LG becomes crucial, because proper vibration controls maintain a consistent electricity output and maximize the efficiency of the engine. Present study proposed by using a linear motor (LM) to generate an anti-phase momentum to counter the impact forces due to PRA as shown in Figure 1.3. The proposed method is known as active vibration cancellation (AVC), where the vibration is attacked with a counter-force that drives the system of interest to respond in a way that is exactly opposite to the system's response due to other inputs or from within the system. The total response of the system at the location of interest can then be driven to zero, or at least be significantly reduced.

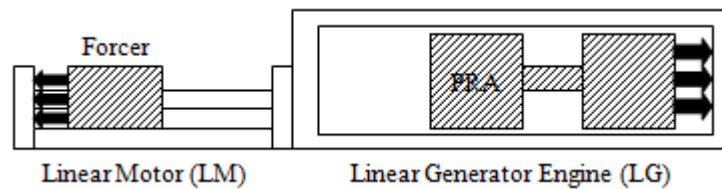


Figure 1.3: Proposed AVC mechanism for LG

Operation of PRA involved internal forces reaction which included friction forces, magnetic cogging forces, compression-expansion forces with or without combustion, and motoring forces. However, only the impact forces which resulted from the reaction will be considered. The forces reaction is assumed to be ideal and limited to 120mm of stroke. The available driven forces are:

- a) 3 batteries motoring force (3BM)
- b) 5 batteries motoring force (5BM)
- c) 3 batteries motoring forces with light combustion (3BC)

Overall aim for this research is to create an effective way to counter impact forces that act on engine block. However, to obtain a full vibration cancellation for LG will be very time consuming and involved complex procedures. Present work will base on analytical model with numerical software MATLAB to illustrate the basic principle and concept of the vibration cancellation. The parameters for simulation are calculated based on preliminary

experimental data. LM is assumed to be efficiently providing counter forces to the LG. Simulation illustrates the responds of LG before and after the application of AVC in frequency and time domains. Verification is carried out to investigate the reliability of the mathematical modeling method, together with a case study to examine the best available driven force that drives the PRA for LG on current experimental stage.

### **1.3 Dissertation Organization**

The introduction in **CHAPTER I** provides the reader with background information of the LG, the cause of LG's vibration problem, definition of vibration, and the importance of vibration control. The research scope and focus are discussed. The objective is identified.

**CHAPTER II** provides some important descriptions taken from literatures which are relevant with this research. This section covers all major issues about LG, active vibration control and works related to simulation results, such as pole-zero plot, root locus plot, time response, and frequency response. For validation purpose, thesis that provided with detailed simulation or experimental results are briefed.

Research methodology is described in **CHAPTER III**. This section outlined the work flow of current research. All important definitions are briefed and generally discussed, especially for the analytical analysis part. The chapter derived the LG dynamic mechanical interaction forces within the engine to indentify the impact forces which cause vibration problem to the LG.

**CHAPTER IV** shows all detailed theoretical principles followed by simulation results. Transfer functions method is used to investigate the system stability characteristic. Transfer function method is applied to plot pole-zero plots and root locus plots. State-space approach is used to plot non-proportional damped time response. Modal state-space approach is applied to plot proportional damped time response, which the system are assumed lightly damped. Frequency responses obtained are in the form of bode diagram with all approaches. A comparison of results is showed later in the chapter to identify the suitable and relevant approach for validation and case study.

Validation for the simulation is discussed in **CHAPTER V**. The validation model is a lumped-mass quarter car suspension system models. The types of the suspension systems studied are passive, semi-active, active and smart. Three different literatures with different proposed method are used to verify reliability of the simulation.

**CHAPTER VI** is the case study. The purpose of case study is to determine the best available driven force which drives the LG optimally. The case study is simulated using preliminary data on motoring limited stroke.

**CHAPTER VII** concluded present study and proposed future works. This chapter revisits the overall aim and specific objectives of this research study. The limitations of the work are also highlighted. Importantly, the issue of managing the implementation of the recommendations is addressed.

## **CHAPTER II**

### **LITERATURE REVIEW**

#### **2.1 Introduction**

The study within this review of literature focuses on the importance of application of vibration control from different points of view. Literature review will examine all the main issues surrounding:

1. Free-piston linear generator engine (LG)
2. Active vibration control
3. Pole-zero plots and Root locus plots
4. Time response
5. Frequency response
6. Damping properties
7. Quarter car suspension system (validation)

#### **2.2 Free-piston linear generator engine**

According to Van Blarigan and Goldborough, conventional two-stroke engines are plagued by problems of insufficient charging and high short-circuiting emissions throughout parts of their operating regimes, with this generally resulting from the wide range of speeds and power outputs over which the engines operate. For the free piston engine however, a much more narrow range of operating speeds is expected to be utilized. This is due to the electrical generating scheme employed by the device; efficient generation will be achieved by operating at a fixed oscillation rate. Single speed operation significantly simplifies the scavenging system design, in effect allowing the charging process to be optimized about a specific operating point [9].

Mikalsen and Roskilly reviewed the development of past and present researches and works that related with free-piston engine applications. They reviewed the history of free-piston internal combustion engines, from the air compressors and gas generators used in the mid-20th century through to recent free-piston hydraulic engines and linear electric

generators. Unique features of the free-piston engine are presented and their effects on engine operation are discussed, along with potential advantages and disadvantages compared to conventional engines. The paper focuses mainly on developed engines where operational data has been reported. Finally, the potential of the free-piston engine is evaluated and the most promising designs identified [10]. Figure 2.1 shows the early configuration of a single piston and dual piston free-piston engine.

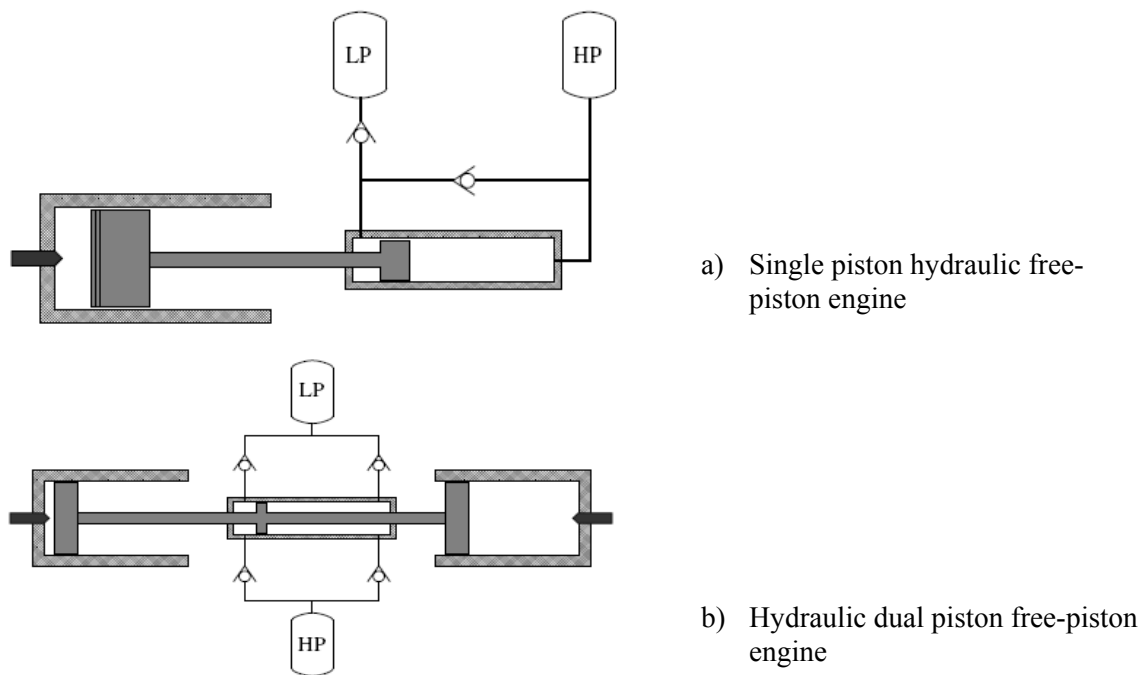


Figure 2.1: Single piston and dual piston free-piston engine, adapted from [10] (LP = low pressure, HP = high pressure)

For the single piston and dual piston engine, however, balancing issues need to be addressed when mounting the engine. Vibrations may be cancelled out by running two or more engines in parallel, but this requires accurate control of engine speed. Another possibility is to apply counterweights. Disadvantages of counterweights are a more complex design, increased engine size and weight and additional friction losses [10].

Mikalsen and Roskilly also work on design and simulate a two-stroke free-piston compression ignition engine for electrical power generation. A simulation program was written using the numerical computation software MATLAB to investigate the influence of design parameters and engine input variables. The simulation program determine the piston speed and position using standard forward Euler numerical integration, with the diesel engine sub-models and the correlations for alternator load force and bounce chamber pressure being solved at each simulation step. The program allows investigation into both steady state outputs and transient response of engine performance [6].

Van Blarigan carried out studies on the multi-fuel potential of free-piston engine. Van Blarigan proposed to use renewable hydrogen-based in an advanced internal combustion electrical generator. The objective of the project is to provide a high-efficiency means of renewable hydrogen-based fuel utilization. The development of a high-efficiency, low-emissions electrical generator will lead to establishing a path for renewable hydrogen-based fuel utilization. This combustion condition leads to the highest possible peak temperatures, and thus the highest possible thermal efficiencies. In general, HCCI combustion has been shown to be faster than spark ignition (SI) or compression ignition combustion. And much leaner operation is possible than in SI engines, while lower NO<sub>x</sub> emissions result [11].

Cosic *et al.* on the other hand, tested on different configuration of magnet, presented a new concept of a linear TFM in which strong emphasis has been put to achieve a design that is simple to manufacture. In this paper a new linear TFM machine has been presented. An analytical model for a surface magnet design has been developed. By using the equations developed the calculated force was found to be 4:1kN and movable mass of the translator 5:8kg. The 2D model has been used to develop analytical expressions and some empirical factors have been used in order to predict leakage in the 3rd dimension. Analysis of the hallbach oriented magnets is still to be performed together with a verification of the analytical model with a 3D FEM simulation [12].

Saiful on the other hand, studied on the starting mechanism for LG. He proposed to drive the LG with motoring force using a series of batteries [13]. Research groups like SANDIA National Lab, Aerodyne Research, Inc., U. West Virginia and Czech Tech had developed prototype of free-piston engine which is still under experimental stage [2, 3, 4, 5, 13, 14].

### 2.3 Active Vibration Control

Many active vibration control methods are suggested and tested in many different cases. According to Nagurka and Kurfess a system can be considered absolutely stable if a transient oscillation decays and ultimately vanishes in time domain. As in frequency domain, the resonance peak can be used to indicate relative stability. The reasons for choosing active control are simply because significantly increase performance [15]. Counter-force control is the more logical choice as it measures and directly reduces the quantity of interest (disturbance force) rather than indirectly [16, 17].

Montanaro and Beale proposed to use feedback control for active vibration propose. They claimed the cancellation is accomplished by applying an alternating force to the surface through a vibrating motor. Applications for which it is desired to reduce vibrations in an object range from home appliances and automobiles to aircraft and high-speed trains. Reducing mechanical vibration provides for improved user comfort and safety, and it increases product reliability and durability by reducing wear. Both  $H_\infty$  and Linear Quadratic Gaussian (LQG) techniques were investigated [18]. The schematic of vibration control system proposed by authors is shown is Figure 2.2.

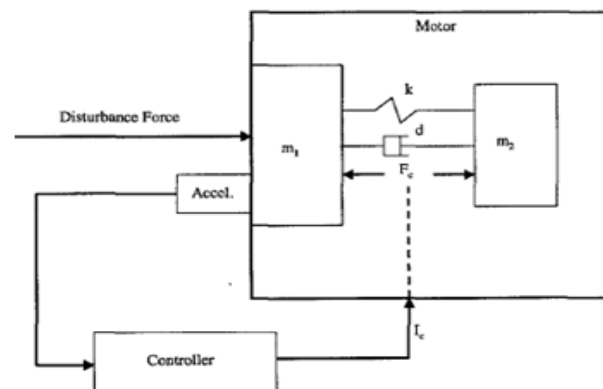


Figure 2.2: Schematic of vibration control system, adapted from [18]



Kwak and Heo investigated the active vibration control for a grid structure using multi-input multi-output (MIMO) positive position feedback (PPF). They claimed the PPF controller is very effective in suppressing a specific vibration mode, thus maximizing the damping in a targeted frequency bandwidth without destabilizing other modes. However tuning is required during the process. The theoretical models are built based on simulink. Both theoretical and experimental results show that the proposed MIMO PPF controller is capable of suppressing first four modes of the grid structure with two sets of sensor and actuator. They concluded that the block inverse technique, the stability prediction formula, and the design methodology can be effectively used for the design of successful vibration suppression controller for smart structures [19].

Chen and Zhu suggested using robust control for active vibration control. They formulated a control strategies using linear matrix inequality to attenuate the transient vibration of a flexible rotor system under a non-stationary seismic excitation. According to authors, the rotating machinery is likely to face more severe vibrations caused by various vibration sources such as mass unbalance, shaft misalignment and exogenous disturbance. These vibrations are in turn responsible for not only performance degradations, but also excessive acoustic noises and fatigue-related damages. Therefore, the vibration suppression is a matter of great significance to rotating machinery systems. In this study, the  $H_2$ ,  $H_\infty$  and multi-objective  $H_2/H_\infty$  state feedback control strategies are described by means of the linear matrix inequality (LMI) and applied to active vibration control of the flexible rotor system under seismic excitation. The multi-objective  $H_2/H_\infty$  control problem is solved by using very efficient convex optimization software MATLAB LMI Tools for a practical control object of the double-disc cantilever flexible rotor system under seismic excitation. The  $H_2$ ,  $H_\infty$  and mixed  $H_2/H_\infty$  control strategies were formulated, respectively, by means of the LMI. An active vibration control for a double-disc cantilever flexible rotor system under seismic excitation were analyzed by the  $H_2$ ,  $H_\infty$  and mixed  $H_2/H_\infty$  control strategies and compares the simulation results in transient domain and frequency domain [20].

Zhu *et al.* used active vibration isolation systems (VIS) as a foundation to stabilize the space shuttle to the ground vehicle [21].

Hillis *et al.* conducted work to control automotive active engine mounts, consisting of a conventional passive mount and an internal electromagnetic actuator. Active engine mounts seek to cancel the oscillatory forces generated by the rotation of out-of-balance masses within the engine. Two active vibration cancellation algorithms which are filtered-x least-mean-square (FXLMS) and error-driven minimal controller synthesis (Er-MCSI) have been tested with an active engine mount in conjunction with a saloon car equipped with a four-cylinder turbo-diesel engine [22].

Olsson studied the active automotive engine vibration isolation both in stationary and transient engine-induced excitations. He proposed an adopted control strategy targets the dominating spectral components of the excitation and achieves narrow band vibration isolation using feedback of disturbance states estimates. A virtual environment consisting of two different software packages have been used for physical modeling of the engine and its suspension system, control system modeling and design of controller, and virtual verification of outcomes, i.e. control algorithms [23]. They are

- a) A multi-body system analysis and simulation software for dynamics (ADAMS),
- b) A real-time analysis and simulation software for control synthesis (MATLAB/Simulink).

## **2.4 Pole-zero Plots and Root Locus Plots**

The purpose to plot the pole-zero plots and root locus is to investigate the cause of system instability. Hara *et al.* stated that ‘poles’ and ‘zeros’ play important roles in the performance of linear time-invariant control systems [24]. Ravuri and Asada also stated that the ‘poles’ and ‘zeros’ move as the location of the mass is varied, because the distribution of the mass and stiffness are essential to the determination of the resonances [25, 26]. Kurfess and Narguka described that the system behavior of the closed-loop system is determined by the eigenvalues or ‘poles’ [27]. Analysis and experiment results

from Ha and Negnevitsky indicate that the maximal damping of two-mass systems depends on the mass ratio of the system described. The conventional approach to the estimation of electromechanical system dynamics relies on the location of the roots of the system's characteristic equation in the complex plane [28].

A simple method for finding the roots of the characteristic equation has been developed by W. R. Evans and used extensively in control engineering. This method, called the root-locus method. It is a graphical solution, which the roots of the characteristic equation are plotted with a range of damping values. It is a set of theorems and techniques that calculates the locations of the closed-loop poles in the  $s$ -plane as a changing parameter (gain) in the open-loop transfer function varies over some defined range. The plot of positive gain is known as root locus (RL), and the locus of negative gain is referred to as complementary root locus (CRL) [29]. The roots corresponding to a particular damping value can then be located on the resulting graph [28]. Root Locus is a graphical technique method purposely to exam the stability of a system and indicates the degree of stability of the system, such as amount of overshoot and the settling time [27].

## **2.5 Time Response**

There will be two types of time responses; a proportional damped time response and a non-proportional damped time response. Proportional damping is the most common approach to model dissipative forces in complex engineering structures. One of the main limitations of the mass and stiffness proportional damping approximation comes from the fact that the arbitrary variation of damping factors with respect to vibration frequency cannot be modeled accurately by using this approach [30]. Proportional damped response is assumed the damping matrix to be a linear combination of mass and stiffness matrix [31]. According to Sorrentino *et al.*, for a linear system, it is often modeled as proportional damping response [32].

However in many real situations, the proportional damping assumption is not valid and does not describe the dynamics of the system with sufficient accuracy [31, 32]. Typically for a proportional damped time response, equivalent viscous damping model does not

accurately represent the damping behavior. According to Adhikari and Woodhouse, linear systems must generally be expected to exhibit non-viscous damping [33]. Normally, a damped system will possess non-proportional damping response [33, 34]. Cha stated, with the present of damping, the characteristic equation will have complex conjugate roots [35]. For a given complex conjugate eigenvalues there are complex conjugate eigenvectors and consequently the system possesses complex modes instead of real normal modes [30]. However, consideration of complex modes in experimental modal analysis has not been very popular among researchers [33].

## 2.6 Frequency Response

Chen and Zhu in their work, proposed robust control for active vibration control purpose. They showed the comparison before and after the application of robust control for a rotor system in time and frequency domain. With or without the  $H_\infty$  control, the frequency responses and the transient responses in the  $x$ -direction of disc A of the cantilever flexible rotor system under EI Centro seismic excitation is shown in Figure 2.3. Without the  $H_\infty$  control, there are five peaks on the frequency response curves which are corresponded to the first five critical angular frequencies of the rotor system. The peaks almost disappear with the  $H_\infty$  control. As for the transient response, the amplitude of excitation reduced with the  $H_\infty$  control [20].

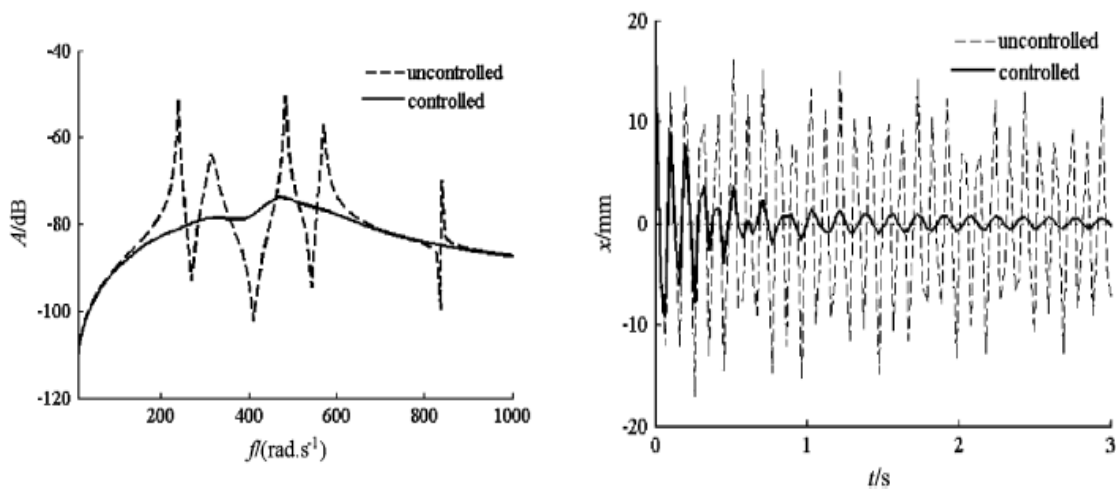


Figure 2.3: Responses of disc A, adapted from Chen and Zhu [20]

Benassi *et al.* showed that with variant in feedback gains, it will affect the location as well as the magnitude of resonance [36]. For a smart grid structure, Kwak and Heo proved the needs and importance of vibration control, with suitable and correct used of piezoceramic sensors and actuator, the resonance is delayed with the reduction of magnitude at the same instant [19]. Stark *et al.* also showed that with suitable control strategy, using state-space model, obtained the same conclusion. They found that with the control mechanism, the resonance can be delayed and the magnitude can be reduced [37].

Olsson in his work on active automotive engine vibration isolation designed an adopted control strategy to achieve narrow band vibration isolation using feedback of disturbance state estimates. He found that by using appropriate control strategy, the resonance occurrence can be delayed with phase shifted back to initial phase [38].

The Bode diagram obtained by Olsson using linear parameter varying (LPV) modeling is shown in Figure 2.4. The solid line represent before the application of feedback. It clearly shows a better performance can be achieved with the application of feedback.

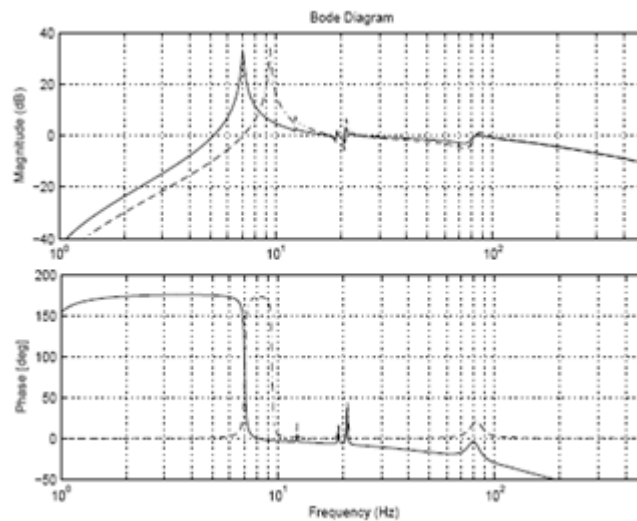


Figure 2.4: Bode diagram adapted from Olsson [38]

## 2.7 Validation: Quarter Car Suspension System

A lumped mass quarter car active suspension system is selected for validation purpose. There are many types of suspension systems, such as passive, semi-active, active and smart suspension system. The study of concept of active suspension system can be traced back to 1960s [39], while works that compare the active, passive and semi-active are available since 1982 [40] and during 90's [41]. The development of active suspension system evolved, involving design of high performance and energy efficient by Beard [42]. Chantra used adaptive robust control to suit with the active suspension system [43]. From times, better approach is proposed for the same suspension model. Optimal Control used for passive, semi-active, and smart suspension system [44], linear quadratic regulator (LQR) used for active suspension system [45], but due to some drawback from LQR, Coprime factorization is proposed to analyze a quarter car suspension system [46].

## 2.8 Damping Properties

Damping in mechanical structures appears in many forms such as viscous, hysteresis, frictional, Coulomb, and so on. The properties of the damping mechanisms differ from each other and not all of them are equally amenable to mathematical formulation. Fortunately, small amounts of damping have very little influence on the resonant frequencies, which are normally calculated by neglecting the effects of damping. However, in calculating the response under forced vibrations, it is necessary to include the damping effects. Often, one has to resort to experimental information to determine the damping present in practical structures [26].

In most vibration problem, the value for damping ratio value is normally assumed. The value of critical damping value can only be determined experimentally. Verma and Balan try to determine damping ratio,  $\zeta$  experimentally [26]. The outcome of the experiment is, under the condition for a two masses and two degree of freedoms system, the critical damping is approximate 0.02032 (0.02), or 2%.

Table 2.1: The values of the damping ratios obtained from the well defined vibration responses, adapted from [26]

**Table 3: Damping-ratios measured at the selected resonances of the stator-shell and the laminated stator models**

Stator-shell model				Laminated stator with windings			
$f$ , Hz	$n$	$m$	$\zeta$	$f$ , Hz	$n$	$m$	$\zeta$
1242	2	0	0.00043	470	2	0	0.01241
1432	2	1	0.00046	631	2	4	0.01624
3032	1	1	0.00024	1801	3	2	0.01292
3197	3	0	0.00012	1907	2	2	0.02032
3432	3	1	0.00019	2055	3	4	0.03558
3456	1	2	0.00031	2306	3	2	0.03066
3942	0	0	0.00017	2491	4	0	0.04232
4254	0	1	0.00021	3016	0	0	0.05165
5513	4	0	0.00011	3339	0	0	0.03021
5729	4	1	0.00008	3820	5	4	0.01748
8012	5	0	0.00017	4325	1	6	0.01638
8193	5	1	0.00014				

## 2.9 Conclusion

Many works and researches related to the development for free-piston linear generator are presented particularly on the combustion aspects. Many methods of active vibration control are proposed. However, no researches related directly to the active vibration cancellation of a free-piston linear generator engine is recorded or documented yet. Present study introduces the first trial to deal with vibration problem for a free-piston linear generator engine.

## **CHAPTER III**

### **RESEARCH METHODOLOGY**

#### **3.1 Introduction**

The research work started with vibration sources identification of LG. A study of internal forces reactions within LG is carried out to investigate the main vibration source. Active vibration cancellation is proposed as the vibration control strategy based on analytical analysis aspect. The methods proposed for analysis are the transfer function approach, the state-space modeling and the modal state-space analysis with a defined mathematical model. Transfer function approach is used to plot pole-zero plots and root locus plots. State-space modeling is applied to obtain non-proportional damped time response. Modal state-space analysis is carried out to determine the proportional damped time response. Frequency responses (Bode Plots) are obtained using all methods. All simulation results are obtained using MATLAB. Results comparison is made to select the most relevant approach for validation. With the justified results, case study is carried out to decide the best driven force that offer better operating condition for LG. Eventually, the work is concluded and future works are also suggested. The work flow is shown in Figure 3.1.



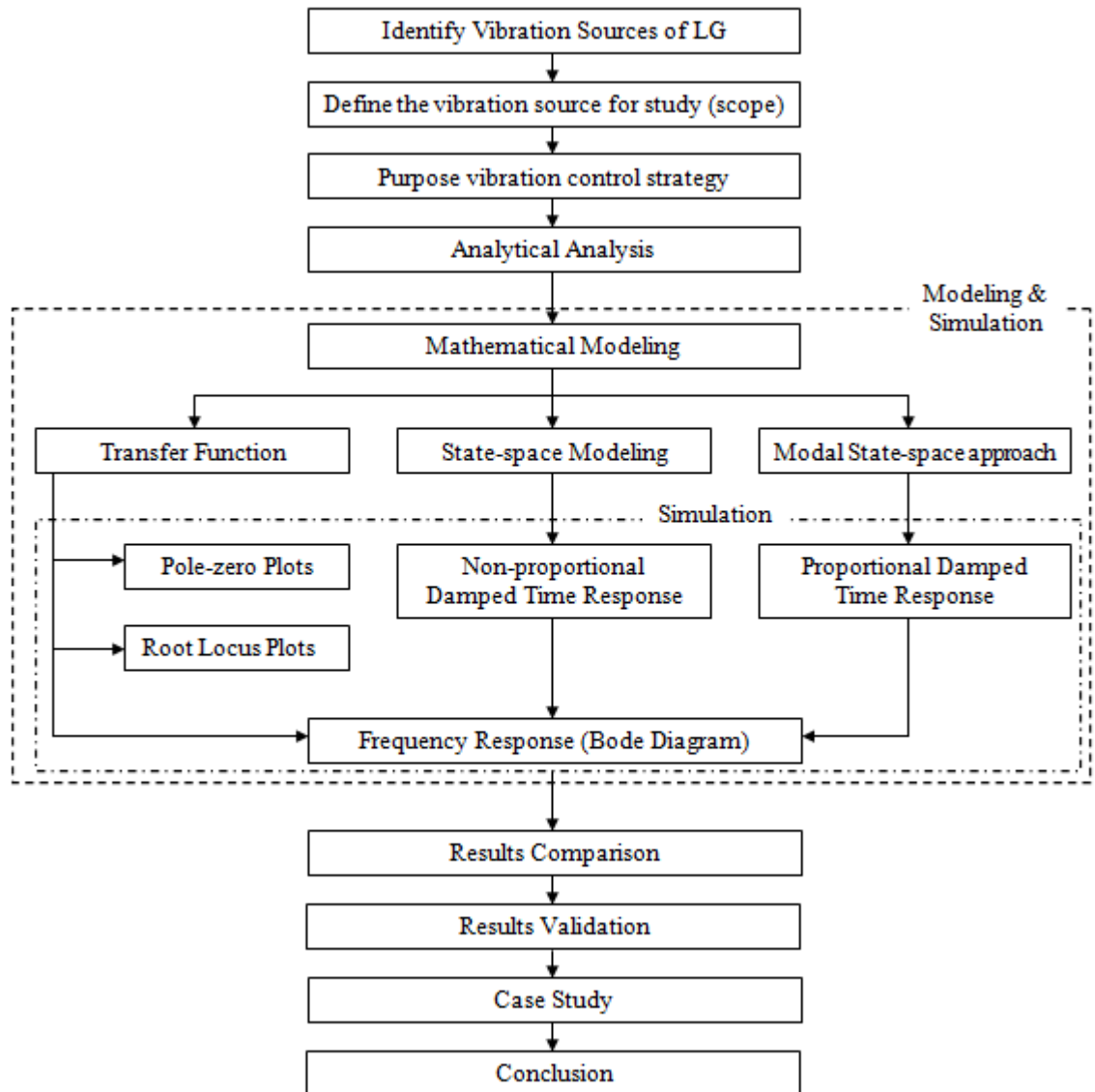


Figure 3.1: The research methodology of active vibration cancellation for LG

### 3.2 LG Mechanical Forces

In order to determine the required counter forces generated from LM, a full mathematical description showing all forces reaction of LG is shown in Figure 3.2. The free-body diagram depicts the forces reaction with or without the presence of internal combustion.

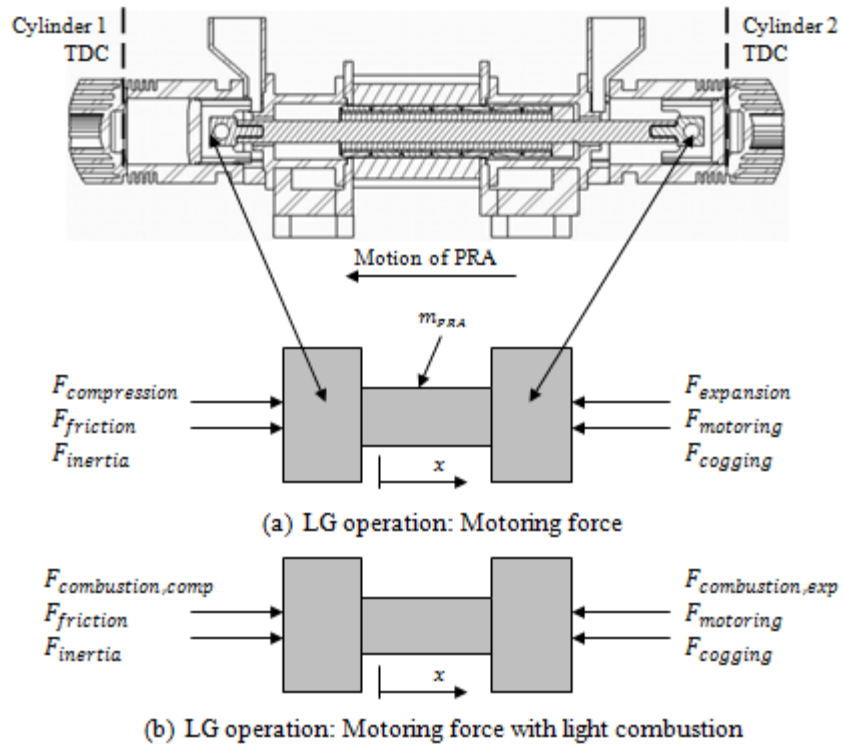


Figure 3.2: LG free-body diagram

Compression force ( $F_{comp}$ ) and expansion force ( $F_{exp}$ ) arise due to pressure built in combustion chambers. The forces generated when the gap between the piston head and cylinder head is closing. The LG is dual-opposed configuration, when one side of PRA is compressed, the other side experiences expansion, and vice versa during the operation. However, with the presence of combustion, higher compression force ( $F_{comb,comp}$ ) and expansion forces ( $F_{comb,exp}$ ) are expected. For an ideal gas, the expressions for compression force based on function of  $x$  is

$$F_{comp} = P_{atm} \cdot A \left( \frac{V_2}{V_1} \right)^k \quad (3.1)$$

The constant  $k$  is the adiabatic constant of the medium undergoing the compression-expansion process. The  $P_{atm}$  is the atmospheric pressure,  $V_1$  is the compressed volume which will varies according to displacement of PRA,  $V_2$  is the trapped cylinder volume just before the exhaust port is close and  $A$  is the surface of the piston. The equation (3.1) can be rewritten as:

$$F_{comp}(x) = K_1 \cdot \left( \frac{K_2}{x+l} \right)^k \quad (3.2)$$

Where  $K_1$  and  $K_2$  are constant determined by atmospheric pressure  $P_{atm}$ , and piston surface are  $A$  and trapped volume  $V_{trapped}$ . Parameter  $l$  is the equivalent crevice length of the cylinder head and is constant, and  $x$  is the piston distance from TDC and is thus the only variable in equation (3.2). Similarly, the expansion force is expressed as:

$$F_{exp}(x) = K_3 \cdot \left( \frac{K_4}{x+l} \right)^k \quad (3.3)$$

Where  $K_3$  and  $K_4$  are constant determined by compressed pressure of the previous stroke and corresponding final compressed volume  $V_{comp}$ , which acting on the piston surface area,  $A$ . Thus, with the expression of (3.2) and (3.3), the non-linearly of the compression and expansion force can be eliminated. The purpose for that is to determine the air spring constant using a normal linear mechanical spring relation:

$$F(x) = k \cdot x \quad (3.4)$$

The inertia forces ( $F_{int}$ ) are created due to the linear oscillation motions of PRA in LG. The inertia forces are affected by the way and direction of motion of PRA as well as PRA's mass. The higher the mass of PRA, the larger the inertia forces may be expected.

It is difficult to determine the friction forces ( $F_f$ ) instantaneous magnitude to generate an accurate friction profile against displacement. Thus, the value of the friction is assumed to be fixed based on reliable measurements. The value of friction is adjusted to meet the requirement to implement motoring force as well as combustion force.

Magnetic cogging force ( $F_{cog}$ ) resulted from the interaction between the permanent magnet's magnetic field and the iron-cored stator. The cogging force may be positive or negative depending on the position of PRA. This also means that the cogging force may be assisting or impeding PRA motion. The magnitudes of the cogging force over the entire stroke with or without combustion is shown in Figure 3.3, which is obtained via finite-element analysis performed by *UM* LG team [5]. Plot for magnetic cogging and other mechanical forces of LG is shown in *Appendix A*.

### 3.3 LG Dynamic Equations

Newton's second law is used to express all internal reaction forces as shown in Figure 3.2. Two dynamic equations are derived with LG operates on motoring force ( $F_{mot}$ ) and motoring force with combustion. Since the operation of LG is only in one single axis (linear), if LG is operates only with motoring force,

$$\Sigma F_{x,mot} = F_{exp} + F_{mot} + F_{cog} - F_{comp} - F_f = m_{PRA} \frac{d^2 x_{PRA}}{dt^2} \quad (3.5)$$

The forces acting on the engine block is therefore assumed and defined as,

$$Impact\ force_{mot} = m_{PRA} \frac{d^2 x_{PRA}}{dt^2} \quad (3.6)$$

which turn out to be the inertia force due to PRA oscillations. This is the force that needs to be phasing out using LM. Similarly, if LG operates with motoring force and combustion,

$$\Sigma F_{x,mot+comb} = F_{comb,exp} + F_{mot} + F_{cog} - F_{comb,comp} - F_f = m_{PRA} \frac{d^2 x_{PRA}}{dt^2} \quad (3.7)$$

And the impact force is assumed as,

$$Impact\ force_{mot+comb} = m_{PRA} \frac{d^2 x_{PRA}}{dt^2} \quad (3.8)$$

The forces showed in Figures 3.3, 3.4 and 3.5 are the profile of all driven forces. Under a single full cycle (assumed 120mm of stroke and idealized internal forces reaction), the forces acting on one side of the engine block are,

- a) Case when 3BM:  $F_{impact} = 75\text{ N}$
- b) Case when 5BM:  $F_{impact} = 87.5\text{ N}$
- c) Case when 3BC:  $F_{impact} = 212.5\text{ N}$

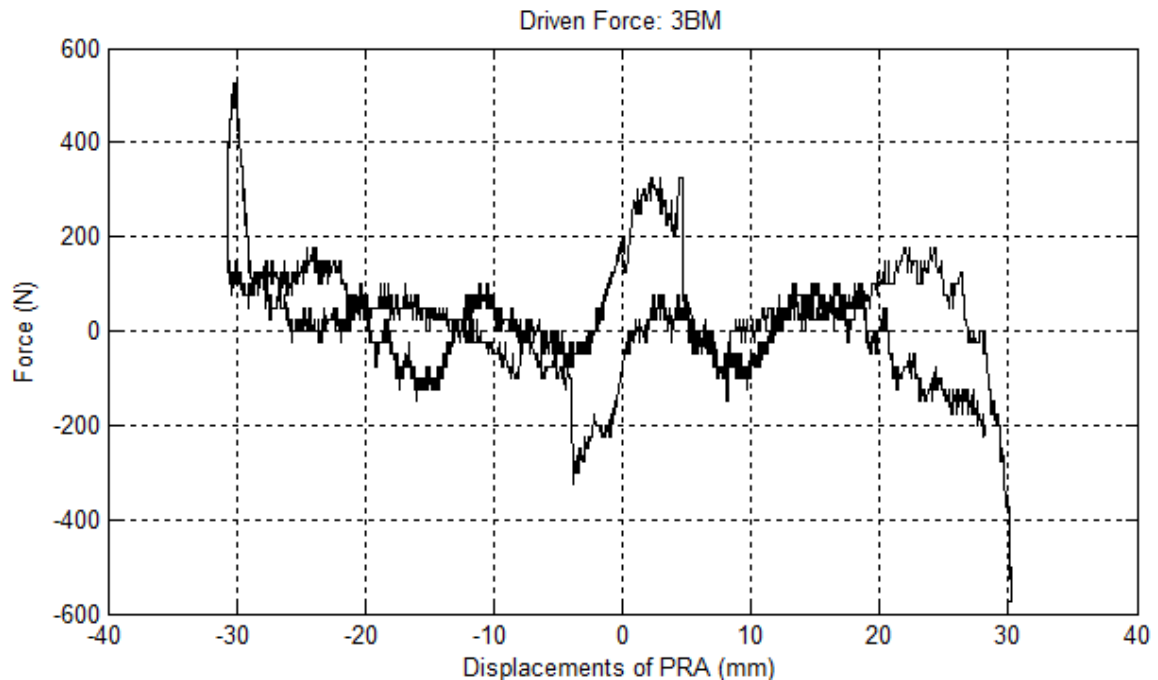


Figure 3.3: Force generated by 3BM (complete cycle = 0.22s), adapted from [3, 13]

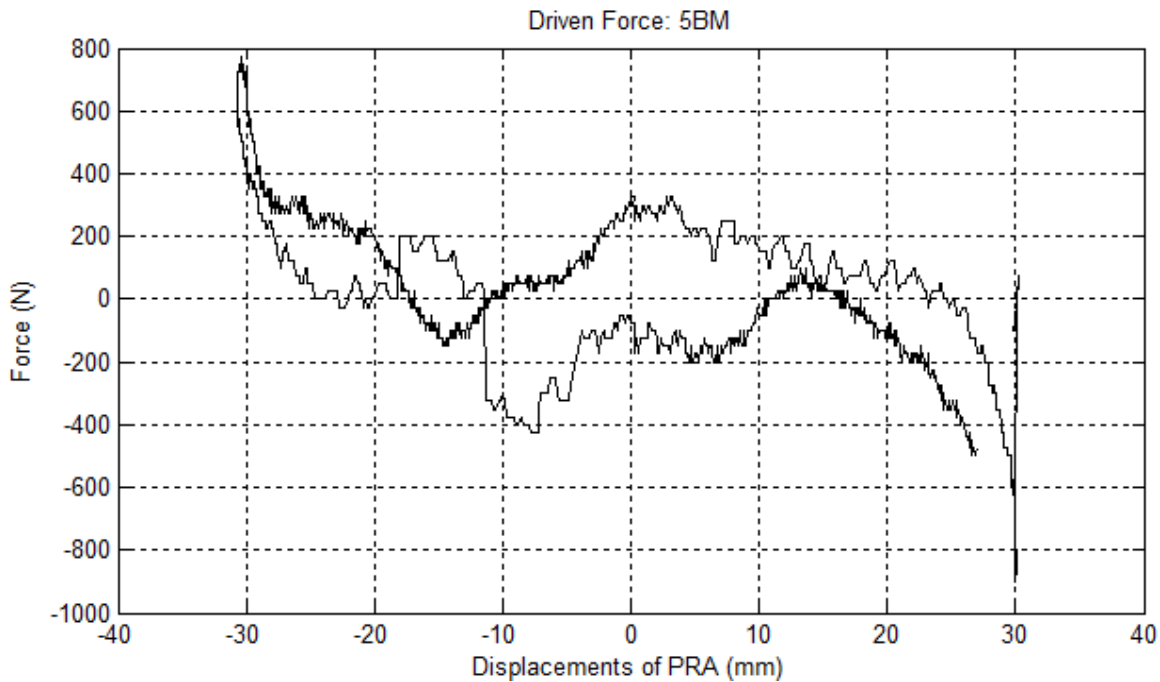


Figure 3.4: Force generated by 5BM (complete cycle = 0.14s), adapted from [3, 13]

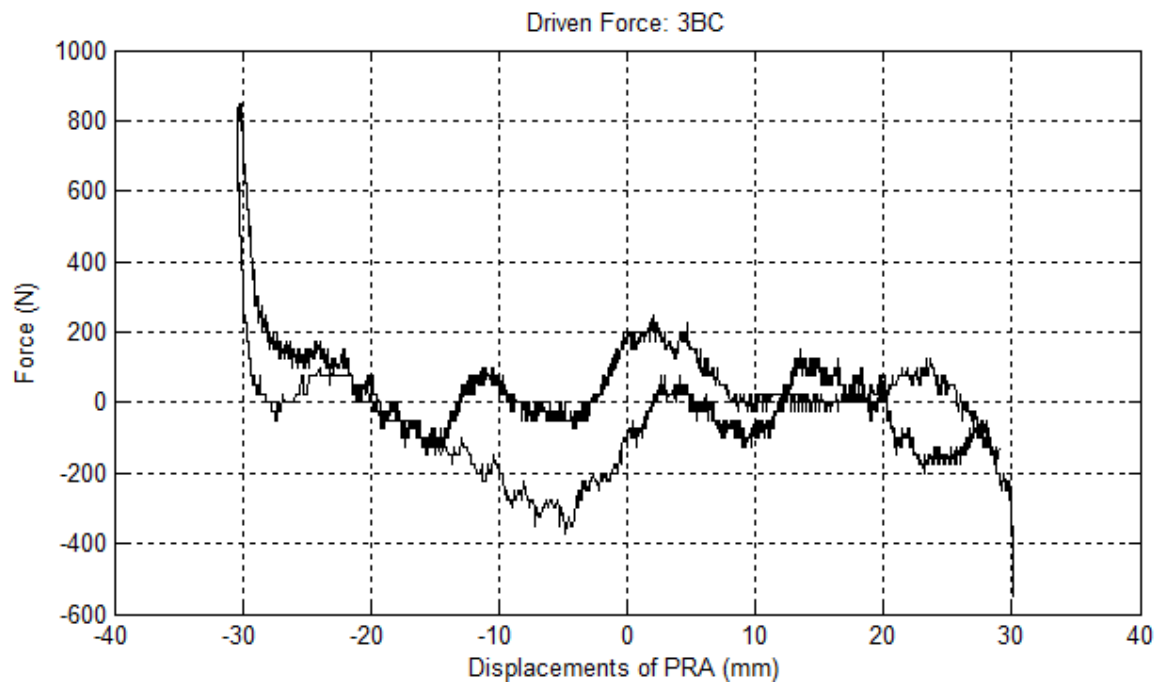


Figure 3.5: Force generated by 3BC (complete cycle = 0.22s), adapted from [3, 13]

### 3.4 Analytical Analysis

#### 3.4.1 Mathematical Modeling

A mathematical model is defined as a set of differential equations that represents the dynamics of the system. A compromise between the simplicity of the model and the accuracy of the results of the analysis must be made when obtaining a mathematical model. However a mathematical is not unique to a given system; the system can be represented in many ways depending on one's perspective. The fundamentals of vibration analysis can be understood by studying the simple mass–spring–damper model. Even a complex structure such as an automobile body can be modeled as a "summation" of simple mass–spring–damper models. Mass-spring-damper models for free-damped and forced-damped are showed on Figure 3.6.

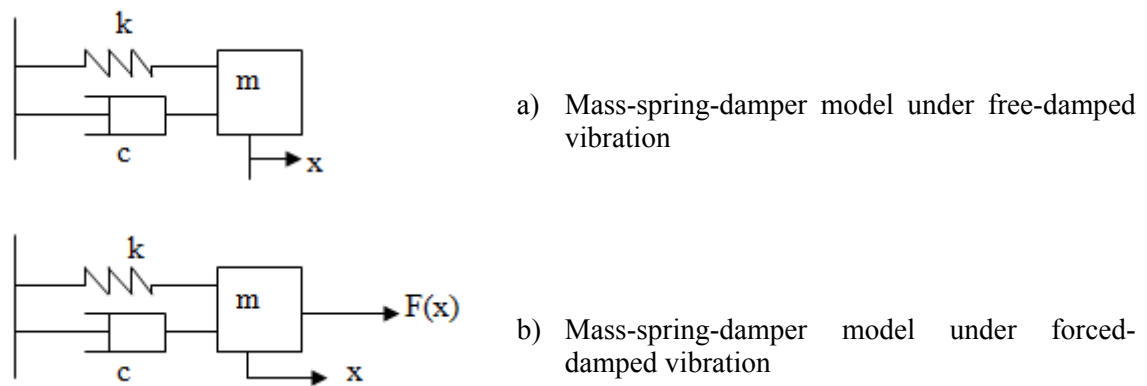


Figure 3.6: Mass-spring-damper models

By summing the forces on the mass using Newton's Law, the following governing equation or equation of motion (EOM) obtained:

For free-damped:

$$m\ddot{x} + c\dot{x} + kx = 0 \quad (3.9)$$

For forced-damped:

$$m\ddot{x} + c\dot{x} + kx = F(x) \quad (3.10)$$

### **3.4.2 Transfer Function Approach**

Transfer functions are commonly used to characterize the input-output relationships of a system. The transfer function is a property of a system itself, *independent of the magnitude and nature of the input or driving function*. The transfer function does not provide any information concerning the physical structure of the system. Typical form of transfer function:

$$G(s) = \frac{\text{numerator}(s)}{\text{denominator}(s)} \quad (3.11)$$

Transfer function is obtained by Laplace transformation of the equations of motion with all initial conditions assumed zero. The transformed equation will then be rearranged to show the ratio of output to input. Other properties of transfer function:

#### **3.4.2.1 Poles**

The ‘poles’, eigenvalues, or resonant frequencies, are the roots of the characteristic equation or denominator ‘den’. ‘Poles’ show the frequencies where the system will amplify inputs. All the transfer functions will have the same ‘poles’ or characteristic equation. The ‘poles’ of a system depend only on the distribution of mass, stiffness, and damping throughout the system, without considering on where the forces are applied or where displacements are measured [25].

#### **3.4.2.2 Zeros**

The ‘zeros’ of each SISO transfer function are defined as the roots of its numerator. ‘Zeros’ show the frequencies where the system will attenuate inputs. ‘Zeros’ can be different for every transfer function and some transfer functions may have no ‘zeros’.

#### **3.4.2.3 Pole-zero plots**

In mathematics, signal processing and control theory, a pole-zero plot is a graphical representation of a rational transfer function in the complex plane which helps to convey certain stability properties of the system.



### 3.4.2.4 Root Locus Plots

Root Locus is a graphical technique method purposely to exam the stability of a system and indicates the degree of stability of the system. There are two general conclusions from the root locus plots [7, 47]:

- a) The additional of a ‘zeros’ to a system has the general effect of pulling the root locus to the left, tending to make it more stable and faster-responding system.
- b) The additional of a ‘poles’ to a system has the effect of pulling the root locus to the right, tending to make it a less stable and slower-responding system.

### 3.4.3 State-space Modeling

A state-space representation is a mathematical model of a physical system as a set of input, output and state variable related by first-order differential equations. The state-space representation is useful to model and analyze a MIMO system [48]. States-space modeling is achieved by converting the second-order differential equations or equations of motion to first-order differential equations. The first-order differential equations will then be rearranged in matrix form and defined in state equation and output equation.

#### 3.4.3.1 State-space equation

For a linearized state equation and output equation, the  $\dot{\mathbf{x}}(t)$  is the state equation,  $\mathbf{y}(t)$  is the output equation,  $\mathbf{u}(t)$  is the inputs and  $\mathbf{x}(t)$  is the outputs.

$$\dot{\mathbf{x}}(t) = \mathbf{A}(t)\mathbf{x}(t) + \mathbf{B}(t)\mathbf{u}(t) \quad (3.12)$$

$$\mathbf{y}(t) = \mathbf{C}(t)\mathbf{x}(t) + \mathbf{D}(t)\mathbf{u}(t) \quad (3.13)$$

Where  $\mathbf{A}(t)$  is called the state matrix,  $\mathbf{B}(t)$  the input matrix,  $\mathbf{C}(t)$  the output matrix, and  $\mathbf{D}(t)$  the direct transmission matrix. For a linear, time-invariant system (LTI):

$$\dot{\mathbf{x}}(t) = \mathbf{A}\mathbf{x}(t) + \mathbf{B}\mathbf{u}(t) \quad (3.14)$$

$$\mathbf{y}(t) = \mathbf{C}\mathbf{x}(t) + \mathbf{D}\mathbf{u}(t) \quad (3.15)$$

A typical state-space modeling under LTI condition is shown in Figure 3.10.

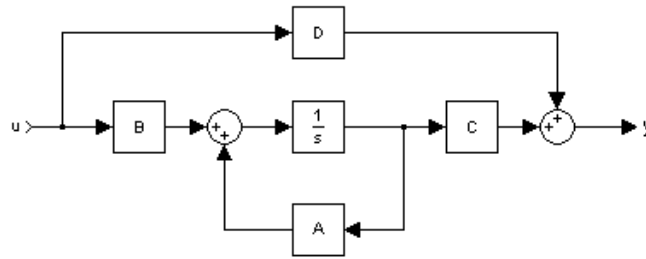


Figure 3.7: Typical state-space model

### 3.4.3.2 Non-proportional Damped Time Response

A non-proportional damped time response can be obtained, when the dynamic system is treated with damped condition initially. With the presence of damping during the dynamic analysis, the characteristic equation will have complex conjugate eigenvalues. For a given complex conjugate eigenvalues there are complex conjugate eigenvectors and consequently the system possesses complex modes instead of real normal modes. However, the consideration of complex modes in experimental modal analysis has not been very popular among researchers. The main reasons are:

- a) By contrast with real normal modes, the ‘shapes’ of complex modes are not in general clear.
- b) The imaginary parts of the complex modes are usually very small compared to the real parts, especially when the damping is small. This makes it difficult to reliably extract complex modes using numerical optimization methods in conjunction with experimentally obtained transfer function residues.
- c) The phases of the complex modes are highly sensitive to experimental errors, ambient conditions and measurement noise and often not repeatable in a satisfactory manner.

### 3.4.4 Modal State-space approach

#### 3.4.4.1 Modal Analysis

Modal analysis is the most popular and efficient method for solving engineering dynamic problems. The concept of modal analysis, as introduced by Rayleigh was originated from the linear dynamics of un-damped system. Most of the problems for modal analysis require using the finite element method to define a model with ANSYS for analysis.

The diagram in Figure 3.8 shows the methodology for analyzing a lightly damped structure using normal modes. As with the coupled equation solution above, the solution starts with deriving the un-damped equations of motion in physical coordinates. The next step is solving the eigenvalue problem, yielding eigenvalues (natural frequencies) and eigenvectors (mode shapes). This is the most intuitive part of the problem and gives one considerable insight into the dynamics of the structure by understanding the mode shapes and natural frequencies [48].

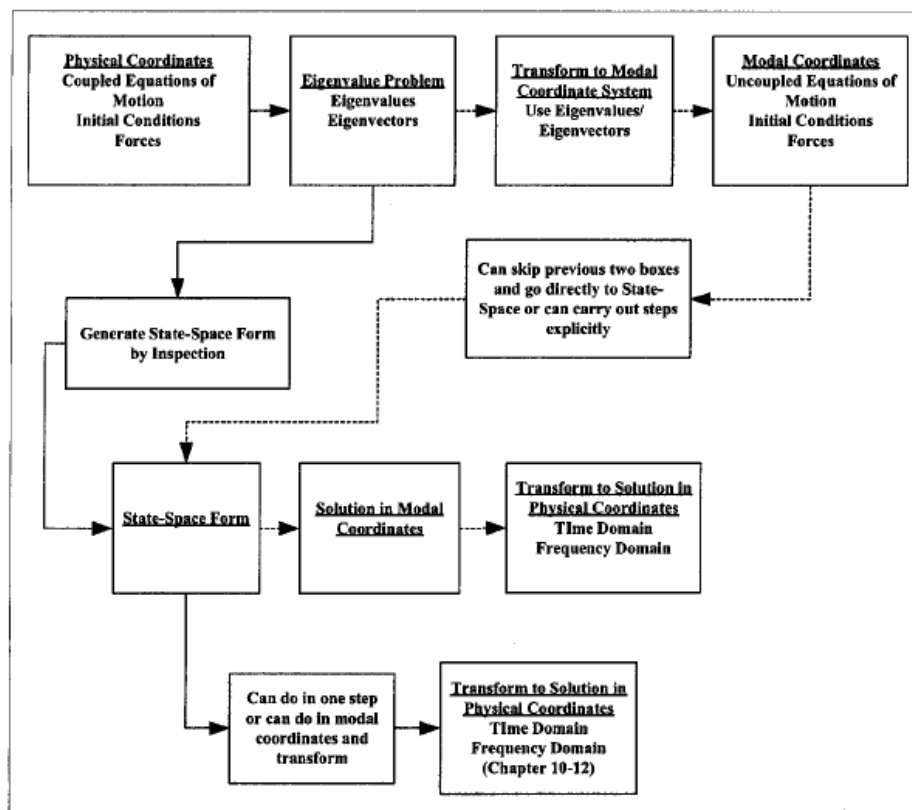


Figure 3.8: Modal analysis model flow chart, adapted from [48]

To solve for frequency and time domain responses, it is necessary to transform the model from the original physical coordinate system to a new coordinate system, the modal or principal coordinate system, by operating on the original equations with the eigenvector matrix. In the modal coordinate system the original un-damped coupled equations of motion are transformed to the same number of un-damped uncoupled equations. Each uncoupled equation represents the motion of a particular mode of vibration of the system. It is at this step that proportional damping is applied. It is trivial to solve these uncoupled equations for the responses of the modes of vibration to the forcing function and/or initial conditions because each equation is the equation of motion of a simple single degree of freedom system. The desired responses are then back-transformed into the physical coordinate system, again using the eigenvector matrix for conversion, yielding the solution in physical coordinates [48].

The modal analysis sequence of taking a complicated system,

- 1) Transforming to a simpler coordinate system,
- 2) Solving equations in that coordinate system and
- 3) Back-transforming into the original coordinate system is analogous to using Laplace transforms to solve differential equations.

The original differential equation is

- 1) Transformed to the “s” domain by using a Laplace transform,
- 2) The algebraic solution is then obtained and
- 3) Back-transformed using an inverse Laplace transform.

It will be shown that once the eigenvalue problem has been solved, setting up the zero initial condition state space form of the uncoupled equations of motion in principal coordinates can be performed by inspection. The solution and back-transformation to physical coordinates can be performed in one step in the MATLAB solution.

#### ***3.4.4.2 Modal Analysis: State-space form***

Modal analysis in state-space form or Modal state-space approach is a combination technique using both modal analysis and state-space modeling. In most cases, modal analysis is solved using ANSYS, but current method uses MATLAB to solve modal analysis problem.

In normal occasion, MATLAB used to solve for both frequency and time domain responses without the knowledge about eigenvalues and eigenvectors. Reason behind is that most mechanical simulations are performed using finite element techniques (ANSYS), and the equations of motion are too numerous to be able to be used directly in MATLAB. Current study will use MATLAB to determine eigenvalues and eigenvectors which result from the state space eigenvalues problem but contain the same information as from ANSYS. Eigenvalues will be used to uncoupled homogeneous equations of motion in the state space principal coordinate system. Forcing function and initial conditions will then be converted to principal coordinates using the normalized modal matrix. The final state equation of motion in the principal coordinate system is then created. With a completed form of equation of motion, proportional damping can be added to the modal formulation. The solution in principal coordinates back-transformed to physical coordinates for the final result.

#### ***3.4.4.3 Proportional Damped Time Response***

Proportional damping is the most common approach to model dissipative forces in complex engineering structures. The method treats a dynamic system under un-damped or lightly damped condition.

The un-damped modes or classical normal modes satisfy an orthogonality relationship over the mass and stiffness matrices and uncouple the equations of motion. This significantly simplifies the dynamic analysis because complex multiple degree-of-freedom (MDOF) systems can be effectively treated as a collection of single degree-of-freedom oscillators.

For an un-damped system, the eigensolutions are real. These eigensolutions, also known as the modes of vibration, are characterized by the natural frequencies and the mode shapes of the system. For a damped system, the eigensolutions are typically complex. To obtain the eigensolutions exactly, state equations are used, resulting in a generalized eigenvalue problem with complex eigenvalues and eigenvectors that require extensive computations. However, in many real situations this simplified approach does not describe the dynamics of the system with sufficient accuracy.

### ***3.4.5 Frequency Response (Bode Plots)***

Frequency response is the measure of any system's spectrum response at the output to a signal of varying frequency at its input. The frequency response is typically characterized by the *magnitude* of the system's response, measured in dB, and the *phase*, measured in radians, versus frequency. Magnitude represents the *ratio of output amplitude to input amplitude*. From control theory point of view, magnitude or gain can be positive or negative. Positive gain refers to positive feedback, while negative gain refers to negative feedback. For a system with positive feedback, the increase in some variable or signal leads to a situation in which that quantity is further amplified. This has a destabilizing effect and is usually accompanied by a saturation that limits the growth of the quantity. The negative feedback attempts to regulate the system by reacting to disturbances in a way that decreases the effect of those disturbances [49].

The frequency response using magnitude and phase diagram also known as *logarithmic plots or bode diagram*. Typically there are two conclusions can be shown using the bode diagram:

- a) The magnitude of resonance or 'peak' is preferable to be negative at a desirable frequency range.
- b) The phase remains constant except during the resonance.

## CHAPTER IV

### MODELING AND SIMULATION

#### 4.1 Mathematical Modeling

##### 4.1.1 Modeling of AVC

The LTI modeling of AVC as shown in Figure 4.1 matches the configuration of Figure 1.3. The masses  $M_1$  and  $M_2$  are the mass for the LM and LG respectively, with  $x_0$ ,  $x_1$  and  $x_2$  as the reference coordinates. The spring coefficients  $k_1$  represent the motions for the LM due to ‘forcer’ and  $k_3$  to illustrate the motion of LG due oscillation motion of PRA. The spring constant  $k_2$  is the equivalent spring coefficient of  $k_1$  and  $k_3$  in parallel configuration, together with applied damping rates,  $c$ . The force  $F_1$  is counter force from LM which is anti-phase to the impact force  $F_2$  from LG.

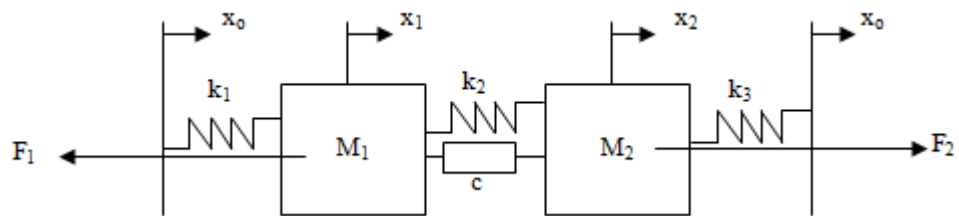


Figure 4.1: AVC Mathematical Modeling

The coordinates  $x_1$ ,  $x_2$  and  $x_0$  represent the motion of LM, LG and the whole system. Assuming,  $x_2 > x_1 > x_0$ , hence  $x_1 - x_0 \triangleq z_1$  and  $x_2 - x_0 \triangleq z_2$ .

##### 4.1.2 Free Body Diagram

The free body diagram of AVC mathematical model is shown in Figure 4.2.

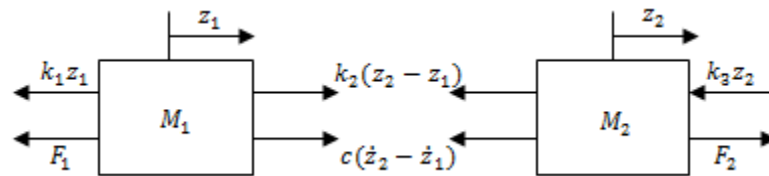


Figure 4.2: FBD of the mathematical model

### 4.1.3 Equations of Motion (EOM)

From Figure 4.2,

$$-F_1 - k_1 z_1 + k_2(z_2 - z_1) + c(\dot{z}_2 - \dot{z}_1) = M_1 \ddot{z}_1 \quad (4.1)$$

$$F_2 - k_3 z_2 - k_2(z_2 - z_1) - c(\dot{z}_2 - \dot{z}_1) = M_2 \ddot{z}_2 \quad (4.2)$$

Rearranging equations (4.1) and (4.2):

$$M_1 \ddot{z}_1 + c\dot{z}_1 - c\dot{z}_2 + (k_1 + k_2)z_1 - k_2 z_2 = -F_1 \quad (4.3)$$

$$M_2 \ddot{z}_2 - c\dot{z}_1 + c\dot{z}_2 - k_2 z_1 + (k_2 + k_3)z_2 = F_2 \quad (4.4)$$

Redefine the equations (4.3) and (4.4) in matrix form:

$$\begin{bmatrix} M_1 & 0 \\ 0 & M_2 \end{bmatrix} \begin{bmatrix} \ddot{z}_1 \\ \ddot{z}_2 \end{bmatrix} + \begin{bmatrix} c & -c \\ -c & c \end{bmatrix} \begin{bmatrix} \dot{z}_1 \\ \dot{z}_2 \end{bmatrix} + \begin{bmatrix} (k_1 + k_2) & -k_2 \\ -k_2 & (k_2 + k_3) \end{bmatrix} \begin{bmatrix} z_1 \\ z_2 \end{bmatrix} = \begin{bmatrix} -F_1 \\ F_2 \end{bmatrix} \quad (4.5)$$

### 4.1.4 Simulation parameters

The impact forces acting on one side of the engine block are (section 3.3.1):

- a) Case when 3BM:  $F_{impact} = 75 \text{ N}$
- b) Case when 5BM:  $F_{impact} = 87.5 \text{ N}$
- c) Case when 3BC:  $F_{impact} = 212.5 \text{ N}$

Table 4.1 shows all the parameters calculated based on the mass ratio, damping ratio and time for a complete single full cycle. The ‘forcer’ is assumed completing a single full cycle as when PRA complete a single full cycle in opposed phase. The spring coefficients and damping rate are the same for 3BM and 3BC. It is only a special case because the displacements and amount of impact forces are different for both the driven forces.



Table 4.1: Simulation Parameters

	$M_1 = 10\text{kg}$	$M_2 = 25\text{kg}$	
3BM	$k_1 = 101.17 \text{ N/m}$	$k_2 = 266.16 \text{ N/m}$	$F_1 = 75\text{N}$
	$k_3 = 165.29 \text{ N/m}$	$c = 3.26 \text{ Ns/m}$	$F_2 = 75\text{N}$
5BM	$k_1 = 249.82 \text{ N/m}$	$k_2 = 657.98 \text{ N/m}$	$F_1 = 87.5\text{N}$
	$k_3 = 408.16 \text{ N/m}$	$c = 5.113 \text{ Ns/m}$	$F_2 = 87.5\text{N}$
3BC	$k_1 = 101.17 \text{ N/m}$	$k_2 = 266.16 \text{ N/m}$	$F_1 = 212.5\text{N}$
	$k_3 = 165.29 \text{ N/m}$	$c = 3.26 \text{ Ns/m}$	$F_2 = 212.5\text{N}$

Mass ratio: PRA/ LG engine block = 1/4, ‘forcer’/LM block = 2.9/7.1 and  $\zeta = 2\%$ .

\*For the case of before the application of AVC, the FBD and EOM are shown in Appendix A

#### 4.2 Transfer Function Approach

Laplace transforms equation (4.5) by assuming all initial conditions are zero,

$$\begin{bmatrix} M_1 & 0 \\ 0 & M_2 \end{bmatrix} \begin{bmatrix} s^2 Z_1 \\ s^2 Z_2 \end{bmatrix} + \begin{bmatrix} c & -c \\ -c & c \end{bmatrix} \begin{bmatrix} s Z_1 \\ s Z_2 \end{bmatrix} + \begin{bmatrix} (k_1 + k_2) & -k_2 \\ -k_2 & (k_2 + k_3) \end{bmatrix} \begin{bmatrix} Z_1 \\ Z_2 \end{bmatrix} = \begin{bmatrix} -F_1 \\ F_2 \end{bmatrix} \quad (4.6)$$

Rearranging equation (4.6):

$$\begin{bmatrix} [M_1 s^2 + cs + (k_1 + k_2)] & -cs - k_2 \\ -cs - k_2 & [M_2 s^2 + cs + (k_2 + k_3)] \end{bmatrix} \begin{bmatrix} Z_1 \\ Z_2 \end{bmatrix} = \begin{bmatrix} -F_1 \\ F_2 \end{bmatrix} \quad (4.7)$$

##### 4.2.1 Denominator

Denominator or ‘Den’ is the characteristic equation for the transfer functions. The determinant of the left side of equation (4.7),

$$\begin{aligned} \text{Den} &= [M_1 s^2 + cs + (k_1 + k_2)][M_2 s^2 + cs + (k_2 + k_3)] - (cs - k_2)^2 \\ &= (M_1 M_2) s^4 + (M_1 c + M_2 c) s^3 + [M_1(k_2 + k_3) + M_2(k_1 + k_2)] s^2 \\ &\quad + [c(k_2 + k_3) + c(k_1 + k_2) - 2ck_2] s + [(k_1 + k_2)(k_2 - k_3) - k_2^2] \end{aligned} \quad (4.8)$$

All the transfer functions will have the same denominator. Since there are two inputs and two outputs, there will be four SISO functions. These four transfer functions assumed to be *four different SISO*, which means that only single force is applying to the system at a time.  $F_1$  and  $F_2$  will only be taking the displacement of a single degree of freedom  $z_1$  or  $z_2$ . This leads to four distinct transfer functions,

$$Z_1/F_1 = [M_1s^2 + c_1s + (k_1 + k_2)]/\text{Den} \quad (4.9a)$$

$$Z_1/F_2 = -cs - k_2/\text{Den} \quad (4.9b)$$

$$Z_2/F_1 = -cs - k_2/\text{Den} \quad (4.9c)$$

$$Z_2/F_2 = [M_2s^2 - c_4s + (k_2+k_3)]/\text{Den} \quad (4.9d)$$

Notations:

$Z_1/F_1 (z_{11})$  = displacement of LM due to impact force generated from ‘forcer’.

$Z_1/F_2 (z_{12})$  = displacement of LM due to impact force generated from PRA.

$Z_2/F_1 (z_{21})$  = displacement of LG due to impact force generated from ‘forcer’.

$Z_2/F_2 (z_{22})$  = displacement of LG due to impact force generated from PRA.

**Note: for pole-zero plots and all Bode plots (transfer function, state-space, modal state-space), the focus is on the function  $z_{22}$  which represents the responds of LG.**

#### ***4.2.2 Poles and Zeros***

‘Poles’ are roots for denominator (equation (4.8)), while ‘zeros’ are roots for the numerator (equation (4.9)). If there is no damping, all ‘poles’ should be complex and lied on the imaginary axis. These complex ‘poles’ are known as ‘imaginary poles’ (IP). If there are ‘poles’ on the right hand side of the complex plane, it is known as ‘real poles’ (RHP). The ‘poles’ are the same for all transfer functions while ‘zeros’ are depend on the transfer functions [24, 49, 50].

### 4.2.3 Pole-zero Plots

The pole-zero plots are plotted before and after the application of AVC for all driven forces. The 'poles' are plotted as *asterisks* and 'zeros' as *circles*. Pole-zero plots for 3BM and 3BC are identical because the available forces are not considered using transfer function.

#### 4.2.3.1 Pole-zero plots: 3BM and 3BC

The pole-zero plots of 3BM and 3BC is shown in Figure 4.3. IP are presence because no damping is applied before the application of AVC. The 'poles' and 'zeros' are at the left hand side of the complex plane after the application of AVC. The system is stable since transfer function does not consider the magnitude and direction of available forces.

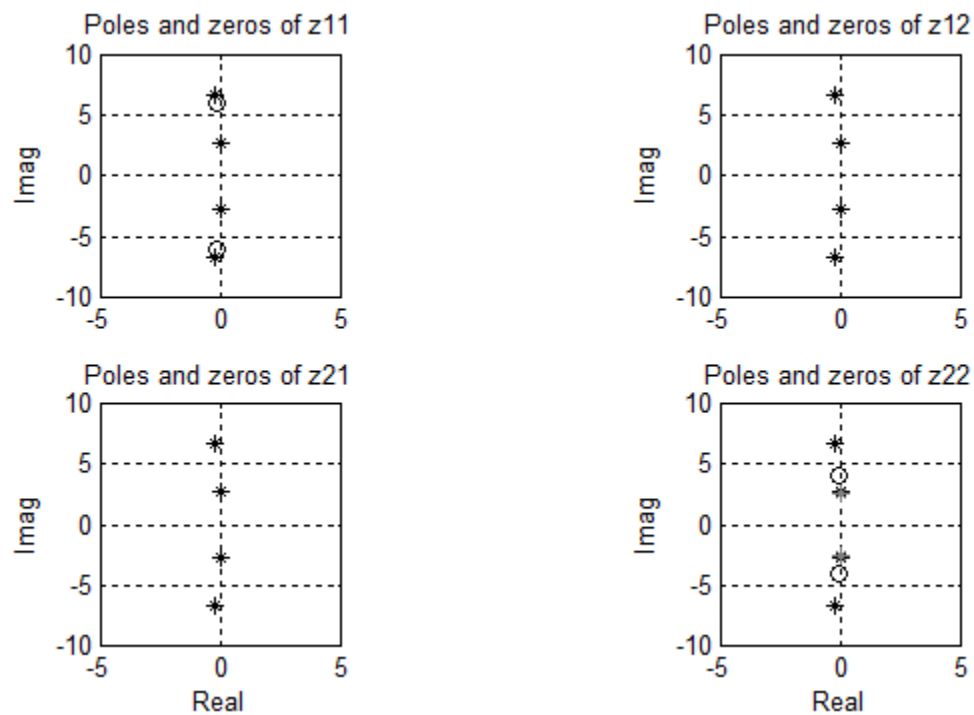


Figure 4.3: Pole-zero plots of 3BM and 3BC (Before AVC, After AVC)

(Note: the 'zeros' for  $z_{12}$  and  $z_{21}$  are not showing for consistency in axis scale, the 'zeros' are far to the left hand side of the complex plane)

#### 4.2.3.2 Pole-zero plots: 5BM

Figure 4.4 below shows the pole-zero plots for 5BM before and after the application of AVC. The results are the same as cases of 3BM and 3BC.

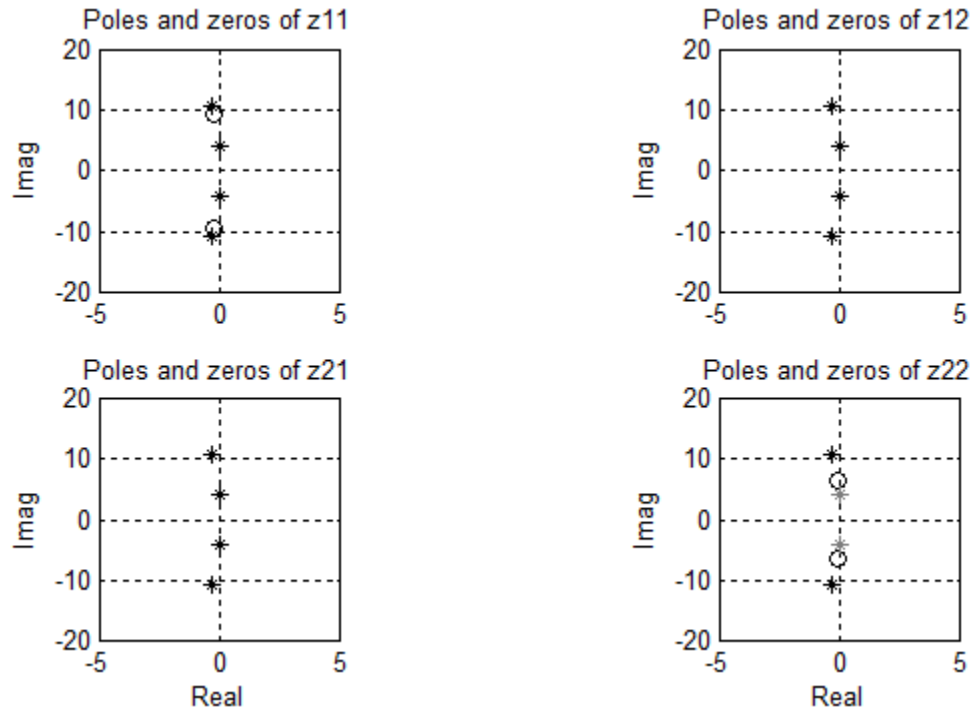


Figure 4.4: Pole-zero plots of 5BM (Before AVC, After AVC)

#### 4.2.4 Root Locus Plots

Root locus plot are obtained using equation (4.9d) under a range of damping rates,  $c$ . Figure 4.5 represents the root locus for LG with damping rate is increased with the application of AVC. The Figure shows IP stay at the imaginary axis. The remain 'poles' are pulled to the left hand side of the complex plane due to the presence of 'zeros'.

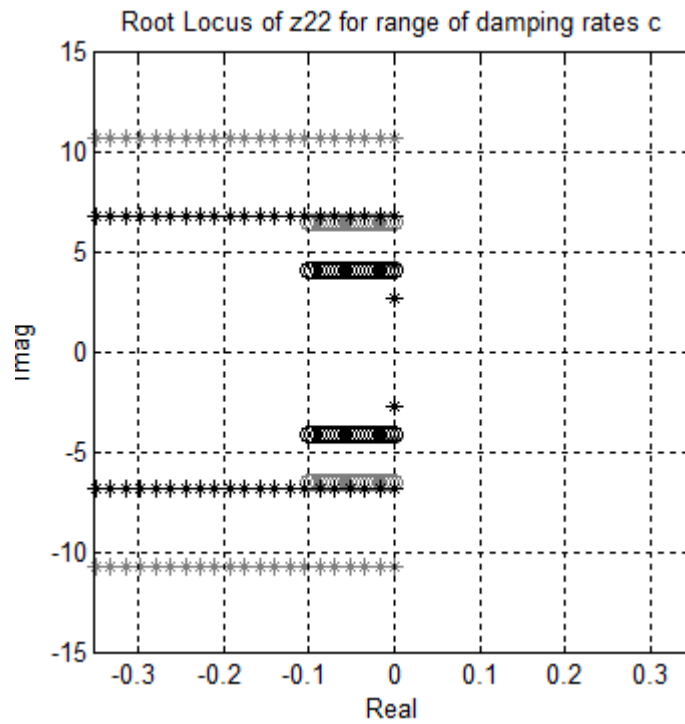


Figure 4.5: Root locus for LG after the application of AVC (\*-3BC & 3BM, \*-5BM)

#### 4.2.5 Frequency Response – Transfer Function Approach

The frequency responses are plotted based on equations (4.8) and (4.9) for all driven forces before and after the application of AVC. The plots for 3BC and 3BM are overlapping.

##### 4.2.5.1 Before the application of AVC

Before the application of AVC, only LG is presence in the system as shown in Figure 4.6. The phase of LG shifted permanently from 0 deg to 180 deg for all driven forces. (Note: 3BM & 3BC: \_\_\_\_, 5BM: ---)

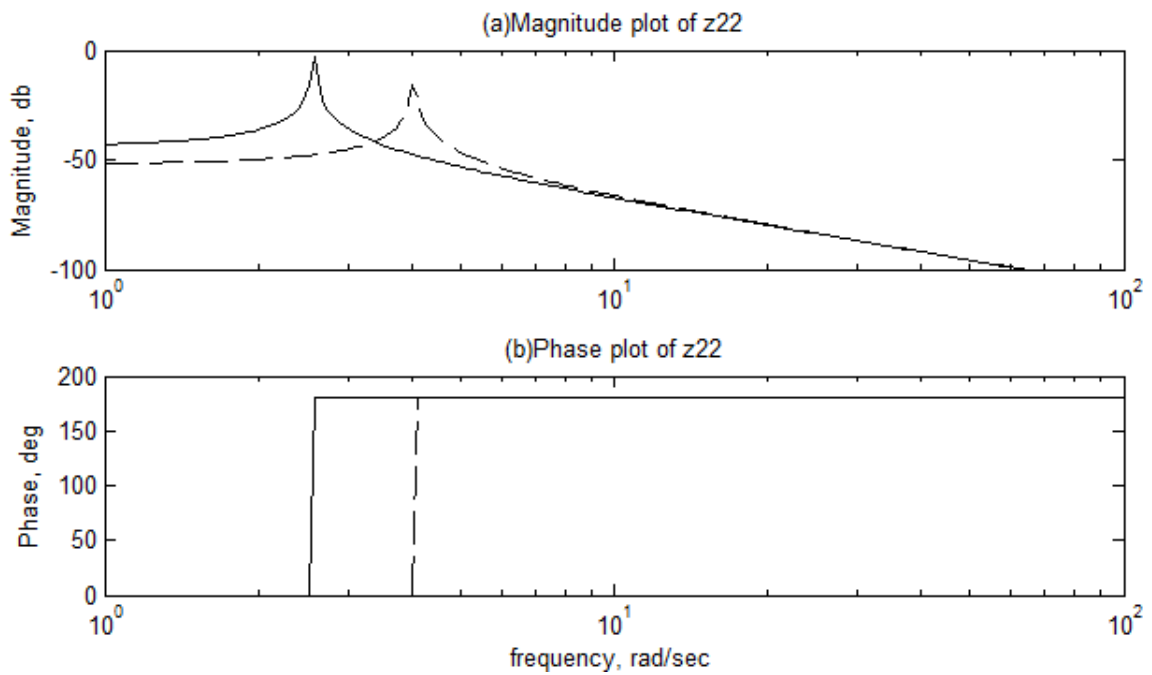


Figure 4.6: Bode plot before the application of AVC

#### 4.2.5.2 After the application of AVC

Figures 4.7 and 4.8 are the Bode plots for all driven forces after the application of AVC.

(Note: 3BM & 3BC: \_\_\_\_, 5BM: ---)

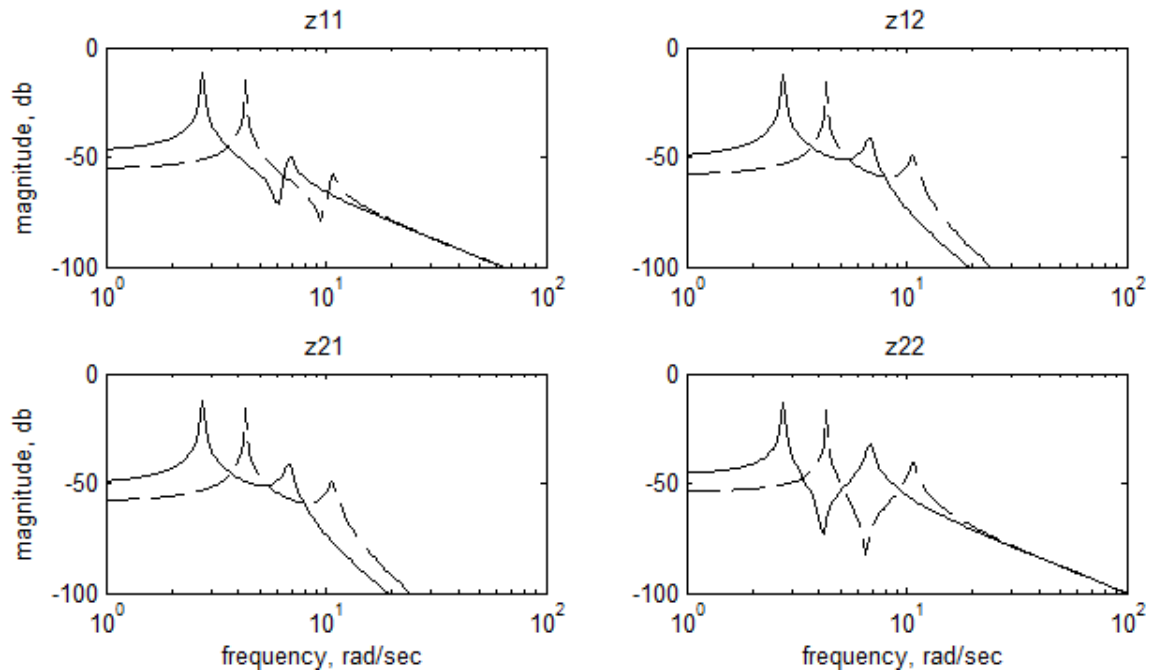


Figure 4.7: Magnitude plots after the application of AVC – transfer function

Magnitude plots of function  $z_{22}$  in Figure 4.7 shows two peaks, the first represent LM while the second peak is the LG. A peak head downward is the sign of presence of damping. All the peaks are having a negative magnitude. Phase plot for function  $z_{22}$  in Figure 4.8 shows initially the phase shifted from 0 deg to 180 deg due to the presence of LM. Then the phase remains consistent except during resonance. However, the phase crosses a range of frequencies to become constants. This show LG has stability limitation after the application of AVC. Besides, the phases for  $z_{12}$  and  $z_{21}$  should be opposing to meet the objective of present study.

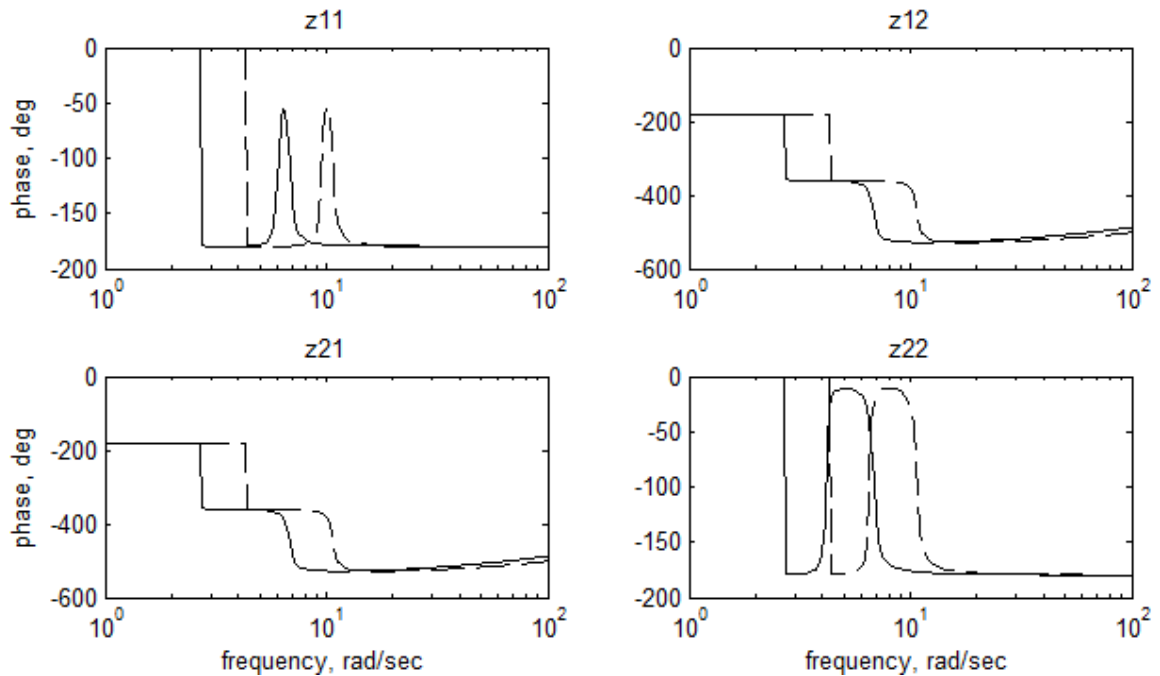


Figure 4.8: Magnitude plots after the application of AVC – transfer function

Magnitude plots in Figures 4.6 and 4.7 shows the resonant frequency is delayed with the application of AVC. The applications of LM will actually swift the location of resonance for LG to a higher range of frequency, because the switching from single-degree to two-degrees of freedom. Resonance happens because unsymmetrical weight distribution occurs during the operation of LG.



### 4.3 State-space Modeling Approach

#### 4.3.1 State-space equation

Rearranging equations (4.3) and (4.4) for the highest derivatives:

$$\ddot{z}_1 = (-F_1 - c\dot{z}_1 + c\dot{z}_2 - (k_1 + k_2)z_1 + k_2z_2)/M_1 \quad (4.10a)$$

$$\ddot{z}_2 = (F_2 + c\dot{z}_1 - c\dot{z}_2 + k_2z_1 - (k_2 + k_3)z_2)/M_2 \quad (4.10b)$$

Changing the notation, using 'x' to define the four states; two positions and two velocities:

$$x_1 = z_1 \quad \text{Position of LM} \quad (4.11a)$$

$$x_2 = \dot{z}_1 \quad \text{Velocity of LM} \quad (4.11b)$$

$$x_3 = z_2 \quad \text{Position of LG} \quad (4.11c)$$

$$x_4 = \dot{z}_2 \quad \text{Velocity of LG} \quad (4.11d)$$

The state equations:

$$\dot{x}_1 = x_2 \quad (4.12a)$$

$$\dot{x}_2 = (-F_1 - cx_2 + cx_4 - (k_1 + k_2)x_1 + k_2x_3)/M_1 \quad (4.12b)$$

$$\dot{x}_3 = x_4 \quad (4.12c)$$

$$\dot{x}_4 = (F_2 + cx_2 - cx_4 + k_2x_1 - (k_2 + k_3)x_3)/M_2 \quad (4.12d)$$

Rewriting the state equations (4.12) in matrix:

$$\begin{bmatrix} \dot{x}_1 \\ \dot{x}_2 \\ \dot{x}_3 \\ \dot{x}_4 \end{bmatrix} = \begin{bmatrix} 0 & 1 & 0 & 0 \\ -\frac{(k_1+k_2)}{M_1} & -\frac{c}{M_1} & \frac{k_2}{M_1} & \frac{c}{M_1} \\ 0 & 0 & 0 & 1 \\ \frac{k_2}{M_2} & \frac{c}{M_2} & -\frac{(k_2+k_3)}{M_2} & -\frac{c}{M_2} \end{bmatrix} \begin{bmatrix} x_1 \\ x_2 \\ x_3 \\ x_4 \end{bmatrix} + \begin{bmatrix} 0 & 0 \\ -\frac{F_1}{M_1} & 0 \\ 0 & 0 \\ 0 & \frac{F_2}{M_2} \end{bmatrix} \quad (4.13)$$

The output equations:

$$y_1 = x_1 \quad (4.14a)$$

$$y_2 = x_3 \quad (4.14b)$$

Output equations (4.13) in matrix form:

$$\begin{bmatrix} y_1 \\ y_2 \end{bmatrix} = \begin{bmatrix} 1 & 0 & 0 & 0 \\ 0 & 0 & 1 & 0 \end{bmatrix} \begin{bmatrix} x_1 \\ x_2 \\ x_3 \\ x_4 \end{bmatrix} + \begin{bmatrix} 0 \\ 0 \end{bmatrix} u \quad (4.15)$$

Notations for state equation are:

$$\dot{\mathbf{x}} = \mathbf{A}\mathbf{x} + \mathbf{B}u \quad (4.16)$$

Where,

$$\text{State matrix, } \mathbf{A} = \begin{bmatrix} 0 & 1 & 0 & 0 \\ -\frac{(k_1+k_2)}{M_1} & -\frac{c}{M_1} & \frac{k_2}{M_1} & \frac{c}{M_1} \\ 0 & 0 & 0 & 1 \\ \frac{k_2}{M_2} & \frac{c}{M_2} & -\frac{(k_2+k_3)}{M_2} & -\frac{c}{M_2} \end{bmatrix} \quad (4.16a)$$

$$\text{Input matrix, } \mathbf{B} = \begin{bmatrix} 0 & 0 \\ -\frac{F_1}{M_1} & 0 \\ 0 & 0 \\ 0 & \frac{F_2}{M_2} \end{bmatrix} \quad (4.16b)$$

Notation for the output matrix:

$$\mathbf{y} = \mathbf{C}\mathbf{x} + \mathbf{D}u \quad (4.17)$$

Where,

$$\text{Output matrix, } \mathbf{C} = \begin{bmatrix} 1 & 0 & 0 & 0 \\ 0 & 0 & 1 & 0 \end{bmatrix} \quad (4.17a)$$

$$\text{Direct transmission matrix, } \mathbf{D} = \begin{bmatrix} 0 \\ 0 \end{bmatrix} \quad (4.17b)$$

The matrix  $\mathbf{D}$  is 'zero' because there is no couple relation between the input and the output.

### 4.3.2 Complex Eigenvalue and Eigenvector – State-space form

If there are no limitations on the presence of the damping terms defined during the simulation, this could result in complex eigenvalues and eigenvectors. The ‘complex’ eigenvalue and eigenvectors lead to establishment of non-proportional damped time response [32, 53, 54]. Setting the forcing function to zero and write the homogeneous state equations of motion (4.16) into

$$\dot{\mathbf{x}} = \mathbf{A}\mathbf{x} \quad (4.18)$$

Motion in principal mode defined as:

$$\mathbf{x}_i = \mathbf{x}_{mi}e^{\lambda_i t} \quad (4.19)$$

Where,

$\lambda_i$  =  $i^{\text{th}}$  eigenvalue, the natural frequency of the  $i^{\text{th}}$  mode of vibration,

$\mathbf{x}_i$  = vector of states at the  $i^{\text{th}}$  frequency,

$\mathbf{x}_{mi}$  =  $i^{\text{th}}$  eigenvector, the mode shape for the  $i^{\text{th}}$  mode.

Substituting equation (4.19) into the homogeneous state equation (4.18) and canceling the exponential terms leads to:

$$\dot{\mathbf{x}} = \mathbf{A}\mathbf{x} \quad (4.20a)$$

$$\lambda \mathbf{x}_{mi} e^{\lambda t} = \mathbf{A} \mathbf{x}_{mi} e^{\lambda t} \quad (4.20b)$$

$$\lambda \mathbf{x}_{mi} = \mathbf{A} \mathbf{x}_{mi} \quad (4.20c)$$

$$(\lambda \mathbf{I} - \mathbf{A}) \mathbf{x}_{mi} = 0 \quad (4.20d)$$

Equation (4.20d) is the classic “eigenvalue problem”. If  $\mathbf{x}_{mi}$  is not equal to zero, a solution exists only if the determinant below is zero:

$$|(\lambda \mathbf{I} - \mathbf{A})| = 0 \quad (4.21)$$

Taking the system matrix  $\mathbf{A}$  from (4.16a) and inserting in (4.21):

$$(\lambda \mathbf{I} - \mathbf{A}) = \lambda \mathbf{I} - \begin{bmatrix} 0 & 1 & 0 & 0 \\ -\frac{(k_1+k_2)}{M_1} & -\frac{c}{M_1} & \frac{k_2}{M_1} & \frac{c}{M_1} \\ 0 & 0 & 0 & 1 \\ \frac{k_2}{M_2} & \frac{c}{M_2} & -\frac{(k_2+k_3)}{M_2} & -\frac{c}{M_2} \end{bmatrix} \quad (4.22)$$

Equation (4.22) provides the solution for eigenvalues. Since the form of the eigenvalues is not specified, in most general case can be complex. The real and imaginary parts will be defined using  $\sigma_{nx}$  and  $\omega_{nx}$ , respectively:

$$\lambda_{n1} = \sigma_{n1} + j\omega_{n1} \quad (4.23)$$

### 4.3.3 Complex Eigenvalue combining to give real motion

To describe “real” and physical observable motions with complex eigenvalues and eigenvectors is by summing the conjugate eigenvalue/eigenvector for that mode.

$$\begin{aligned} \mathbf{x}(t) &= e^{\lambda_{n1}t} \mathbf{x}_{n1} + e^{\lambda_{n2}t} \mathbf{x}_{n2} \\ &= e^{\lambda_{n1}t} \mathbf{x}_{n1} + e^{\lambda_{n1}^*t} \mathbf{x}_{n1}^* \\ &= e^{(\sigma_{n1}+j\omega_{n1})t} \mathbf{x}_{n1} + e^{(\sigma_{n1}-j\omega_{n1})t} \mathbf{x}_{n1}^* \\ &= e^{\sigma_{n1}t} (e^{j\omega_{n1}t} \mathbf{x}_{n1} + e^{-j\omega_{n1}t} \mathbf{x}_{n1}^*) \\ &= 2e^{\sigma_{n1}t} \text{Re}(\mathbf{x}_{n1}) \end{aligned} \quad (4.24)$$

The  $e^{j\omega_{n1}t} \mathbf{x}_{n1}$  term represents a vector of magnitude  $|\mathbf{x}_{n1}|$  which is *rotating counter-clockwise* at the rate of  $\omega_{n1}$  radians/sec. The  $e^{-j\omega_{n1}t} \mathbf{x}_{n1}^*$  term represents a vector of magnitude  $|\mathbf{x}_{n1}^*|$  which is *rotating clockwise* at the rate of  $\omega_{n1}$  radians/sec. This counter-rotation will indicate the ‘real’ motion for the mode. Since the two counter-rotating eigenvector terms are complex conjugates, their imaginary portions are of opposite sign and as they rotate, the sum of the two results in only a real component as the two imaginary portions cancel each other.

#### 4.3.4 Non-proportional damped time response

The non-proportional damped time responses are plot using concepts as explained in section 4.3.3. The non-proportional damped time responses are obtained after the application of AVC of all three driven forces. The sequences of development of non-proportional damped time response using MATLAB are

- 1) Solve original damped system equation for complex eigenvalues and eigenvectors
- 2) Normalize the eigenvector entries to unity
- 3) Calculate the motions of the two masses (LM and LG)
- 4) Plot the real and imaginary displacements of the system after application of AVC.

Figure 4.9 shows the non-proportional damped time responses for 3BM and 3BC after the application of AVC. The Figures show the interactions between the LM and LG with the overall amplitude of the responds are reducing.

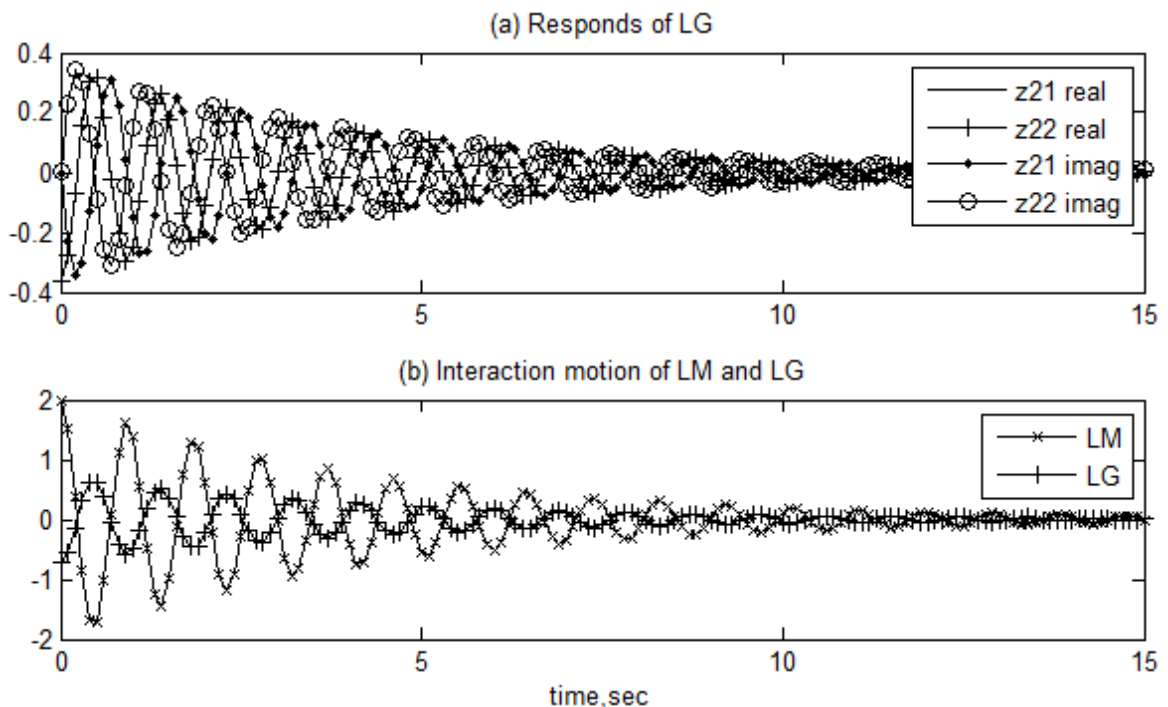


Figure 4.9: Non-prop damped time response for 3BM and 3BC

Figure 4.9(a) shows the complex components out-phasing each other and the amplitude for both masses are decreasing. The amplitude of LM is higher compare to LG is because LM has less weight than LG as shown in Figure 4.9(b). Figure 4.10 below is the non-proportional damped time response for 5BM which shows the same results are obtained.

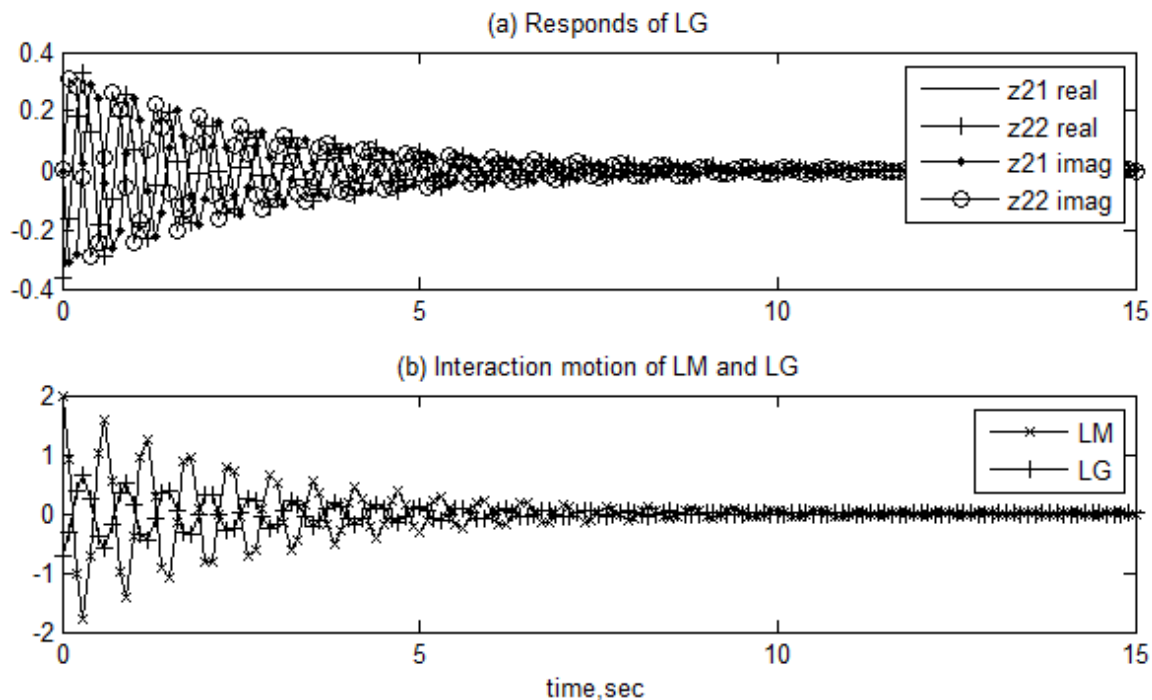


Figure 4.10: Non-prop damped time response for 5BM

### 4.3.5 Frequency Response – State-space modeling approach

The frequency responses for all driven forces after the application of AVC are plotted using equations (4.14) and (4.15). The frequency responses before the application of AVC is not showing because are the same results as obtained by transfer functions approach. (Note: 3BM: ..., 5BM: ---, 3BC \_\_\_\_)

The Bode plots for three driven forces are shown in Figures 4.11 and 4.12. Figure 4.12 shows the phases of 3BM and 3BC are overlapping.

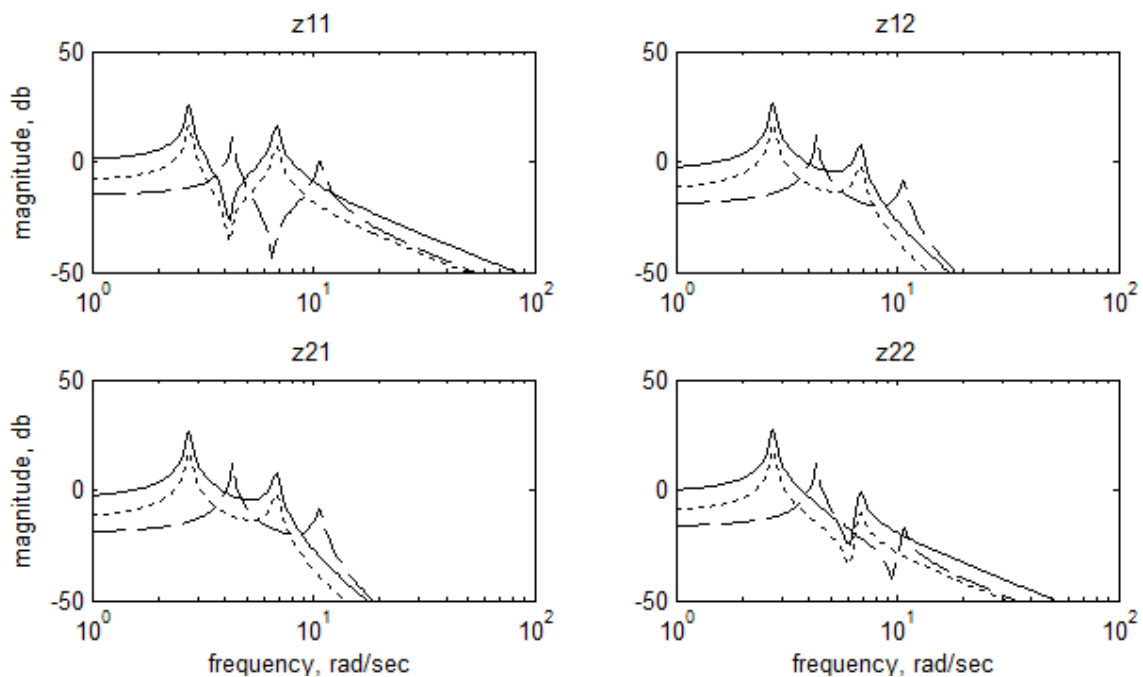


Figure 4.11: Magnitude plots after application of AVC – state-space approach

Magnitude plot of function  $z_{22}$  show two peaks which are the LM and LG. All peaks of LG are negative for all driven forces. However, the LM has a positive magnitude. The reason is the output responses of LM must be amplified (positive gain) to counter the high impact forces from LG. ( $m_{forcer} < m_{PRA}$ )

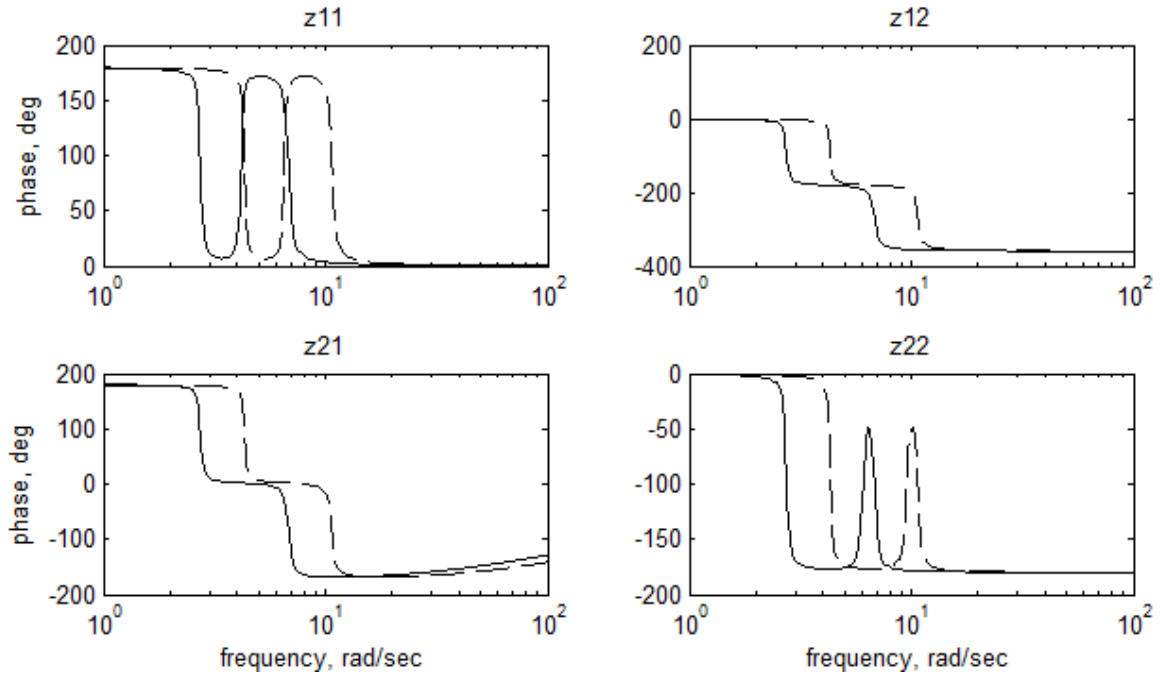


Figure 4.12: Phase plots after the application of AVC – state-space approach

Initially the phase shifted from 0 deg to -180 deg, and then the phase remains constant. The phase shifted back right after the resonance without delay. This provides the LG better stability after the application of AVC. In addition to that, phases for  $z_{12}$  and  $z_{21}$  are in different phases due to the consideration of available forces.



## 4.4 Modal State-space Approach

### 4.4.1 Eigenvalues

Taking the matrix Laplace transform of the homogeneous state equation (4.18) and solving for  $\mathbf{x}(s)$ :

$$s\mathbf{I}\mathbf{x}(s) = \mathbf{A}\mathbf{x}(s) \quad (4.25a)$$

$$(s\mathbf{I} - \mathbf{A})\mathbf{x}(s) = 0 \quad (4.25b)$$

To obtain the characteristic equation, the term  $(s\mathbf{I} - \mathbf{A})$  has to equal zero,

$$|(s\mathbf{I} - \mathbf{A})| = 0 \quad (4.26)$$

Inserting state matrix  $\mathbf{A}$  from equation (4.16a) into the term  $(s\mathbf{I} - \mathbf{A})$

$$(s\mathbf{I} - \mathbf{A}) = s\mathbf{I} - \begin{bmatrix} 0 & 1 & 0 & 0 \\ -\frac{(k_1+k_2)}{M_1} & -\frac{c}{M_1} & \frac{k_2}{M_1} & \frac{c}{M_1} \\ 0 & 0 & 0 & 1 \\ \frac{k_2}{M_2} & \frac{c}{M_2} & -\frac{(k_2+k_3)}{M_2} & -\frac{c}{M_2} \end{bmatrix} \quad (4.27)$$

### 4.4.2 Eigenvectors

Typically, a normal mode is defined

$$\mathbf{x}_i = \mathbf{x}_{mi} \sin(\omega_i t + \phi_i) = \mathbf{x}_{mi} \text{Im}(e^{j\omega_i t + \phi_i}) \quad (4.28)$$

Where,

- $\mathbf{x}_i$  = vector of displacements for all dof's at the  $i^{\text{th}}$  frequency
- $\mathbf{x}_{mi}$  = the  $i^{\text{th}}$  eigenvector, the mode shape for the  $i^{\text{th}}$  resonant frequency
- $\omega_i$  = the  $i^{\text{th}}$  eigenvalue,  $i^{\text{th}}$  resonant frequency
- $\phi_i$  = an arbitrary initial phase angle

For a two degree of freedoms ( $z_1$  and  $z_2$ ), four state ( $x_1$  to  $x_4$ ) system, equation (4.28) becomes,

$$\begin{bmatrix} z_{1i} \\ \dot{z}_{1i} \\ z_{2i} \\ \dot{z}_{2i} \end{bmatrix} = \begin{bmatrix} x_{1i} \\ x_{2i} \\ x_{3i} \\ x_{4i} \end{bmatrix} = x_{mi} \sin(\omega_i t + \phi_i) = \begin{bmatrix} x_{m1i} \\ x_{m2i} \\ x_{m3i} \\ x_{m4i} \end{bmatrix} \sin(\omega_i t + \phi_i) \quad (4.29)$$

Typically, states  $x_1$  and  $x_3$  are the position entries, while  $x_2$  and  $x_4$  are the velocity entries (as equation (4.11)). The position entries are ‘real’ numbers while the velocity entries are “complex” numbers. Since only real numbers will show the motion in time response, the mode will be in “real” mode. A real mode time response is a *proportional damped time response* [30, 31, 35].

#### 4.4.3 Normalizing Eigenvectors

The eigenvectors are normalized with respect to mass. Multiply the original mass and stiffness matrices by the normalized eigenvectors to check the results diagonalization. Since only the displacement entries of the 4x4 modal matrix needed to transform the 2x2 mass and stiffness matrix, the  $x_m$  matrix is only displacement entries. For mass matrix; diagonalized by pre- and post- multiplying by the normalized eigenvector matrix, which yields the identity matrix:

$$\mathbf{x}_n^T \mathbf{m} \mathbf{x}_n = \mathbf{I} \quad (4.30)$$

The stiffness matrix also diagonalized by pre- and post- multiplying by the normalized eigenvector matrix, which yield the stiffness matrix in principal:

$$\mathbf{x}_n^T \mathbf{k} \mathbf{x}_n = \mathbf{k}_p \quad (4.31)$$

#### 4.4.4 Writing Homogeneous EOM

The sequence to write a homogeneous EOM:

- 1) Use the eigenvalues to write the homogeneous equations of motion in the principal coordinate system by inspection.
- 2) Use the normalized eigenvectors to transform the forcing function and initial conditions to principal coordinates, yielding the complete solution for transient or frequency domain problems in principal coordinates.
- 3) Then, back transform the physical coordinate system to get the desired results in physical coordinates. Through the modal formulation, the contributions of various modes to the total response can be defined.

#### 4.4.5 EOM – Physical Coordinates

Equation of motion in physical coordinates with forces, and zero initial conditions with consideration on damping effect (IC:  $\dot{z}_1, \ddot{z}_1, \dot{z}_2, \ddot{z}_2 = 0$ ):

$$\begin{aligned} m\ddot{z}_1 + 4kz_1 - 3kz_2 &= -F_1 \\ m\ddot{z}_2 - 3kz_1 + kz_2 &= F_2 \end{aligned} \quad (4.40)$$

Knowing the eigenvalues and eigenvectors normalized with respect to mass, the damped homogeneous equations of motion in principal coordinates can write by inspection. The forces in principal coordinates,  $F_{p1}$  and  $F_{p2}$  are obtained by pre-multiplying the force vector in physical coordinates by transpose of the normalized eigenvector:

$$\mathbf{F}_p = \mathbf{x}_n^T \mathbf{F} \quad (4.41)$$

$\mathbf{x}_n$  was defined in equation (4.39) as a 2x2 matrix of normalized displacement eigenvectors. The multiplication then results in a 2x1 vector of forces in principal

coordinates. The resulting elements are entered in the appropriate positions in the equations in principal coordinates below.

#### 4.4.6 EOM – Principal Coordinates

The two equations of motion in principal coordinates become:

$$\ddot{x}_{p1} = -F_{p1} \quad (4.42a)$$

$$\ddot{x}_{p2} = F_{p2} - 2\zeta_2\omega_2\dot{x}_{p2} - \omega_2^2x_{p2} \quad (4.42b)$$

Where,  $\omega$  = eigenvalue, with units of radians/sec and  $\zeta$  = represent the percentages of critical damping (assumed 2% or 0.02). Defining states:

$$x_1 = x_{p1} \quad \text{displacement of mode 1}$$

$$x_2 = \dot{x}_{p1} \quad \text{derivative of displacement of mode 1}$$

$$x_3 = x_{p2} \quad \text{displacement of mode 2}$$

$$x_4 = \dot{x}_{p2} \quad \text{derivative of displacement of mode 2}$$

Rewriting the equations of motion using the states:

$$\dot{x}_1 = x_2 \quad (4.43a)$$

$$\dot{x}_2 = -F_{p1} \quad (4.43b)$$

$$\dot{x}_3 = x_4 \quad (4.43c)$$

$$\dot{x}_4 = F_{p2} - \omega_2^2x_3 - 2\zeta_2\omega_2x_4 \quad (4.43d)$$

Rewriting in matrix form: (completed state space equation)

$$\begin{bmatrix} \dot{x}_1 \\ \dot{x}_2 \\ \dot{x}_3 \\ \dot{x}_4 \end{bmatrix} = \begin{bmatrix} 0 & 1 & 0 & 0 \\ 0 & 0 & 0 & 0 \\ 0 & 0 & 0 & 1 \\ 0 & 0 & -\omega_2^2 & -2\zeta_2\omega_2 \end{bmatrix} \begin{bmatrix} x_1 \\ x_2 \\ x_3 \\ x_4 \end{bmatrix} + \begin{bmatrix} 0 \\ -F_{p1} \\ 0 \\ F_{p2} \end{bmatrix} u \quad (4.44)$$

The output matrix equation then becomes, where  $\mathbf{y}_p$  is the displacement in principal coordinates:

$$\mathbf{y}_p = \mathbf{C}\mathbf{x} = \begin{bmatrix} 1 & 0 & 0 & 0 \\ 0 & 1 & 0 & 0 \\ 0 & 0 & 1 & 0 \\ 0 & 0 & 0 & 1 \end{bmatrix} \begin{bmatrix} x_1 \\ x_2 \\ x_3 \\ x_4 \end{bmatrix} = \begin{bmatrix} x_1 \\ x_2 \\ x_3 \\ x_4 \end{bmatrix} \quad (4.45)$$

For the case before the application of AVC, modal state-space approach derived at *Appendix A* eliminated the presence of damping ratio with zero natural frequency. Hence, the case of before application of AVC cannot be applied using modal state-space approach.

#### ***4.4.7 Proportional damped time response***

Proportional damped time responses applied when the system is treated with un-damped initially and involved in transformation from physical coordinates to principal coordinates. Proportional damped time responses are plot after the application of AVC with all three driven forces. The methodology to plot proportional damped time response using MATLAB:

- 1) Solve the un-damped system equation for eigenvalues and eigenvectors.
- 2) Normalize the displacement eigenvectors entries with respect to mass, converting from physical coordinated to principal coordinates.
- 3) Form the completed state space form system matrix with proportional damping.
- 4) Solve the system matrix for eigenvalues and eigenvector with critical damping value of 2%.
- 5) Back transform to physical coordinates using the normalized displacement eigenvectors.
- 6) Plot the real and imaginary displacement of the system after the application of AVC

Figures 4.13 and 4.14 are the proportional damped time responses for 3BM, 3BC and 5BM. The responds for 3BC and 3BM are overlapping.

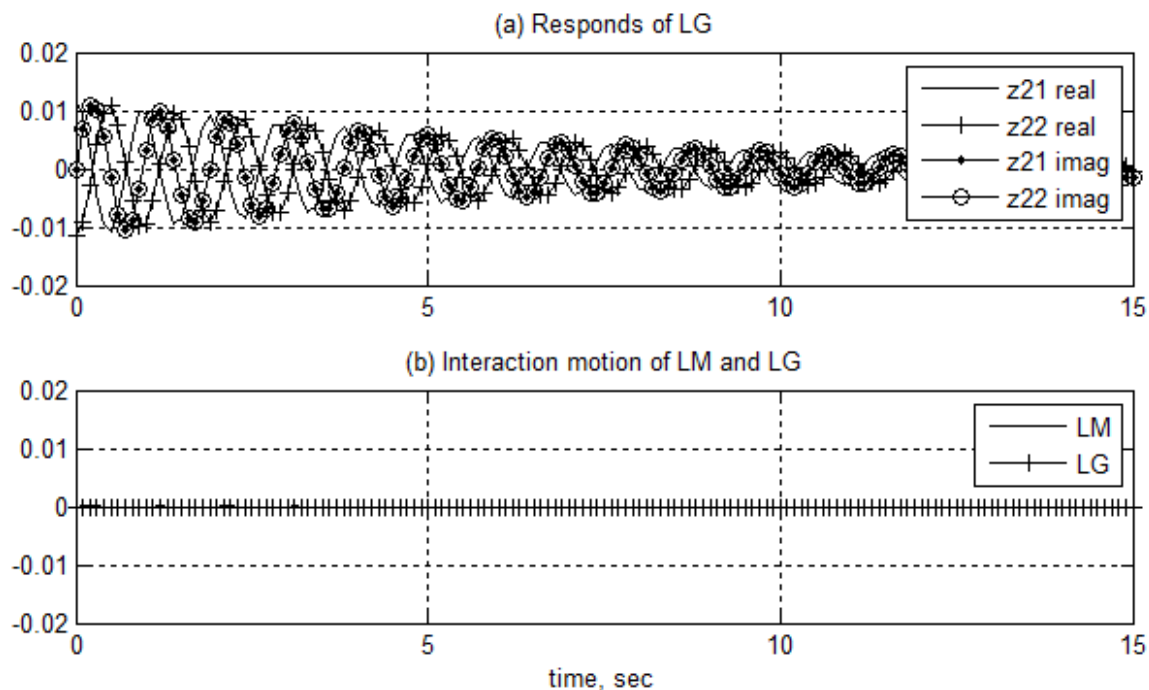


Figure 4.13: Proportional damped time responses for 3BM and 3BC

Figure 4.13(a) shows the imaginary components are overlapping, while the real components are out phasing each other. Accordingly, the real components are showing the displacement of LG. After the imaginary components are removed, the result as shown in Figure 4.13(b) shows no motion. The same results are expected for 5BM:

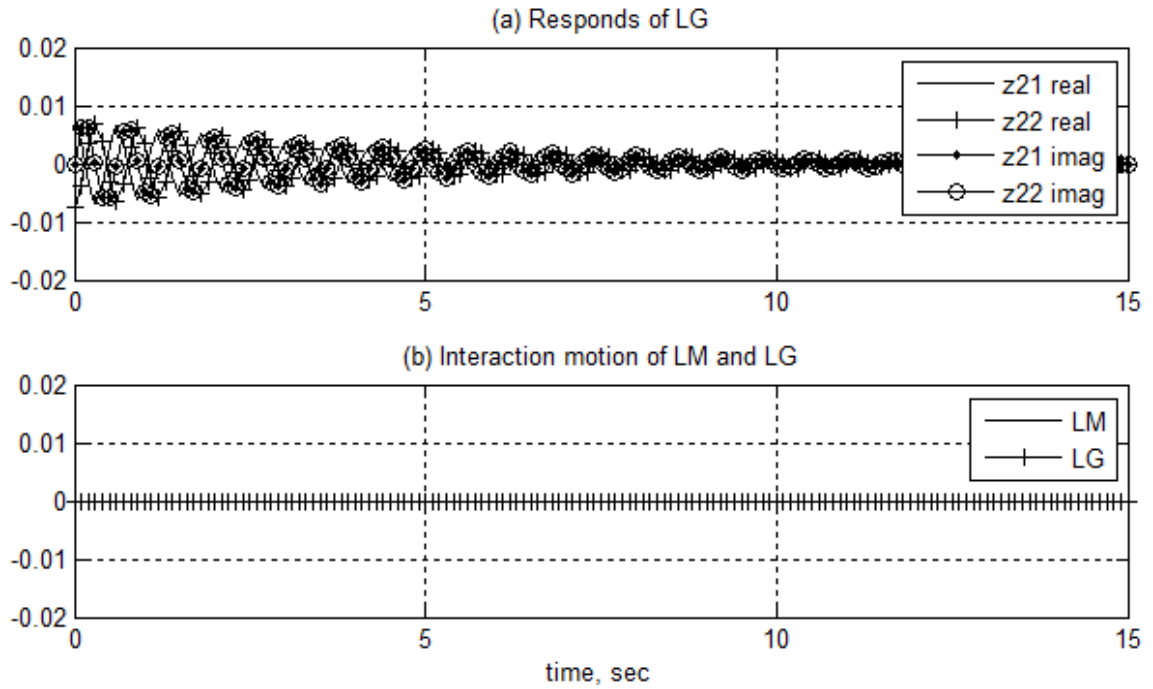


Figure 4.14: Proportional damped time responses for 5BM

The results show that, modal state-space approach creates contradiction to the dynamic modeling which causing unexpected results [31].

#### 4.4.8 Frequency Response – Modal state-space approach

Frequency responses are plotted based on equations (4.44) and (4.45) using all three driven forces after the application of AVC. Bode plots are shown in Figures 4.15 and 4.16. (Note: 3BM: ..., 5BM: ---, 3BC \_\_\_\_\_)

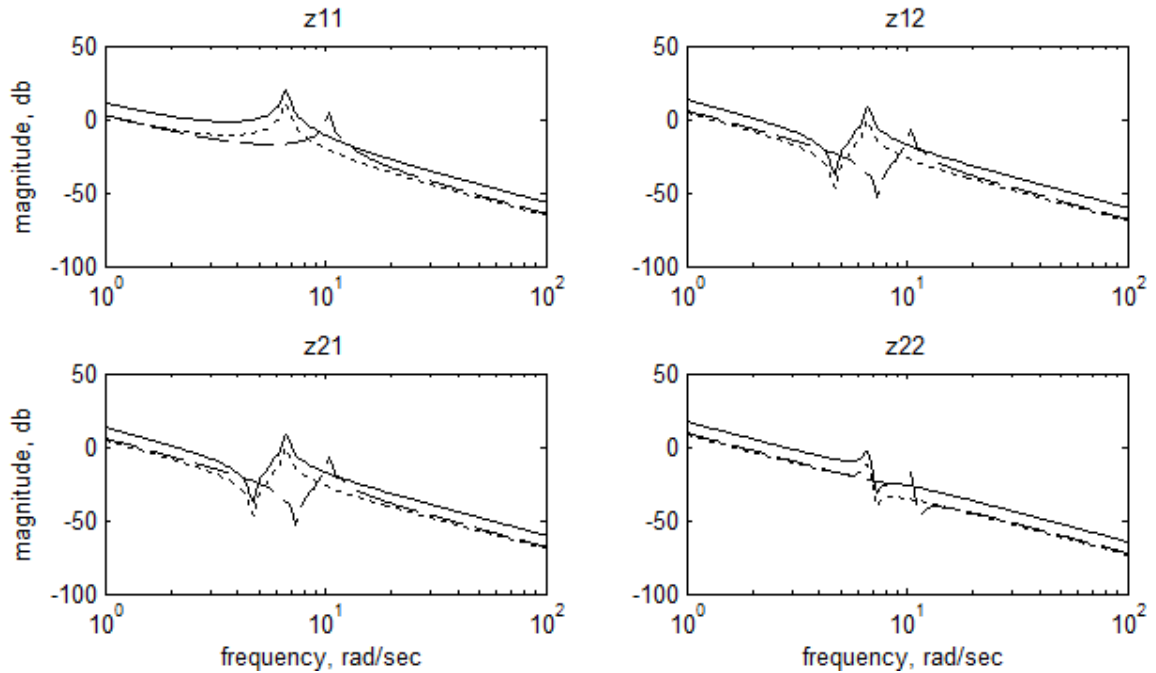


Figure 4.15: Magnitude plots after application of AVC – Modal state-space approach

Function  $z_{22}$  of Figure 4.15 shows all the resonances having negative magnitude, which indicates the LG is in a lower vibration level, together with applied damping effects. The application of AVC almost eliminated the resonances.

In Figure 4.16, the phase of function  $z_{22}$  remains consistent except during the resonance. However, unlike state-space approach, function  $z_{22}$  shows the phase never shifted after the application of AVC. Besides, the interaction phases between LM and LG are constant which is contracted to the present study objective.



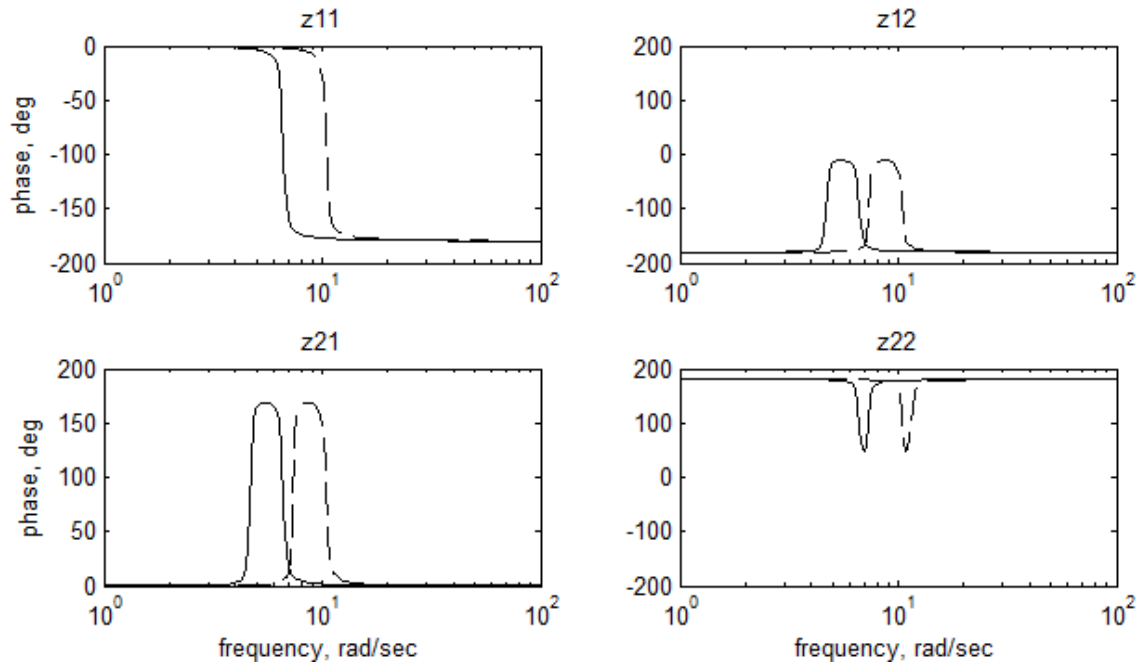


Figure 4.16: Phase plots after the application of AVC – Modal state-space approach

#### 4.5 Results Comparison

The non-proportional damped time responses show the interaction motions of LM and LG. However, proportional damped time responses do not show the interaction motions between LM and LG. Therefore, state-space approach is more suitable to represent the time response.

Consideration for the case without the application of AVC is neglected. Frequency response obtained using transfer function approach is not considered, because the method does not consider the amount and direction of applied force. State-space is more suitable approach because it meets objective of present study without idealization of the model.

## CHAPTER V

### SIMULATION RESULTS VALIDATION

*A lumped-mass quarter car suspension system* is chosen for validation purposes, due to the lack of literature and experimental works related directly to AVC for LG. The quarter car suspension systems are categorized into passive, semi-active, smart and active type (for more details see *Appendix C*). The parameters defined in the literature will be used to obtain similar results using selected approach (state-space approach). The reasons of selection lumped-mass quarter car model are because

- a) Both models can be assumed as LTI system.
- b) Both models are treated as two degree of freedom system.
- c) Both models involved only linear motion.
- d) The forces interactions within the systems are similar.

The focus is on the time response and frequency response of suspension displacement in all the literatures. The selected literatures are:

- 1) Development and control of an automotive smart suspension system [44].
- 2) Active suspension simulation through software interfacing [45].
- 3) Aspect of achievable performance for quarter car active suspensions [46].

## 5.1 Development and control of an automotive smart suspension system

Three different types of suspension system are focused; passive, semi-active and smart for quarter-car, half-car, and full-car model. The objective of the study is to assess the performance of the control laws on different car model, and concluded that smart suspension system offers better performance based on Optimal Control Theory (for more details see *Appendix D*). All the suspension systems' descriptions are adapted from [44].

Table 5.1: Parameters defined in simulation for passive, semi-active and smart quarter car model suspension system, adapted from [44]

$m_s = 240\text{kg}$	$k_s = 16000\text{ N/m}$	$b_s = 1000\text{ Ns/m}$
$m_u = 360\text{kg}$	$k_t = 160000\text{ N/m}$	$b_t = 100\text{ Ns/m}$

### 5.1.1 Passive suspension system

The passive suspension system is shown in Figure 5.1 and is modeled as parallel combination of a linear spring with stiffness  $k_s$  and a linear damper with damping rate  $b_s$ . A linear tire model is used, i.e., a spring of stiffness  $k_t$  and a damper rate  $b_t$ . It is assumed that the tire does not leave the ground and that  $z_s$  and  $z_u$  are measured from the static equilibrium position. The linear equations of motion can be easily derived as follows:

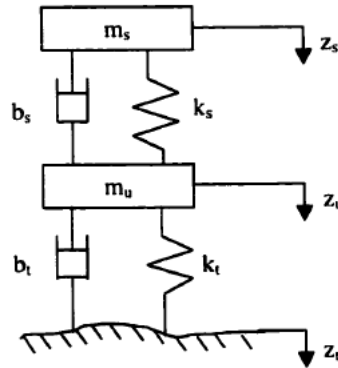


Figure 5.1:  $\frac{1}{4}$  car models with passive suspension system, adapted from [44]

Equations of motion for passive suspension system:

$$m_s \ddot{z}_s + b_s (\dot{z}_s - \dot{z}_u) + k_s (z_s - z_u) = 0 \quad (5.1)$$

$$m_u \ddot{z}_u + b_t (\dot{z}_u - \dot{z}_r) + k_t (z_u - z_r) - b_s (\dot{z}_s - \dot{z}_u) - k_s (z_s - z_u) = 0 \quad (5.2)$$

The state variables are chosen to be:

$$x_1 = z_s - z_u \quad \text{Suspension deflection} \quad (5.3)$$

$$x_2 = \dot{z}_s \quad \text{Absolute velocity of sprung mass} \quad (5.4)$$

$$x_3 = z_u - z_r \quad \text{Tire deflection} \quad (5.5)$$

$$x_4 = \dot{z}_u \quad \text{Absolute velocity of unsprung mass} \quad (5.6)$$

Equations (5.1) and (5.2) can be rewritten in state-space form using definitions (5.3)-(5.6):

$$\dot{\mathbf{x}} = \mathbf{A}_0 \mathbf{x} + \mathbf{L} \dot{z}_r \quad (5.7)$$

Or equivalently,

$$\begin{bmatrix} \dot{x}_1 \\ \dot{x}_2 \\ \dot{x}_3 \\ \dot{x}_4 \end{bmatrix} = \begin{bmatrix} 0 & 1 & 0 & -1 \\ -k_s/m_s & -b_s/m_s & 0 & b_s/m_s \\ 0 & 0 & 0 & 1 \\ k_s/m_u & b_s/m_u & -k_t/m_u & -b_t/m_u - b_s/m_u \end{bmatrix} \begin{bmatrix} x_1 \\ x_2 \\ x_3 \\ x_4 \end{bmatrix} + \begin{bmatrix} 0 \\ 0 \\ 1 \\ b_t/m_u \end{bmatrix} \dot{z}_r$$

### 5.1.2 Semi-active suspension system

A quarter-car model with semi-active suspension is shown in Figure 5.2. The assumptions used for the model development are the same as those used in conjunction with the passive suspension model. In this case:  $k_s$ ,  $k_t$ ,  $b_t$ ,  $b_s$  are constants, and  $v(t)$  is the variable damping coefficient ( $0 < v(t) < v_{max}$ ) and the force provided by the variable damping damper can be expressed as:

$$f_s = -v(x_2 - x_4) \quad (5.8)$$

The state variables are chosen as being the same as those chosen with the passive suspension system. The equations of motion for the semi-active suspension system are in the bi-linear form:

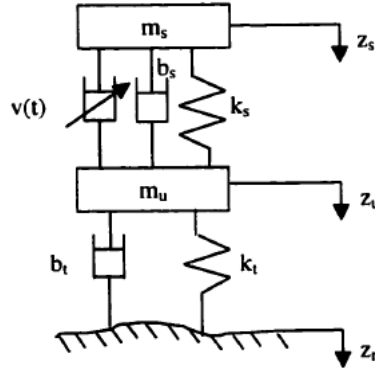


Figure 5.2:  $\frac{1}{4}$  car models with semi-active suspension system, adapted from [44]

$$\dot{\mathbf{x}} = \mathbf{A}_0 \mathbf{x} + \mathbf{B} f_s + \mathbf{L} \dot{z}_r = \mathbf{A}_0 \mathbf{x} + \Phi(\mathbf{x}) v + \mathbf{L} \dot{z}_r \quad (5.9)$$

Where:

$$\mathbf{A}_0 = \begin{bmatrix} 0 & 1 & 0 & -1 \\ -k_s/m_s & -b_s/m_s & 0 & b_s/m_s \\ 0 & 0 & 0 & 1 \\ k_s/m_u & b_s/m_u & -k_t/m_u & -b_t/m_u - b_s/m_u \end{bmatrix} \quad \mathbf{B} = \begin{bmatrix} 0 \\ 1/m_s \\ 0 \\ -1/m_u \end{bmatrix}$$

$$\mathbf{L} = (0 \quad 0 \quad -1 \quad b_t/m_u)^T \quad \Phi(\mathbf{x}) = -\mathbf{B}(x_2 - x_4)$$

$v$  is the variable damping coefficient of the shock absorber and  $\dot{z}_r$  represents the road velocity disturbance.

### 5.1.3 Smart suspension system

A quarter-car model with smart suspension is shown in Figure 5.3. Where:  $k_t$ ,  $b_t$  are constants,  $v_1(t)$  is the variable damping coefficient, ( $0 < v_1(t) < v_{1max}$ ) and  $v_2(t)$  it the variable stiffness ( $0 < v_2(t) < v_{2max}$ ). The forces  $u_1$  and  $u_2$  are provided by the variable damping damper and the variable stiffness spring respectively can be expresses as:

$$u_1 = -v_1(x_2 - x_4) \quad (5.10)$$

$$u_2 = -v_2 x_1 \quad (5.11)$$

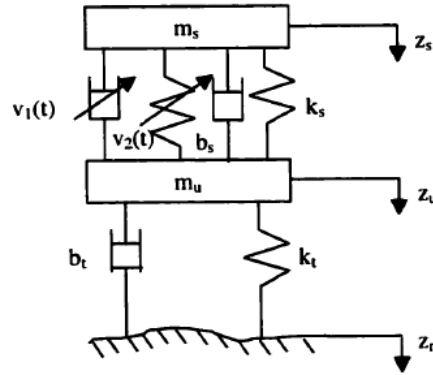


Figure 5.3:  $\frac{1}{4}$  car models with smart suspension system, adapted from [44]

The state variables are chosen as being the same as those selected for the passive suspension system. The dynamic equations of motion for this smart suspension system are written in the following state-space form:

$$\dot{\mathbf{x}} = \mathbf{A}_0 \mathbf{x} + \mathbf{B} \mathbf{f} + \mathbf{L} \dot{z}_r \quad (5.12)$$

Where,

$$\mathbf{A}_0 = \begin{bmatrix} 0 & 1 & 0 & -1 \\ -k_s/m_s & -b_s/m_s & 0 & b_s/m_s \\ 0 & 0 & 0 & 1 \\ k_s/m_u & b_s/m_u & -k_t/m_u & -b_t/m_u - b_s/m_u \end{bmatrix} \quad \mathbf{B} = \begin{bmatrix} 0 & 0 \\ 1/m_s & 1/m_s \\ 0 & 0 \\ -1/m_u & -1/m_u \end{bmatrix}$$

$$\mathbf{L} = \begin{bmatrix} 0 \\ 0 \\ 1 \\ b_t/m_u \end{bmatrix} \quad \mathbf{f} = \begin{bmatrix} \mathbf{u}_1 \\ \mathbf{u}_2 \end{bmatrix}$$

$\mathbf{u}_1$  and  $\mathbf{u}_2$  are control variables which correspond to the damper control force and the spring control force, respectively.

### 5.1.4 Time Response

Figure 5.4 shows the step response of the suspension deflection of a lumped-mass  $\frac{1}{4}$  car suspension model. The response is obtained using optimal controller. Figure 5.5 shows the verified step response of the suspension deflection using state-space approach.

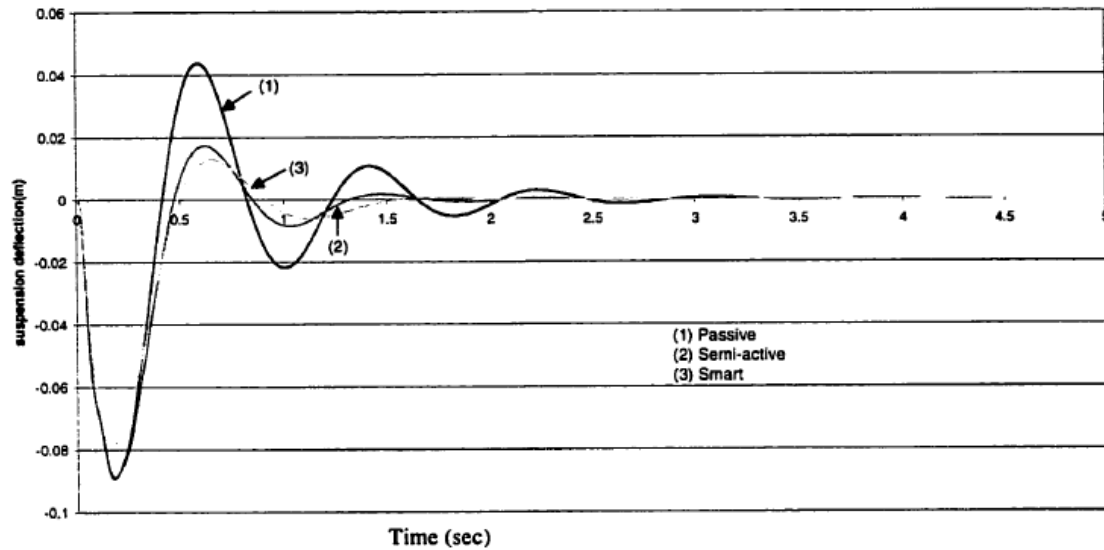


Figure 5.4: Time response of suspension deflection, adapted from [44]

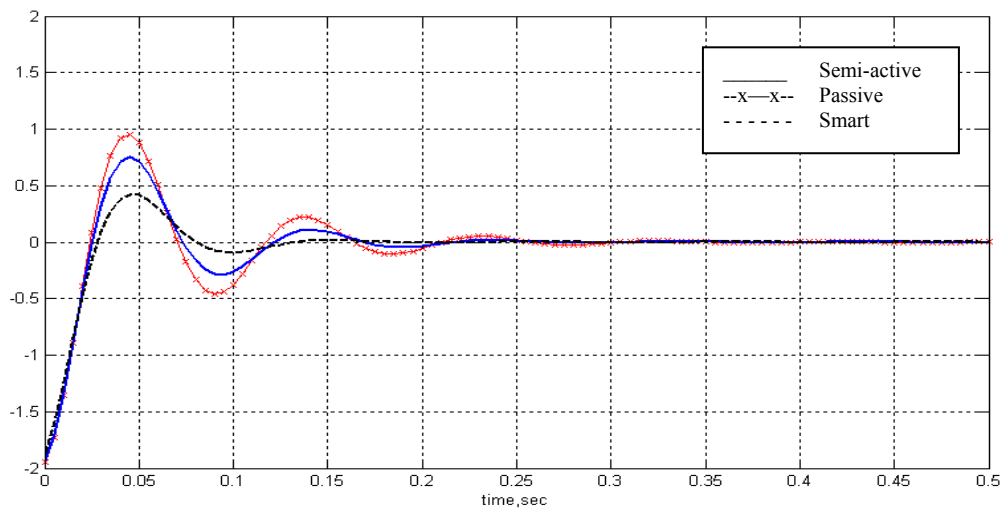


Figure 5.5: Verified time response for passive, semi-active and smart suspension system

Figures 5.4 and 5.5 compare two time responses obtained using different approach. The differences appear in the amplitude of the suspension deflection, the initial condition and the settling time.

### 5.1.5 Frequency Response

The frequency response of a lumped-mass quarter car suspension model using optimal control law is shown in Figure 5.6, and the justified frequency response based on state-space approach is shown in Figure 5.7.

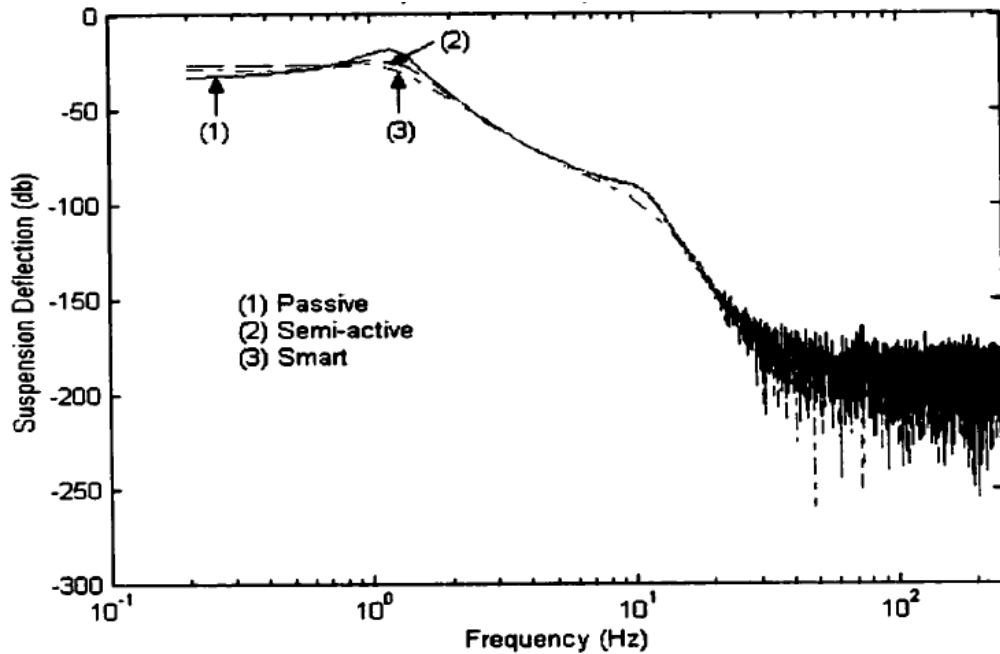


Figure 5.6: Frequency response of suspension deflection, adapted from [44]

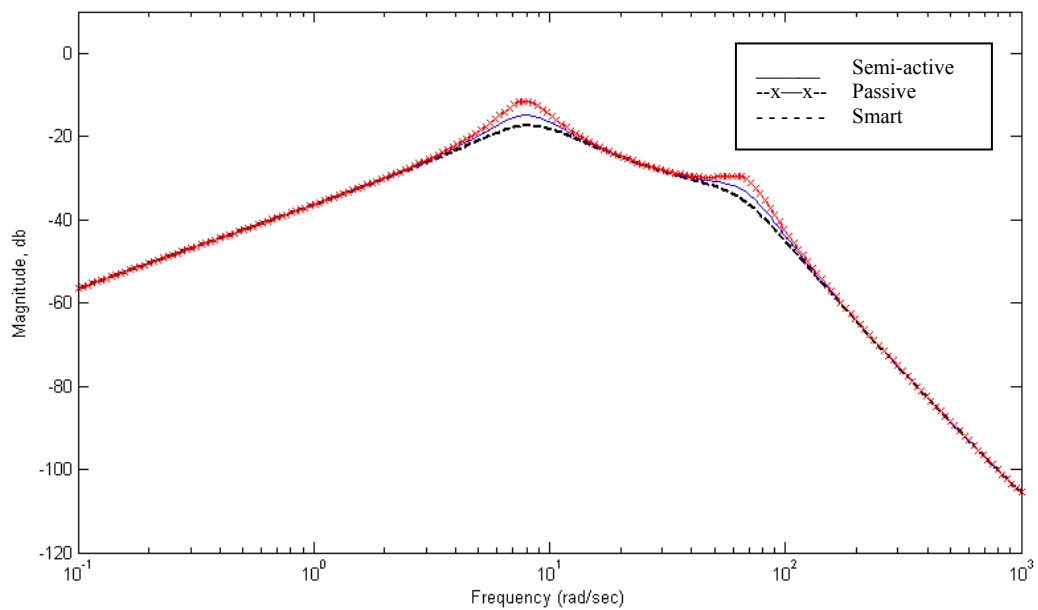


Figure 5.7: Verified frequency response for passive, semi-active and smart suspension system



Figures 5.6 and 5.7 compare the frequency responses using two different approaches. The major differences are seen on the resonance frequency and the magnitude for the resonance.

Optimal control laws constraint the inputs to the system, which physically limited the system reaction. The laws also limited the amplitude, because with lower amplitude suspension, the better handling for the vehicle. State-space approach on the other hand, does not constraint on the control loop. The approach is used to predict the reaction of the system with the same parameters in the literature.

From the time responses, the suspension deflection will stays at 'zero' as long as there is no road disturbance. However due to modeling condition, state-space approach will always have a non-zero initial condition. State-space approach leads with approximate 10 times faster compare to optimal control law in settling time. This also means state-space approach have a faster response but reacts to higher amplitude.

Figure 3.8 shows the state-space model that is used for the validation. The loop shows a feed forward under the influence of direct transmission matrix, **D** and a feedback affected by state matrix **A**.

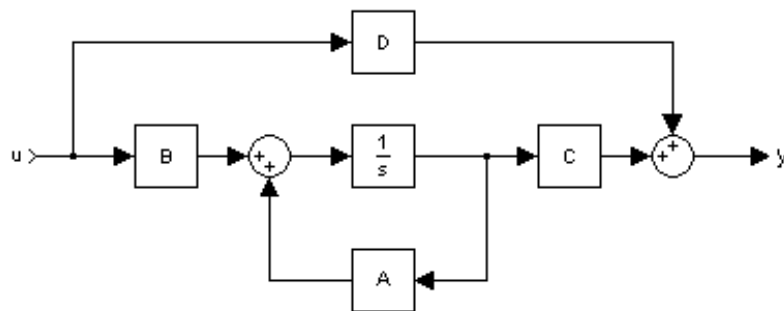


Figure 3.8: Typical state-space model

Figure 5.8 shows the block diagram for a semi-active suspension system which is adapted from literature [44]. The loop shows the only input is from road velocity and has three feedbacks under the influence of **A**<sub>0</sub>, **C** and **G**.

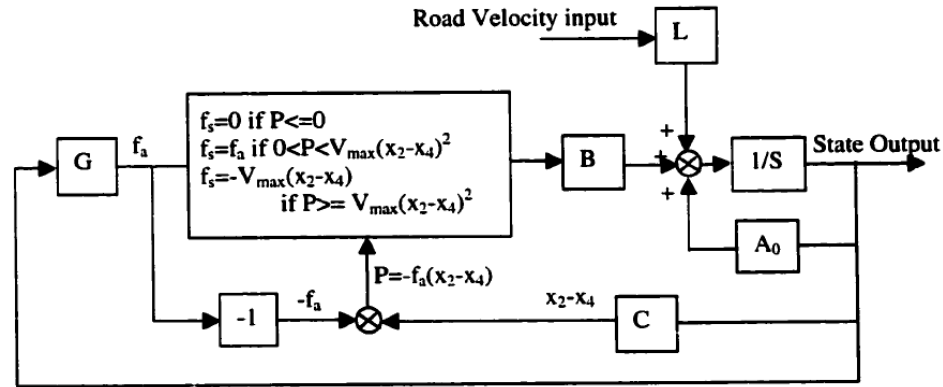


Figure 5.8: Block diagram of a  $\frac{1}{4}$  car model equipped with a semi-active suspension system using optimal control law, adapted from [44]

The reason that state-space approach has a faster response is because the control loop responds more directly with less control (feedback). Optimal control on the other hand consisted with too many constraints on the output that significantly delay the response time.

Frequency response from the literature shows that, resonance happens between the ranges of 1 Hz to 10 Hz, with a very high feedback gain. This can be seen from the optimal control loop, where the errors from **G** and **C** are then fed forward to **B**, and this error is only able to be controlled using **A<sub>0</sub>**. This creates an undesirable situation where there is only one control (**A<sub>0</sub>**) for three inputs (**L**, **BC** and **GB**)

Typically during the state-space modeling, the direct transmission, **D** is neglected. With this condition the state-space loop will only possess with only a feedback influenced by **A**. With such a controllable output, state-space approach delayed the resonance into a range of 10 Hz to 100 Hz, with less feedback gain required. In other words, state-space approach can improve the performance of suspension, by providing better stability with less power required to stabilize the system.

The reason the author used optimal control law is because with a slower response, the car can gain more controllability and passenger comfort can be improved. Figure 5.4 shows the small amplitude for all of the suspensions are achieved.

## 5.2 Active suspension simulation through software interface

Linear Quadratic Regulator (LQR) (for more details see Appendix E) is used to generate the control algorithm for the simulation. LQR defined regulation on input, state, output, and the trajectory. However, LQR does not provide exact solution. It required trial-and-error on the Error Weighted Matrix  $\mathbf{Q}(t)$  and Control Weighted Matrix  $\mathbf{R}(t)$ .

The active suspension system is shown in Figure 5.9 and is modeled in series configuration with an expandable stroke that consisted with linear spring stiffness  $k_s$  and linear damper with damping rate  $c_{st}$ . A linear tire model is used, i.e., a spring of stiffness  $k_t$ . It is assumed that the tire does not leave the ground and that  $z_s$  and  $z_u$  are measured from the static equilibrium position [45]. The linear equations of motion can be easily derived as follows:

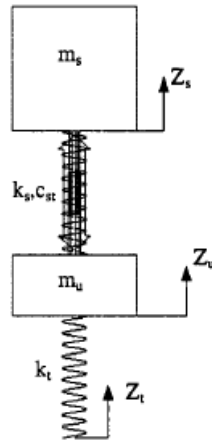


Figure 5.9:  $\frac{1}{4}$  car models with active suspension system, adapted from [45]

Table 5.2: Parameters defined for simulation for  $\frac{1}{4}$  car active suspension system using LQR, adapted from [45]

$m_u = 40\text{kg}$	$m_t = 730\text{kg}$	$m_s = 234\text{kg}$
$k_s = 19.96\text{kN/m}$	$k_t = 175.5\text{kN/m}$	$c_{st} = 1.29\text{kNs/m}$

Tire force:

$$F_t = k_t(Z_u - Z_t) \quad (5.13)$$

Suspension force:

$$F_{sc} = k_s(Z_s - Z_u) + c_{st}(\dot{Z}_s - \dot{Z}_u) \quad (5.14)$$

Equations of Motion:

$$m_s \ddot{Z}_s = -k_s(Z_s - Z_u) - c_{st}(\dot{Z}_s - \dot{Z}_u) - F_u \quad (5.15)$$

$$m_u \ddot{Z}_u = k_s(Z_s - Z_u) + c_{st}(\dot{Z}_s - \dot{Z}_u) + F_u - k_t(Z_u - Z_t) \quad (5.16)$$

State Variables:

$$\dot{\mathbf{x}} = \mathbf{A}\mathbf{x} + \mathbf{B}_1\mathbf{u} + \mathbf{B}_2\mathbf{w} \quad (5.17)$$

Where,

$$\mathbf{A} = \begin{bmatrix} -c_{st}/m_u & -k_s/m_s & c_{st}/m_s & k_s/m_s \\ 1 & 0 & 0 & 0 \\ c_{st}/m_u & k_s/m_u & -c_{st}/m_u & -(k_s + k_t)/m_u \\ 0 & 0 & 1 & 0 \end{bmatrix}$$

$$\mathbf{B}_1 = \begin{bmatrix} -1/m_s \\ 0 \\ 1/m_u \\ 0 \end{bmatrix} \quad \mathbf{B}_2 = \begin{bmatrix} 0 \\ 0 \\ k_t/m_u \\ 0 \end{bmatrix}$$

### 5.2.1 Time Response

Figure 5.10 outlines the response of the sprung mass acceleration of the LQR system compared to the linear passive suspension. Graphed are two different model responses for the LQR controller, one by Simulink ('LQR Simulink') and other by ADAMS model ('LQR interface'). Figure 5.11 shows the verified time response obtained using state-space approach. The time response using state-space approach is based on MATLAB.

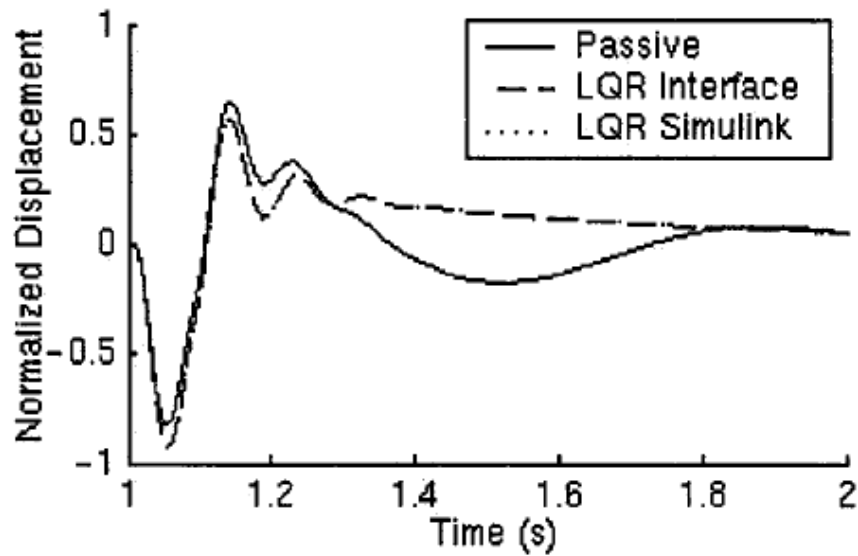


Figure 5.10: Time response of suspension displacement for a  $\frac{1}{4}$  car model active suspension system, adapted from [45]

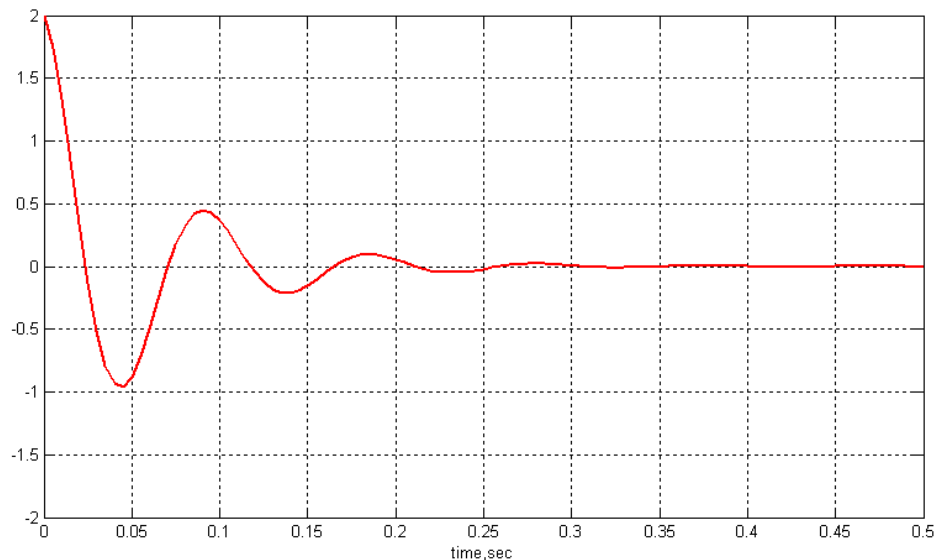


Figure 5.11: Verified time response for active suspension system

Figure 5.10 and 5.11 compare the same  $\frac{1}{4}$  car active suspension model using different approach. The main differences are on the initial condition aspects and the response time, while slightly similarity is achieved for the amplitude.

### ***5.2.2 Frequency Response***

To explore the influence of the weighting matrices on the system response, the frequency response of suspension displacement is shown in Figure 5.12.

- 1) LQR A:  $Q = \text{diag} [1e8 \ 100 \ 100 \ 1e8]$  &  $R = [1]$
- 2) LQR B:  $Q = \text{diag} [1e8 \ 100 \ 100 \ 100]$  &  $R = [10]$
- 3) LQR C:  $Q = \text{diag} [1e9 \ 100 \ 100 \ 1e8]$  &  $R = [1]$
- 4) LQR D:  $Q = \text{diag} [1e6 \ 100 \ 1e4 \ 2e8]$  &  $R = [0.1]$
- 5) LQR E:  $Q = \text{diag} [100 \ 100 \ 1e4 \ 2e9]$  &  $R = [0.1]$

The LQR A is the nominal setting, LQR B decreased the force output of the active actuator and weight the unsprung mass displacement less. LQR C weights the sprung mass velocity even more heavily and the last two system reverse the trend by putting most of the emphasis on decreasing the unsprung mass motion with more available actuator force.

Figure 5.13 shows the frequency response obtained using state-space approach. The comparison will be made between LQR C and state-space approach. The reason selecting the LQR C is because the system shows the most improvement using LQR C.

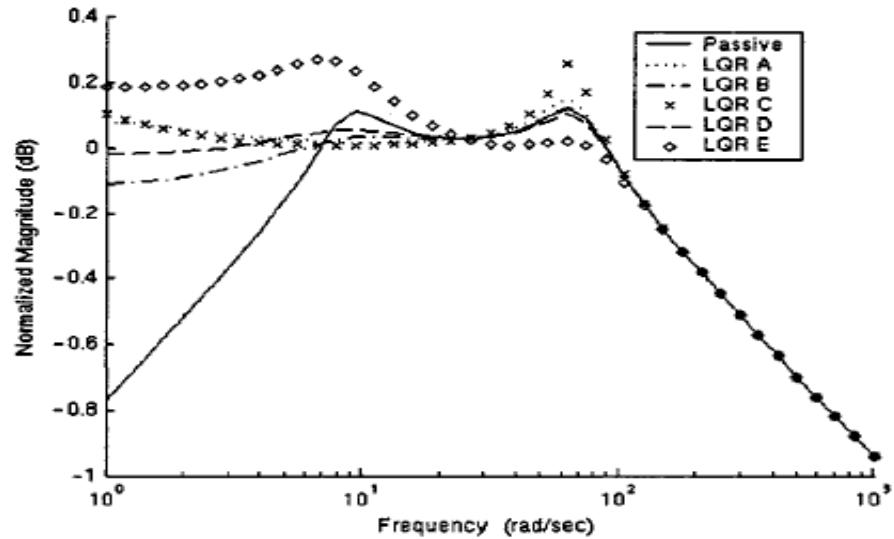


Figure 5.12: Frequency response of suspension displacement for a  $\frac{1}{4}$  car model active suspension system, adapted from [45]

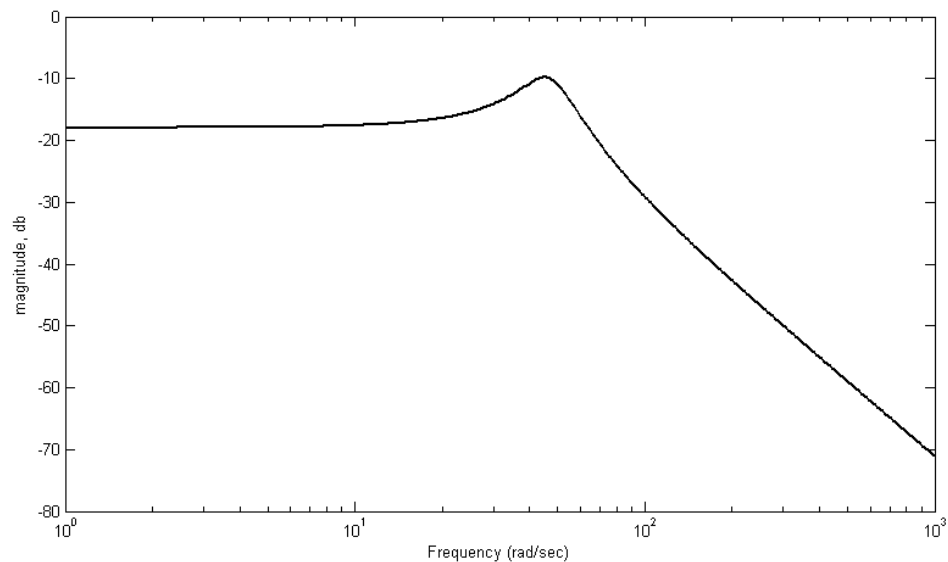


Figure 5.13: Verified Frequency response for active suspension system

Comparison of frequency responses are made between LQR C responses with verified response using state-space approach. Figures 5.12 and 5.13 show the main different at the magnitude of 'peak', the frequency range for the resonance are almost similar at the range  $\approx 10e2$ .

After enhancements are made to the control loop with more constraint, higher similarities are achieved. In time response, beside the initial condition (explained on the previous case) and settling time, the displacement range shows the same for both approaches, from -1 to 0.5. The different in settling time, because state-space approach only deal with sprung and un-sprung mass, while author deals with the total car mass.

Figure 5.12 shows frequency response using LQR approach has a positive gain (positive magnitude). A positive feedback system will have destabilizing effect and is usually accompanied by a saturation that limits the growth of the quantity. State-space approach obtains negative gain, which the system attempts to regulate the system by reacting to disturbances in a way that decreases the effect of those disturbances.

A typical closed control loop for the use of LQR is shown in Figure 5.14. As seen in the control loop, where there are two feedback influenced by  $\mathbf{A}$  and  $\mathbf{K}$ . The additional feedback control in the loop delays the respond time of the control system. On the other hand, state-space model control loop offers a more direct approach to deal with the dynamic system with only one feedback loop.

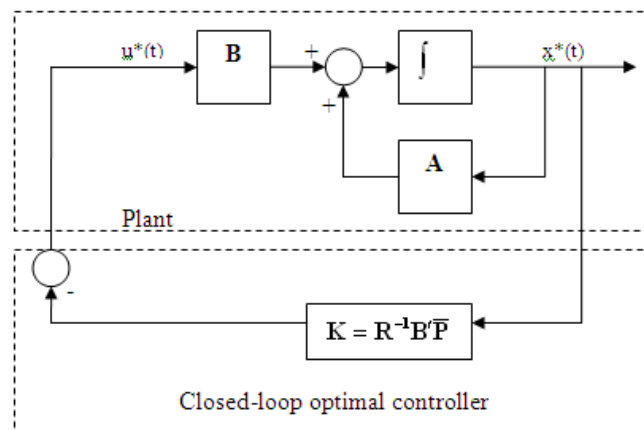


Figure 5.14: Closed-loop optimal control (LQR)

The reason of the frequency response using LQR has a positive magnitude is because, the input  $\mathbf{B}$  is amplified by  $\mathbf{K}$ , this result in a ‘more feed forward’ effect rather than feedback. (LQR required the trial and error of Control Weight Matrix,  $\mathbf{R}$ )



### 5.3 Aspect of achievable performance for quarter car active suspension

To avoid the unnecessary trial-and-error difficulties using LQR approach, author parametrizes all the controllers that stabilize a given plant in terms of a free parameter  $Q(s)$  (a stable proper transfer matrix), also known as Youla Parametrization (Appendix F).

A two-degree-of-freedom quarter-car model is shown in Figure 5.15. In this model, the sprung and unsprung masses are denoted, respectively, by  $m_s$  and  $m_u$ . The suspension system is represented by a linear spring of stiffness  $k_s$  and a linear damper with damping rate  $c_s$ . The tire is modeled by a linear spring of stiffness  $k_t$  and a linear damper with a damping rate  $c_t$ . The parameter values, except  $c_t$ , chosen for this study are shown in Table 5.3 [46].

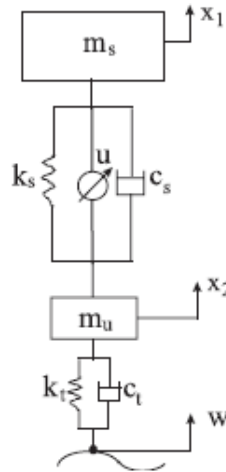


Figure 5.15: The  $\frac{1}{4}$  car model of the vehicle suspension system, adapted from [46]

Table 5.3: Parameters defined for simulation for  $\frac{1}{4}$  car active suspension system using Coprime Factorization, adapted from [46]

$m_u = 36 \text{ kg}$	$k_s = 16 \text{ kN/m}$	$c_s = 980 \text{ Ns/m}$
$m_t = 240 \text{ kg}$	$k_t = 160 \text{ kN/m}$	$c_t = 980 \text{ Ns/m}$

Equations of motion for active suspension system:

$$m_s \ddot{x}_1 = -k_s(x_1 - x_2) - c_s(\dot{x}_1 - \dot{x}_2) - u \quad (5.18)$$

$$m_u \ddot{x}_2 = k_s(x_1 - x_2) + c_s(\dot{x}_1 - \dot{x}_2) + u - k_t(x_2 - w) - c_t(\dot{x}_2 - \dot{w}) \quad (5.19)$$

Where  $\mathbf{x}_1$  and  $\mathbf{x}_2$  are, respectively, the displacements of the sprung and unsprung masses, and  $w$  is the road unevenness. The variables  $\mathbf{x}_1$ ,  $\mathbf{x}_2$ , and  $w$  are measured with respect to an inertial frame, and the control input  $u$  is a force.

In the form of state-space,

$$\mathbf{A} = \begin{bmatrix} 0 & 0 & 1 & -1 \\ 0 & 0 & 0 & 1 \\ -k_s/m_s & 0 & -c_s/m_s & c_s/m_s \\ k_s/m_u & -k_t/m_u & c_s/m_u & -(c_s + c_t)/m_u \end{bmatrix} \quad (5.20)$$

$$\mathbf{B}_1 = \begin{bmatrix} 0 \\ -1 \\ 0 \\ c_t/m_u \end{bmatrix} \quad \mathbf{B}_2 = \begin{bmatrix} 0 \\ 0 \\ -1/m_s \\ 1/m_u \end{bmatrix} \quad (5.21)$$

$$\mathbf{C} = \begin{bmatrix} -k_s/m_s & 0 & -c_s/m_s & c_s/m_s \\ 1 & 0 & 0 & 0 \end{bmatrix} \quad (5.22)$$

$$\mathbf{D} = \begin{bmatrix} -1/m_s \\ 0 \end{bmatrix} \quad (5.23)$$

The author only shows the frequency response using coprime factorization.

### 5.3.1 Frequency Response

Figure 5.16 shows the frequency response magnitudes of the passive and active suspensions are plotted. Figure 5.17 shows the verified frequency response using state-space approach based on the same model as used in the literature. The comparison is made only with the active suspension system.

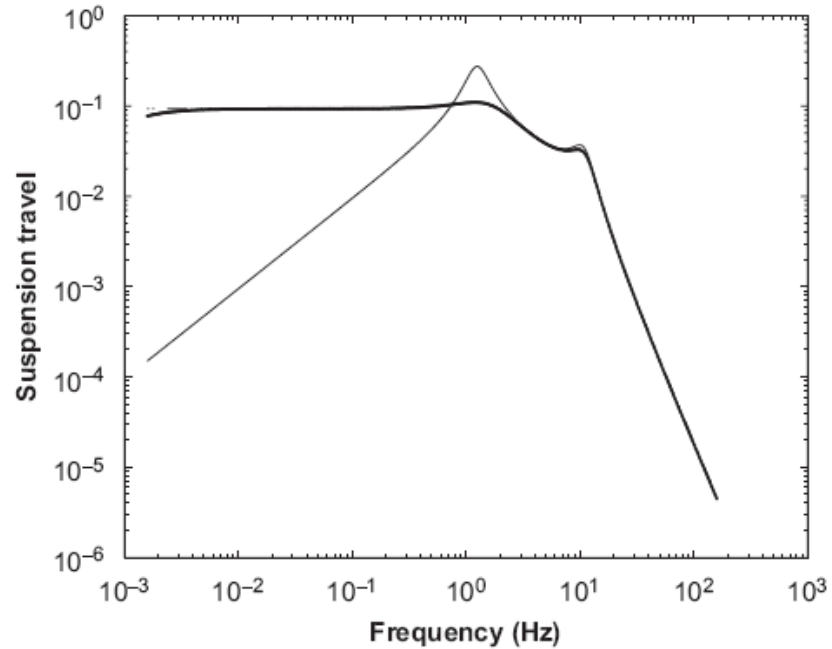


Fig. 4. The suspension travel frequency response magnitude: (—) passive suspension; (---) active suspension using the suspension travel measurement without tire damping; (-·-) active suspension using the acceleration and the suspension travel measurements without tire damping.

Figure 5.16: Frequency response of suspension travel using coprime factorization, adapted from [46]

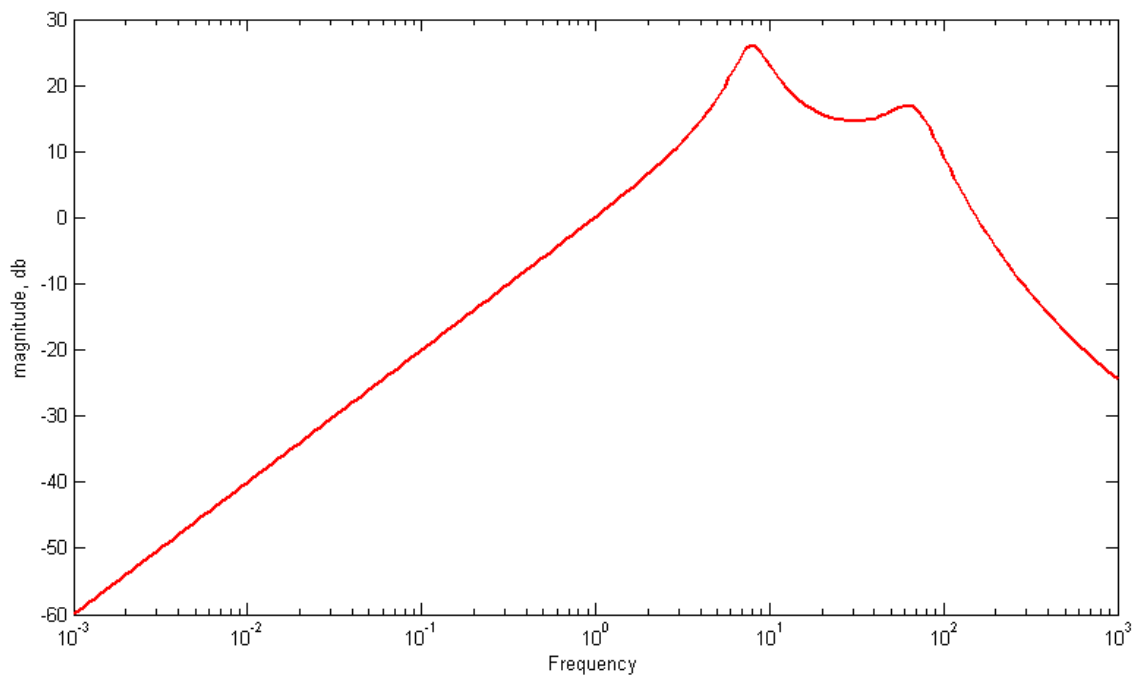


Figure 5.17: Verified frequency response using state-space approach

Figure 5.16 and 5.17 shows differences in magnitude and frequency range of the resonance. State-space approach delays the resonance from 0.1-1Hz to 1-10Hz. But the results also show that, state-space approach has a positive gain, while Youla Parametrization method obtains negative gain.

Youla Parametrization is used to re-define the control loop to achieve better internal stability. It generates optimized gain in control loop, for the system achieve better performance and stability. State-space approach deals only with typical control loop, and does not concern to the system internal stability.

## CHAPTER VI

### CASE STUDY

The displacement or stroke limitation for PRA during LG operation is a crucial and critical factor that significantly influencing the amount of impact forces that may generated. The same principles applied for LM where, the anti-phase forces generated from the LM are affected by the oscillation motion of ‘forcer’.

In reality, the total stroke of LG under full combustion is expected to be 138mm. However, current experiment stage only allows motoring driven or motoring with light combustion driven. This reason affects the stroke, by limiting it to 120mm. All the forces that determined in previous chapter for all three driven forces are operating at a stroke of 120mm. Current case study is to investigate out of all three driven forces, which force will provide a better operating condition for LG. Schematic for a full AVC is showed in Figure 4.1 with calculated simulation parameters in Table 4.1,

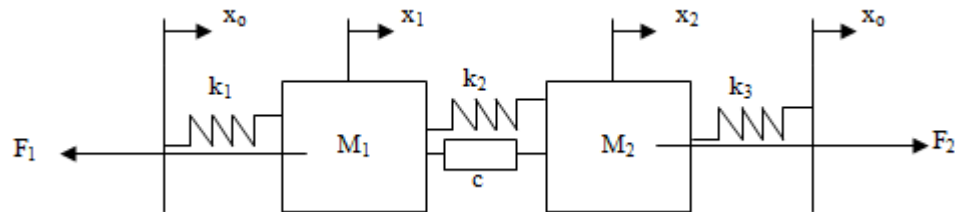


Figure 4.1: AVC Mathematical Modeling

Table 4.1; Simulation parameters

	$M_1 = 10\text{kg}$	$M_2 = 25\text{kg}$	
3BM	$k_1 = 101.17 \text{ N/m}$	$k_2 = 266.16 \text{ N/m}$	$F_1 = 75\text{N}$
	$k_3 = 165.29 \text{ N/m}$	$c = 3.26 \text{ Ns/m}$	$F_2 = 75\text{N}$
5BM	$k_1 = 249.82 \text{ N/m}$	$k_2 = 657.98 \text{ N/m}$	$F_1 = 87.5\text{N}$
	$k_3 = 408.16 \text{ N/m}$	$c = 5.113 \text{ Ns/m}$	$F_2 = 87.5\text{N}$
3BC	$k_1 = 101.17 \text{ N/m}$	$k_2 = 266.16 \text{ N/m}$	$F_1 = 212.5\text{N}$
	$k_3 = 165.29 \text{ N/m}$	$c = 3.26 \text{ Ns/m}$	$F_2 = 212.5\text{N}$

The available driven forces are 3BM, 3BC and 5BM. All Bode plots are obtained using state-space approach with the application of AVC. The focus of the study is on the

function  $z_{22}$  which represents the responds of LG. Figures 4.12 and 4.13 show Bode plots for all functions after the application of AVC.

### 6.1 Before the application of AVC

Figure 6.1 below shows the frequency responses for LG under all driven forces. The resonances appear due to the unsymmetrical weight distribution during the operation of LG. The figure shows driven force 5BM has a higher resonant frequency than 3BM and 3BC. However, all resonances have positive magnitude, which reflect the responds of LG are unstable. Permanent phases shifted happen for all driven forces. Table 6.1 shows the magnitude and frequency for each resonance. (Note: 3BM: ..., 5BM: ---, 3BC \_\_\_\_)

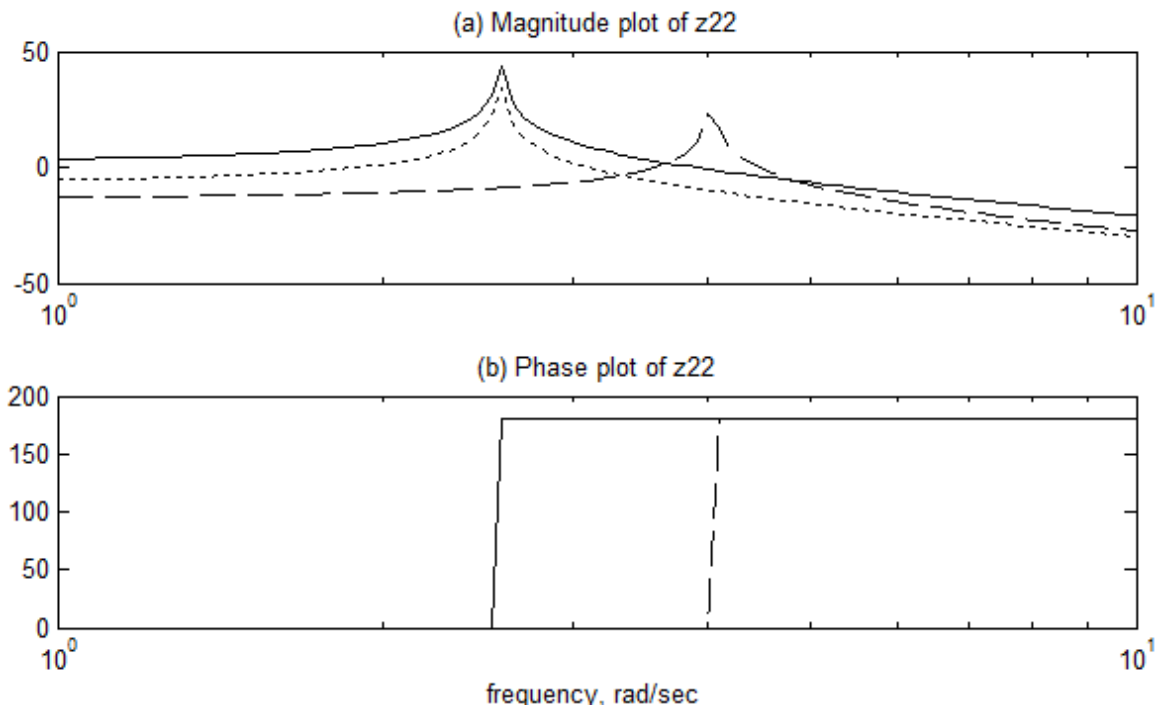


Figure 6.1: Bode plots of LG before the application of AVC

Table 6.1: Magnitudes of ‘Poles’ before the application of AVC

	Poles	
	Frequency (rad/sec)	Magnitude (db)
3BM	2.583	34.23
3BC	2.583	43.27
5BM	4.009	22.72

## 6.2 After the application of AVC

Figure 6.2 shows the Bode plots of LG responses after the application of AVC. (Note: 3BM: ..., 5BM: ---, 3BC \_\_\_\_\_)

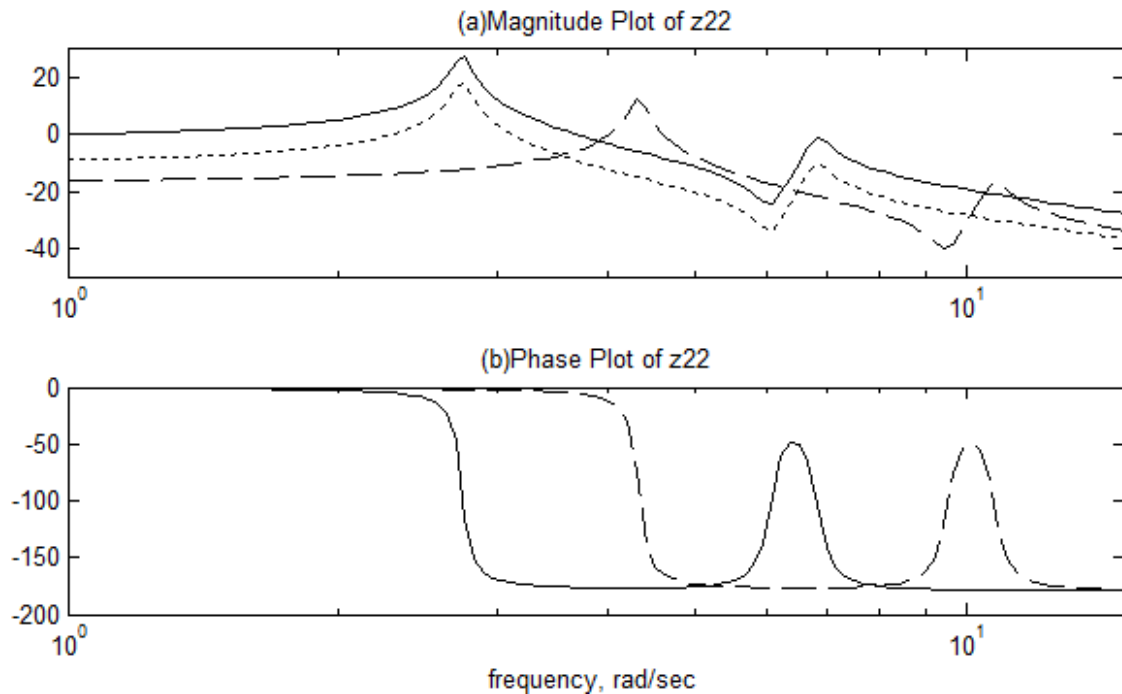


Figure 6.2: Bode plots of LG after the application of AVC

Figure 6.2(a) indicates the presence of two peaks for all driven forces. The first peak is LM and the second peak represents LG. The magnitude of LM is positive, while LG has negative magnitude. Having a positive magnitude allows the LM to generate sufficient forces to counter the impact forces from LG. The higher the impact force, more positive magnitude is needed, as seen for 3BC which possesses the highest impact force. LG has the highest resonant frequency using 5BM.

As for the phase shown in Figure 6.2(b), the phases for 3BC and 3BM are overlapping. After the application of LM, the phase of LG shifted from 0 deg to -180 deg. Then consistent phase is achieved. The peak heads down has a damping effect which reacted to shift the phase back to the initial phase. Table 6.2 shows all the magnitude for 'poles' and 'zeros' after the application of AVC.

Table 6.2: Magnitudes for ‘poles’ and ‘zeros’ after the application of AVC

	Linear Motor (LM)		Linear Generator Engine (LG)			
	Poles		Zeros		Poles	
	Frequency (rad/sec)	Magnitude (db)	Frequency (rad/sec)	Magnitude (db)	Frequency (rad/sec)	Magnitude (db)
3BM	2.768	18.25	6.080	-33.65	6.826	-10.19
3BC	2.768	27.29	6.080	-24.61	6.826	-1.144
5BM	4.297	12.37	9.438	-40.28	10.84	-16.98

Table 6.2 shows the 3BM and 3BC are having the ‘zeros’ and ‘poles’ at the same frequency range. However, the magnitude for 3BM and 3BC are different. LG operates better on 3BM rather than 3BC because the combustion process is very hard to control. In addition to that, combustion process provides additional impact force acting on the LG engine block. Among the driven forces, 5BM is the more suitable. The resonance for 5BM happens after 3BM and 3BC, with much more negative magnitudes are obtained.

The results meet the expectation from the UTP LG group who claimed if the LG is operates using 5BM, a more desirable engine output and performance is achieved. When the PRA is drives using 5BM, a condition similar to combustion only can be achieved.



## CHAPTER VII

### CONCLUSION

#### 7.1 Introduction

This section will revisit the research objectives, summarize the findings of this research work and offer conclusions based on the findings. Recommendations for future research will be discussed, in terms of how to progress this research study. Importantly, the contribution of this research as the initial development of AVC for LG will be clarified.

#### 7.2 Objective of the research

The objective of this research is to reduce LG vibration level with AVC by inserting an anti-phase momentum from LM into the system to cancel out the impact force created. The study is focused on the responds of LG in time and frequency domain, together with pole-zero plots and root locus plots using simulation.

#### 7.3 Summary of finding and conclusions

The pole-zero plots and root locus plots are obtained using transfer function approach. Transfer function approach does not consider the magnitude and direction of available forces, the system is stable initially. No presence of RHP, with all the 'poles' and 'zeros' are on the left hand side of the complex plane.

Two types of time responses are obtained; proportional and non-proportional damped time response. The non-proportional damped time response showed the interactions of masses LM and LG, with the overall amplitude of the interactions reduced after the application of AVC. As for the proportional damped time responses, some contradictions to the mathematical modeling are appealing. Thus, the non-proportional damped time response is a more relevant approach.

Frequency responses are obtained using all approaches derived in four distinct transfer functions. However, only the function that represents the LG is focused. The frequency responses showed that with the application of AVC more consistent of phase is achieved

and the magnitude of resonance is reduced with delay. State-space approach is selected as a more suitable and relevant approach compare to other two methods.

Lumped-mass quarter car suspension model is selected for validation purpose. Three literatures using different methods are evaluated for validation. By using the parameters highlighted in the literatures, similar results are achieved with minor differences due to different approaches.

The case studies examined the LG under motoring limited stroke. The results showed that with the appropriate AVC applied to the LG, the resonance can be delayed and the magnitude of the resonance also can be reduced. The drive force, 5BM offers the optimum operating conditions for LG under motoring limited stroke.

#### **7.4 Recommendations for future work**

A more detailed and specific mathematical modeling should be used. For enhancement, instead of state-space approach, optimal control law or robust control theory can be applied. If possible, experimental works should be carried out to test the effectiveness of AVC for LG.

#### **7.5 Limitation and potential problem**

The lack of real experimental data and related literatures to prove the AVC for LG cause the difficulty to validate the simulation results.

#### **7.6 Contribution to Knowledge**

The review of literature highlighted the importance of active vibration control in structure and machinery. However the literature does not show any related vibration control for free-piston linear generator engine. Present study makes use of some fundamental control approach to investigate the active vibration control for a free-piston linear generator engine. The works conducted still has not been documented yet.

## REFERENCES

1. Mikalsen, R., Roskilly, A.P. (2008). 'Performance simulation of a spark ignited free-piston engine generator', *Applied Thermal Engineering*, 28(14-15):1726-1733.
2. Arshad, W.M., Backstrom, T., Thelin, P., Sadarangani, C. (2002). 'Integrated free-piston generators: an overview', in *Proceedings of the Nordic Workshop on Power and Industrial Electronics, Norpie 2002*, Stockholm.  
Available at: <http://sahkotekniikka.tkk.fi/en/index.html>.
3. Mohd Razali B. Hanipah (2008). Experimental study of combustion process in a two-stroke, H<sub>2</sub>-DI linear Generator Free-piston engine during starting, MSc thesis, Universiti Teknologi PETRONAS: Tronoh.
4. Abdul Rashid Abdul Aziz (2007). *Modeling, design, modification and Test of combustion and fuel system of two stroke free piston linear generator engine*, Technical Report, Universiti Teknologi PETRONAS.
5. Hew Wooi Ping (2006). *Modeling, design modification and testing of EMF linear generator of a new free piston gas generator*, Technical Report, Universiti Malaya.
6. Mikalsen, R., Roskilly, A.P. (2007b). 'The design and simulation of a two-stroke free-piston compression ignition engine for electrical power generation', *Applied Thermal Engineering*, 28(5-6):589-600.
7. De Silva, C.W. (1999). *Vibration: Fundamentals and practice*, Florida: Boca Raton. CRC/Taylor & Francis.
8. Kashani, R. 'Active vibration cancellation' [online].  
Available at: [www.deicon.com](http://www.deicon.com).
9. Van Blarigan, P., Goldborough, S.S. (2003). *Optimizing the scavenging systems for a two-stroke cycle, free piston engine for high efficiency and low emissions: a computational approach*, SAE 2003 Congress, International Multi-dimensional Engine Modeling User Group Meeting.
10. Mikalsen, R., Roskilly, A.P. (2007a). 'A review of free-piston engine history and applications', *Applied thermal Engineering*, 27(14-15):2339-2352.
11. Van Blarigan, P. (2001). 'Advance internal combustion', in *Proceeding of the 2001 DOE Hydrogen Program Review*. NREL/CP-570-30535 Available at: [http://www1.eere.energy.gov/hydrogenandfuelcells/annual\\_review2001.html](http://www1.eere.energy.gov/hydrogenandfuelcells/annual_review2001.html).

12. Cosic, A., Sadarangani, C., Carlsson, F. (2005). 'A novel concept of transverse flux linear free-piston generator', in *Proceeding of the 5<sup>th</sup> International Symposium on Linear Drives for Industry Applications (LDIA2005)*, Hyogo. Available at: <http://www.ee.maritime.kobe-u.ac.jp/ldia2005>.
13. Saiful Azrin Mohd Zulkifli (2007). *Modeling, simulation and implementation of rectangular commutation for starting of free-piston linear generator*, MSc thesis, Universiti Teknologi PETRONAS: Tronoh.
14. Nandkumar, S. (1998). *Two-Stroke Engine*, MSc Theis, West Virginia University: Morgantown.
15. Nagurka, M.L., Kurfess, T.R. (1992). 'Gain and phase margins of SISO systems from modified root locus plots', *IEEE Control Systems Magazine*, 12(3):123-127.
16. Flint, E., Evert, M.E., Anderson, E., Flannery, P. (2000). 'Active/passive counter force vibration control and isolation systems', in *Proceedings of the 2000 IEEE Aerospace Conference*, Montana. Available at: <http://ieeexplore.ieee.org/xpl/RecentCon.jsp?punumber=7042>.
17. Xing, J.T., Xiong, Y.P., Price, W.G. (2005). 'Passive-active vibration isolation systems to produce zero or infinite dynamic modulus: theoretical and conceptual design strategies', *Journal of Sound and Vibration*, 286(3):615-636.
18. Montanaro, J.S., Beale, G.O. (1998). 'Feedback control for canceling mechanical vibration', in *Proceedings of the 24<sup>th</sup> Annual Conference of the IEEE Industrial Electronics Society*, vol.3, IECON'98, Aachen. Available at: <http://ieeexplore.ieee.org/xpl/RecentCon.jsp?punumber=5851>.
19. Kwak, M.K., Heo Seok (2007). 'Active vibration control of smart grid structure by multiinput and multioutput positive position feedback controller', *Journal Sound and Vibration*, 204(1-2):230-245.
20. Chen Youngjun, Zhu C.S. (2008). 'Active vibration control based linear matrix inequality for rotor system under seismic excitation', *Journal of Sound and Vibration*, 314(1-2):53-69.
21. Zhu Wen-Hong; Tryggvason, B.; Piedboeuf, J.C. (2006). 'On active acceleration control of vibration isolation systems', *Control Engineering Practice*, 14(8):863-873.
22. Hillis, A.J., Harrison, L., Stoten D.P. (2005). 'A Comparison of two adaptive algorithms for the control of active engine mounts', *Journal of Sound and Vibration*, 286(1-2):37-54.

23. Olsson, C. (2006). 'Active automotive engine vibration isolation using feedback control', *Journal of Sound and Vibration*, 294(1-2):162-176.
24. Hara, S., Katorim, H., Kondo, R. (1989). 'The relationship between real poles and real zeros in SISO sampled data systems', *IEEE Transaction on Automatic Control*, 34(6):632-635.
25. Ravuri, M., Asada, H. (1998). 'Experimental verification of non-minimum phase endpoint feedback of coordinate measuring machines using asymmetric order doubling', in *Proceedings of the 37<sup>th</sup> IEEE Conference on Decision and control*, vol.3, San Diego.  
Available at: <http://ieeexplore.ieee.org/xpl/RecentCon.jsp?punumber=6103>.
26. Verma, S.P., Balan, A. (1998). 'Experimental investigations on the stators of electrical machines in relation to vibration and noise problems', *IEE Proc.-Electr. Power Appl.*, 145(5):455-461.
27. Kurfess, T.R., Nagurka, M.L. (1991). 'Understanding the root locus using gain plots', *IEEE Control Systems Magazine*, 11(5):37-40.
28. Ha, Q.P., Negnevitsky, M. (1992). 'Root locus application for damping capability estimation of multi-mass electromechanical systems', in *Proceedings of the 1995 IEEE IECON 21<sup>st</sup> International Conference on Industrial Electronics, Control, and Instrumentation*, vol.1, IECON'95, Orlando.  
Available at: <http://ieeexplore.ieee.org/xpl/RecentCon.jsp?punumber=3173>.
29. Eydgahi, A.M., Ghavamzadeh, M. (2001). 'Complementary Root Locus Revisited', *IEEE Transactions on Education*, 44(2):137-143.
30. Adhikari, S (2006). 'Damping modeling using generalized proportional damping', *Journal of Sound and Vibration*, 293(1-2):156-170.
31. Adhikari, S., Woodhouse, J. (2001a). 'Identification of damping: part 1, viscous damping', *Journal of Sound and Vibration*, 243(1):43-61.
32. Sorrentino, S., Marchesiello, S., Piombo, B.A.D. (2003). 'A new analytical technique for vibration analysis of non-proportionally damped beams', *Journal of Sound and Vibration*, 265(4):765-782.
33. Adhikari, S., Woodhouse, J. (2001b). 'Identification of damping: part 2, non-viscous damping', *Journal of Sound and Vibration*, 243(1):63-88.
34. Dukkupati, R.V. (2006). *Advanced mechanical vibrations*, Alpha Science International.

35. Cha, P.D. (2005). 'Approximate eigensolutions for arbitrarily damped nearly proportional systems', *Journal of Sound and Vibration*, 288(4-5):813-827.
36. Benassi, L., Elliot, S.J., Gardonio, P. (2004). 'Active vibration isolation using an inertial actuator with local force feedback control', *Journal of Sound and Vibration*, 276(1-2):157-179.
37. Stark, R.W., Schitter, G., Stark, M., Guckenberger, R., Stemmer, A. (2004). *State-space model of freely vibrating and surface-coupled cantilever dynamics in atomic force microscopy*, Physical review B 69, The American Physical Society, 085412 (1-9).
38. Olsson, C. (2005). *Disturbance observer-based automotive engine vibration isolation dealing with non-linear dynamics and transient excitation*, Technical Report, Department of Information Technology, Uppsala University, 2005-009.
39. Panzer, M. (1960). *The theory and synthesis of active suspension system*, PhD thesis, Polytechnic Institute of Brooklyn: New York.
40. Boonchanta, P. (1982). *Comparison of active, passive and semi-active suspensions for ground vehicles*, PhD thesis, University of California: Berkeley.
41. Su Hong (1990). *An investigation of vibration isolation systems using active, semi-active and tunable passive mechanisms with applications to vehicle suspensions*, PhD thesis, Concordia University: Quebec.
42. Beard, D.C. (1995). *Design of a high performance, energy efficient, active vehicle suspension*, PhD thesis, University of California: Santa Barbara.
43. Chantranuwathana, S. (2001). *Adaptive robust force control for vehicle active suspensions*, PhD thesis, University of Michigan: Ann Arbor.
44. Zhou Haiyan (2002). *Development and control of an automotive smart suspension system*, MSc Thesis, University of Toronto: Toronto.
45. Maiorana, J. (2004). *Active suspension simulation through software interfacing*, MSc Thesis, University of Windsor: Ontario.
46. Turkay, S., Akcay, H. (2008). 'Aspect of achievable performance for quarter-car active suspensions', *Journal of Sound and Vibration*, 311(1-2):440-460.
47. Kuo, B.C. (1997). *Automatic control systems 7<sup>th</sup> edition*, New Jersey. Prentice Hall.
48. Hatch, M.R. (2001). *Vibration simulation using MATLAB and ANSYS*, New York, Chapman & Hall / CRC.

49. Looze, D.P., Freudenberg, J.S. (1991). 'Limitations of feedback properties imposed by open-loop right half plane poles', *IEEE Transaction on Automatic Control*, 36(6):736-739.
50. Saygi, N., Uraz, A. (1998). 'Stable compensation of right half plane zeros in time delay systems', *9<sup>th</sup> Mediterranean Electrotechnical Conference*, vol.1, Tel-Aviv. Available at: <http://ieeexplore.ieee.org/xpl/RecentCon.jsp?punumber=5631>.
51. Freudenberg, J.S., Looze, D.P. (1985). 'Right half plane poles and zeros and design tradeoffs in feedback systems', *IEEE Transaction on Automatic Control*, 30(6):555-565.
52. Goepel, E. (2004). 'Active RC networks: What benefit is there in having conjugate real zeros in the second-order transfer function?' in *Proceedings of the 2004 International Symposium on Circuits and Systems*, vol.1, ISCAS'04, Arizona. Available at: <http://ieeexplore.ieee.org/xpl/RecentCon.jsp?punumber=9255>.
53. Kim Chang-Wan (2006). 'A preconditioned iterative method for modal frequency-response analysis of structures with non-proportional damping', *Journal of Sound and Vibration*, 297(3-5):1097-1103.
54. Adhikari, S. (2004). 'Optimal complex modes and an index of damping non-proportionality', *mechanical Systems and Signal Processing*, 18(1): 1-27.
55. Zhang Xiangqun (1997). *Modeling and simulation of a hybrid-engine*, MSc thesis, University of Regina: Regina.
56. Naidu, D.S. (2003). *Optimal control systems*, London. CRC Press.
57. Zhou Kemin; Doyle, J.C.; Glover, K. (1997). *Robust and optimal control*, New York. Prentice Hall.

## APPENDIX A LG'S DETAILS & EXPERIMENTAL DATA

Prototype:

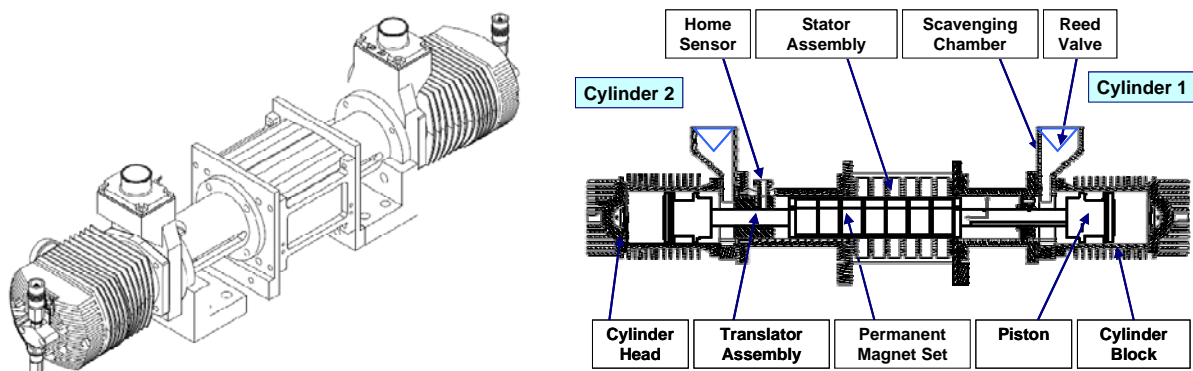


Figure A.1: Linear generator free piston engine prototype assembly and components

Specification:

Table A.1: The specifications of linear generator free-piston engine prototype

Engine type	Two-stroke, DISI
Bore (mm)	76
Maximum Stroke (mm)	69
Maximum Compression ratio	14
Total engine capacity (cc)	626
Exhaust port open-[begins/ends] (mm from origin)	5.5/34.5
Intake port open-[begins/ends] (mm from origin)	22/34.5
Scavenging type	Loop Scavenged Curtis type
Maximum Scavenging compression ratio	1.71
Moving Mass (kg)	$\approx 5$
Linear generator output (kW)	5



Figure A.2 shows a schematic diagram of LG along with a simplistic graph displaying the overlapping and non-overlapping regions of the cylinders' compression and expansion forces.

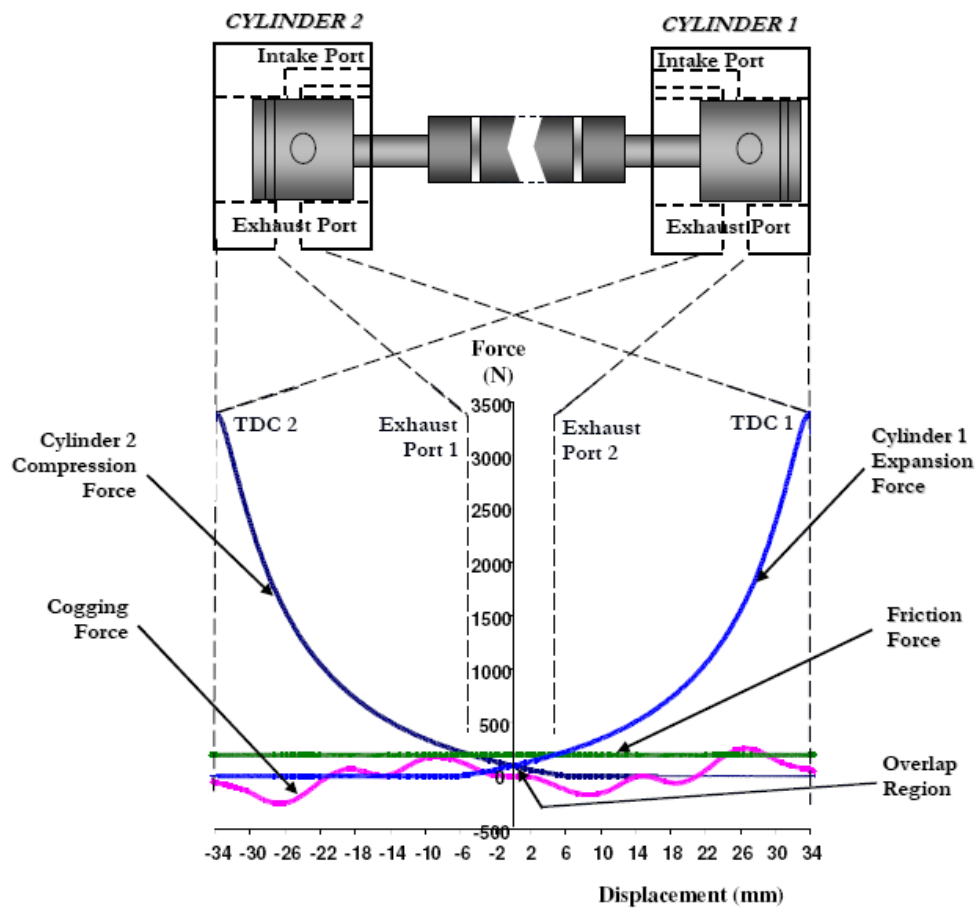


Figure A.2: LG schematic and Graph of Mechanical Forces against Displacement, adapted from [5]

Magnetic cogging forces:

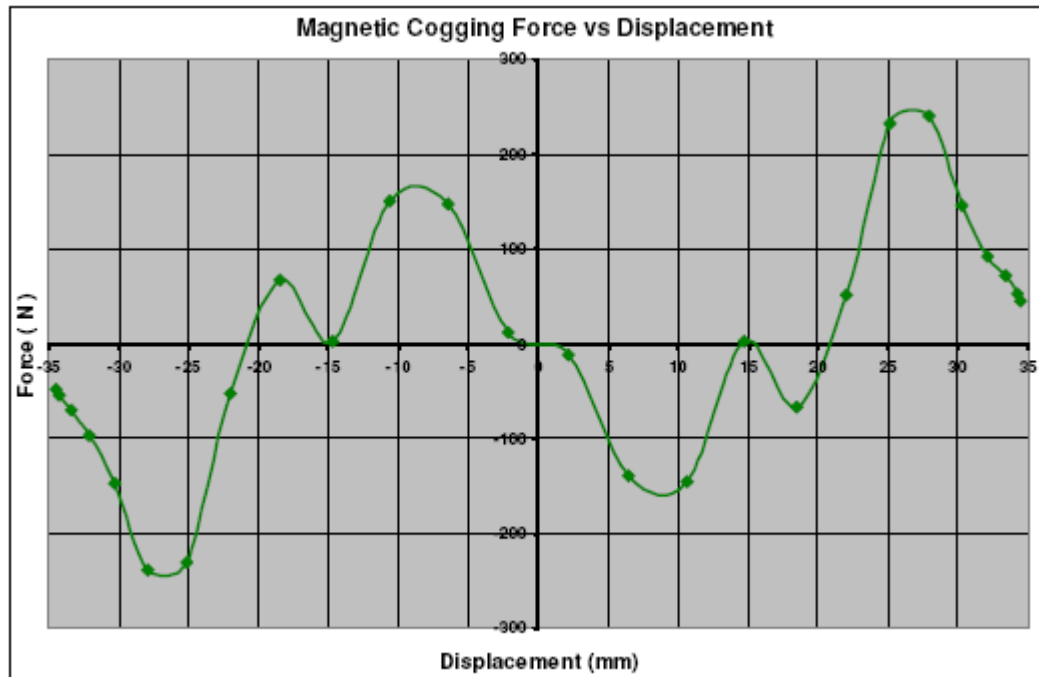


Figure A.3: LG's magnetic cogging force, adapted from [5]

**Before the application of AVC:**

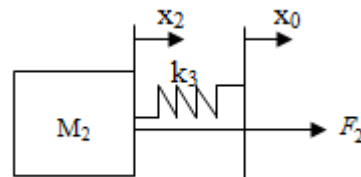


Figure A.2: Schematic for before the application of AVC

EOM:

$$M_2 \ddot{z}_2 + k_3 z_2 = F_2 \quad (\text{A.1})$$

**Transfer Function mode:**

Laplace transforms equation (A.1) assuming all initial conditions are zero:

$$[M_2 s^2 + k_3] Z_2 = F_2 \quad (\text{A.2})$$

In transfer functions mode:

$$Z_2 / F_2 = 1 / (M_2 s^2 + k_3) \quad (\text{A.3})$$

**State-space mode:**

Setting the highest derivatives of equation (A.1),

$$\ddot{z}_2 = (F_2 - k_3 z_2)/M_2 \quad (\text{A.4})$$

States:

$$x_1 = z_2 \quad (\text{A.5a})$$

$$x_2 = \dot{z}_2 \quad (\text{A.5b})$$

State equation:

$$\begin{bmatrix} \dot{x}_1 \\ \dot{x}_2 \end{bmatrix} = \begin{bmatrix} 0 & 1 \\ -k_3/M_2 & 0 \end{bmatrix} \begin{bmatrix} x_1 \\ x_2 \end{bmatrix} + \begin{bmatrix} 0 \\ F_2/M_2 \end{bmatrix} \quad (\text{A.6})$$

Output equation:

$$y_1 = \begin{bmatrix} 1 & 0 \end{bmatrix} \begin{bmatrix} y_1 \\ y_2 \end{bmatrix} + \begin{bmatrix} 0 \end{bmatrix} u \quad (\text{A.7})$$

**Modal state-space mode:**

By inspection:

$$\ddot{x}_{p2} = -F_{p2} \quad (\text{A.8})$$

Defining states:

$$x_1 = x_{p2} \quad (\text{A.9a})$$

$$x_2 = \dot{x}_{p2} \quad (\text{A.9b})$$

Rewriting the equations of motion using the states:

$$\dot{x}_1 = x_2 \quad (\text{A.10a})$$

$$\dot{x}_2 = -F_{p2} \quad (\text{A.10b})$$

Modal state equation:

$$\begin{bmatrix} \dot{x}_1 \\ \dot{x}_2 \end{bmatrix} = \begin{bmatrix} 0 & 1 \\ 0 & 0 \end{bmatrix} \begin{bmatrix} x_1 \\ x_2 \end{bmatrix} + \begin{bmatrix} 0 \\ -F_{p2} \end{bmatrix} u \quad (\text{A.11})$$

Modal output equation:

$$y_p = x_1 \quad (\text{A.12})$$

Equation (A.11) shows no sign of percentage of critical damping,  $\zeta$ . Hence, modal state-space approach cannot apply for the case before the application of AVC.

## APPENDIX B LG ELECTRICITY GENERATION PRINCIPLES

This section discussed about the relation between electricity generations with resonant frequency. Some basic definitions about the electromagnetic induction are explained. All analysis discussion will be based on qualitatively.

The electricity is generated based electromagnetic induction principles. The law for electromagnetic induction is “Faraday’s Law of induction”. Faraday’s law defined as the induced electromotive force or EMF in any closed circuit is equal to the time rate of change of magnetic flux through the circuit.

$$\varepsilon = -\frac{d\Phi_B}{dt}$$

where,  $\varepsilon$  is the EMF in volts and  $\Phi_B$  is the magnetic flux through the circuit in “Weber”. The electricity generation of LG is like sweeping a magnet past a loop of wire. It means that the flux will go through a surface and EMF will go through around a loop. For a tightly-wound coil of wire, composed of N identical loops,

$$\varepsilon = -N\frac{d\Phi_B}{dt}$$

where, N is the number of turns of wire, and  $\Phi_B$  is the magnetic flux through a single loop. Imagine that having a uniform magnetic field, B, direct evaluation of the change in flux will be,

$$\varepsilon = -\frac{d\Phi_B}{dt} = Bvl$$

where  $v$  is the velocity of motion of conductor or magnet. It means by knowing the velocity of permanent magnet passing through the coil built inside LG, the EMF that generated can be calculated. From principle of Lorentz force and Maxwell’s equation, the relation between velocity and frequency is

$$f = \frac{v}{\lambda}$$

where  $\lambda$  defined as the wavelength. The frequency is direct proportional to velocity. This concluded that, if the velocity of the PRA is known, the operation frequency of PRA can be determined. In other words, at resonance frequency, the PRA will move in a velocity with high level of vibration.

## APPENDIX C

### LUMPED MASS QUARTER CAR SUSPENSION SYSTEMS

**Passive suspension systems** include conventional springs and shock absorber. The force versus velocity characteristic of the shock absorber is usually non-linear. These systems contain no sensors, electronics, or controls.

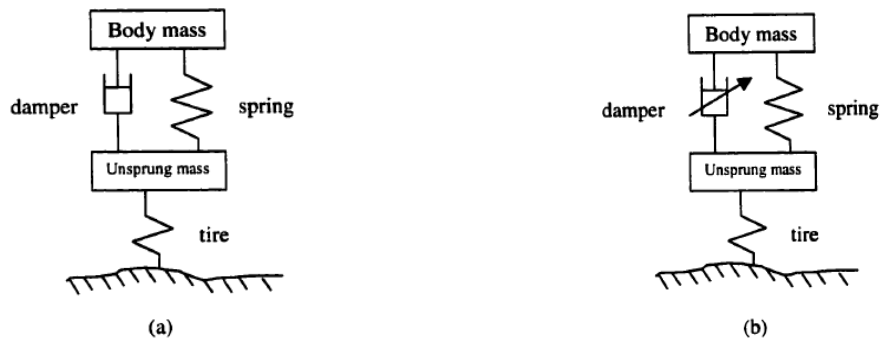


Figure C.1: (a) Passive  $\frac{1}{4}$  car suspension system, (b) Semi-active  $\frac{1}{4}$  car suspension system, adapted from [44]

**Semi-active suspension systems** provide controlled real-time dissipation of energy. For an automotive suspension, this is accomplished through a mechanical device called an active damper use parallel with an ordinary spring. Three types of semi-active systems exist:

1. Continuously variable semi-active control. This type of control requires the electro-mechanical active damper valve modulate its orifice area to any effective size.
2. On/off semi-active control. This type of control requires a simpler valve, which can switch between a large orifice and a small orifice area.
3. CDC (Continuous Damping Control) is a adjustable damping systems. CDC automatically adjusts the damping force to all driving conditions, road surface and load levels.

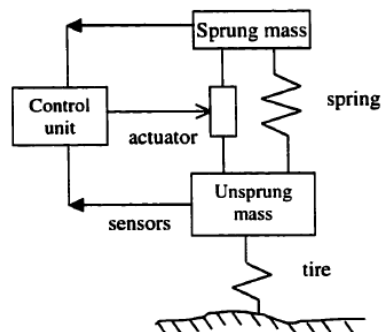


Figure C.2: Active  $\frac{1}{4}$  car suspension system, adapted from [44]

**Fully active suspension** use actuators, which create a desired force in the suspension system. The actuator is often placed in parallel with a passive spring.

A fully active suspension system often comprises an electro-hydraulic actuator and the associated control hardware and software, which are used to control the vehicle much more effectively than the spring and damper that they replace. The actuator force is determined based in a control law, developed such that the vertical body acceleration, suspension working space variability and dynamic tire force are minimized.

Both the semi-active and fully active suspensions may require sensors to be located on the vehicle, which measure the motion of the body, suspension system, and/or the unsprung mass. The information is used in the controller to decide “instantaneously” the force to be supplied by the actuator in a fully active suspension system or the amount of passively generated force to be supplied by the active damper in a semi-active system.

An active suspension system continuously monitors the bounce, pitch, roll, and yaw motions of the vehicle and generates necessary wheel motion compensations, so that disturbance due to terrain irregularities and inertia forces are minimized. It also corrects errors in steering and forces contact forces resulting from undesirable changes in weight distribution during severe maneuvers.

**Smart suspension;** “Active” denotes the controllability of a system state, on demand. Technological advances in material science have bred an advanced group of smart materials. These materials, in both solid and liquid forms, are uniquely controllable by an applied external energy source.

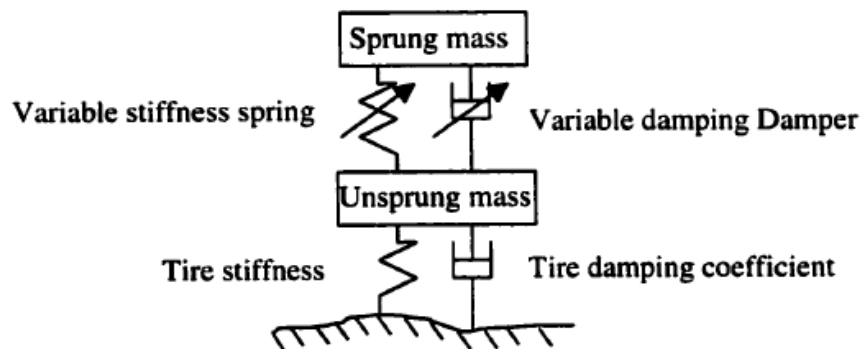


Figure C.3: Smart 1/4 car suspension system, adapted from [44]

The smart suspension system is similar to a traditional or passive suspension system since many of the same components are found in it. An adjustable damping shock absorber or an adjustable damping strut and other suspension components work together to provide good handling and comfortable drive. However, in a smart suspension system, the stiffness of the coil spring coated with piezoceramic can be controlled by a computer.

## APPENDIX D OPTIMAL CONTROL THEORY

The main objective of optimal control is to determine control signals that will cause a system to satisfy some physical constraints and at the same time extremize (maximize or minimize) a chosen performance criterion (performance index) [56]. The formulation of optimal control problem requires

- a) a mathematical description (linear or nonlinear differential or difference equations) of the process to be controlled
- b) a specification of the performance index
- c) a statement of boundary conditions and the physical constraints on the states or controls.

### *Performance Index*

Performance index, the optimal control problem is to find a control which causes the dynamical system to reach a target or follow a state variable (or trajectory) and at the same time extremize a performance index. It is very common, when designing proper control systems, to model reality as a linear system, such as

$$\begin{aligned}\dot{\mathbf{x}}(t) &= \mathbf{A}\mathbf{x}(t) + \mathbf{B}\mathbf{u}(t) \\ \mathbf{y}(t) &= \mathbf{C}\mathbf{x}(t)\end{aligned}$$

Performance index for general optimal control system:

$$J = \mathbf{x}'(t_f)\mathbf{F}\mathbf{x}(t_f) + \int_{t_0}^{t_f} [\mathbf{x}'(t)\mathbf{Q}\mathbf{x}(t) + \mathbf{u}'(t)\mathbf{R}\mathbf{u}(t)]dt$$

Or

$$J = S(\mathbf{x}(t_f), t_f) + \int_{t_0}^{t_f} V(\mathbf{x}(t), \mathbf{u}(t), t)dt$$

Where,  $\mathbf{R}$  is a positive definite matrix, and  $\mathbf{Q}$  and  $\mathbf{F}$  are positive semi definite matrices. Note that the matrices  $\mathbf{Q}$  and  $\mathbf{R}$  maybe time varying. The particular form of performance index is called *quadratic* (in term of the states and controls) form.

### *Constraints*

The control  $\mathbf{u}(t)$  and state  $\mathbf{x}(t)$  vectors are either unconstrained or constrained depending upon the physical situation. The unconstrained problem is less involved and gives rise to some elegant results. Normally,

$$\mathbf{U}_+ \leq \mathbf{u}(t) \leq \mathbf{U}_-, \text{ and } \mathbf{X}_- \leq \mathbf{x}(t) \leq \mathbf{X}_+$$

Where, +, and – indicate the maximum and minimum values the variables can attain.

## APPENDIX E LINEAR QUADRATIC REGULATOR (LQR)

LQR is a closed loop optimal control of linear plants or systems with quadratic performance index or measure, dealing with state regulation, output regulation, and tracking. The interest is to design of optimal linear systems with quadratic performance indices [57].

Some important definitions:

- 1) The Error Weighted Matrix  $\mathbf{Q}(t)$ : to keep the error small, this matrix must remain positive semi-definite.
- 2) The Control Weighted Matrix  $\mathbf{R}(t)$ : the quadratic nature of the control cost indicates that one has to pay higher cost for larger control effort. Since the cost will always remains as positive, the  $\mathbf{R}(t)$  should be positive definite
- 3) The Control Signal  $\mathbf{u}(t)$ : the assumption that there are no constraints on the control  $\mathbf{u}(t)$  is very important in obtaining the closed loop optimal configuration.

A drawback of the LQR algorithm is the requirement of optimizing the response by picking the  $\mathbf{Q}$  and  $\mathbf{R}$  weighting matrices by trial and error. As a result a better set of weighting matrices that those used for these result may exist. Nonetheless, the following still lends insight into the behavior of fully-active suspension. Tuning the LQR controller involves finding the values of the weighting matrices by running the numerical simulations with different  $\mathbf{Q}$  and  $\mathbf{R}$  magnitude until a reasonable ride response is achieved.

The  $\mathbf{Q}$  matrix is equally weighted on the first and last state which is the sprung mass velocity and unsprung mass displacement respectively, thus the controller should decrease these state response the most to give a better trade-off between ride and handling. For a linear time-invariant (LTI) system:

$$\dot{\mathbf{x}}(t) = \mathbf{A}\mathbf{x}(t) + \mathbf{B}\mathbf{u}(t)$$

And the cost functional as

$$J = 0.5 \int_0^{\infty} [\mathbf{x}'(t)\mathbf{Q}\mathbf{x}(t) + \mathbf{u}'(t)\mathbf{R}\mathbf{u}(t)]dt$$

Where,  $\mathbf{x}(t)$  is nth order state vector;  $\mathbf{u}(t)$  is rth order control vector; A is nxn-order state matrix; B is rxr-order control matrix; Q is nxn-order, symmetric, positive semi-definite matrix; R is rxr-order, symmetric, positive definite matrix.

The full state feedback control is:

$$\mathbf{u}^*(t) = -\mathbf{R}^{-1}\mathbf{B}'\bar{\mathbf{P}}\mathbf{x}^*(t) = -\bar{\mathbf{K}}\mathbf{x}^*(t)$$



Where,  $K$  is called Kalman gain, or optimal LQR gain.  $\bar{P}$ , the  $n \times n$  constant, positive definite, symmetric matrix, is the solution of the nonlinear, matrix algebraic Riccati equation (ARE)

$$-\bar{P}A - A'\bar{P} + \bar{P}BR^{-1} - Q = 0$$

The best possible gain is the one that minimizes the quadratic cost function comprised of weighting matrices  $Q$  and  $R$ .

Kalman gain:

$$\bar{K} = R^{-1}B'\bar{P}$$

Alternatively, the full state feedback control:

$$u^*(t) = -\bar{K}_a'x^*(t)$$

Where,  $\bar{K}_a = \bar{P}BR^{-1}$

The optimal state is the solution of the system obtained by using the control in the plant

$$\dot{x}^*(t) = [A - BR^{-1}B'\bar{P}]x^*(t) = Gx^*(t)$$

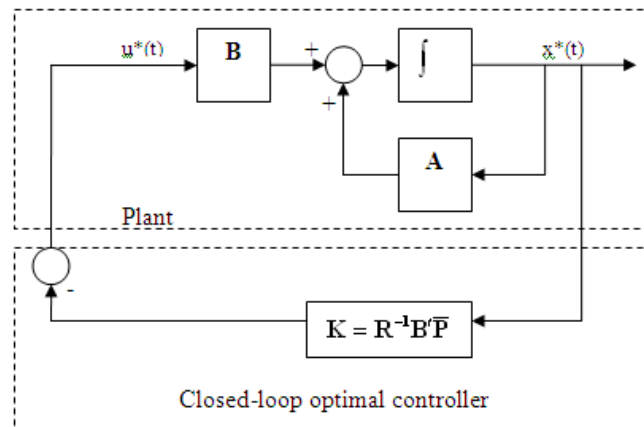
Where, the matrix  $G$  must have stable eigenvalue so that the closed-loop optimal system is stable. This is required since any unstable states with infinite time interval would lead to an infinite cost functional  $J^*$ . Note that no constraints on the stability of the original system. This means that although the original system may be unstable, but the optimal system must definitely stable. The minimum cost:

$$J^* = 0.5x^{*'}(t)\bar{P}x^*(t)$$

The boundary conditions as,

$$x(t_0) = x_0; \quad x(\infty) = 0$$

The closed-loop optimal control (CLOP)



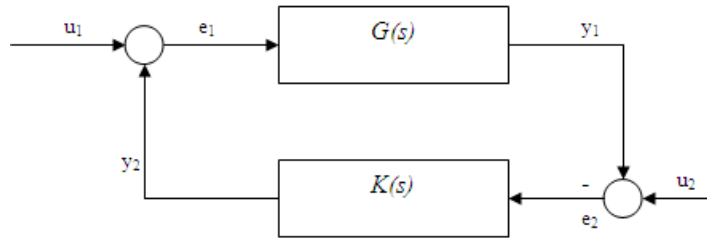
## APPENDIX F COPRIME FACTORIZATION

### *Stabilization*

It is very hard to achieve optimal nominal performance, especially when dealing with how to characterize the stabilizing controller for a common control loop. Hence, more preferable, is to use tools from optimal control theory such as LQR to solve stabilizing problem. However, this requires recasting the performance specifications in terms of Q and R, the state and control weighting matrices used in LQR performance index. Since there are no rules to exactly express the Q and R, in practice this leads to trial-and-error solution [57].

In order to avoid such difficulties, we will parametrize all the controllers that stabilize a given plant in terms of a free parameter  $Q(s)$  (a stable proper transfer matrix), also known as Youla Parametrization.

### *Internal stability*



The loop interconnection shown in the figure is internally stable if and only if all possible input-output transfer functions are stable. To develop a state-space based parametrization of all stabilizing controllers, following Lemma need to obey:

$$G_c = \begin{bmatrix} A_c & B_c \\ C_c & D_c \end{bmatrix}$$

Be the minimal state-space realization of the closed-loop system of the figure. The relations between the input ( $u(s)$ ) and output ( $e(s)$  or  $y(s)$ ) are:

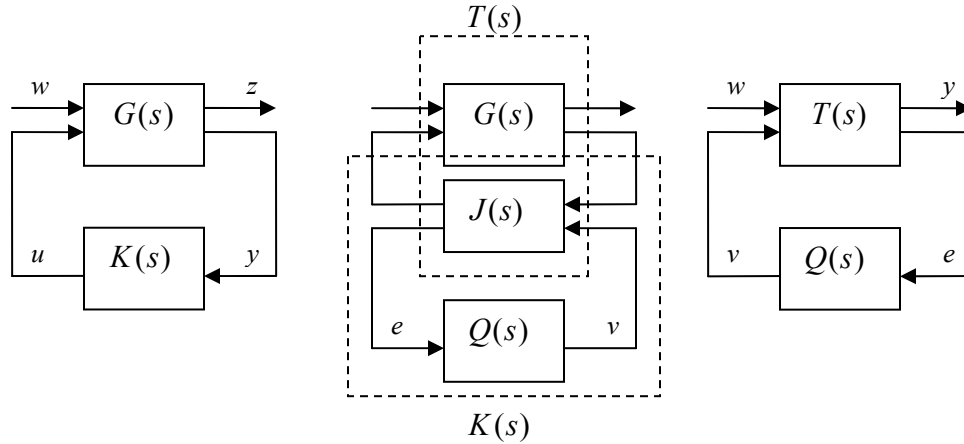
1. The feedback loop is internally stable
2. The eigenvalues of  $A_c$  are in the open left-half complex plane
3. All transfer function have poles in complex plane
4. the transfer matrix  $\begin{bmatrix} I & -K \\ G & I \end{bmatrix}$  is invertible in  $RH_\infty$

### *Open-loop stable plants*

Assume that the interconnection shown in figure is well posed and  $G(s) \in RH_\infty$ . Then, the youla parametrization of all stabilizing controllers takes the form:

$$K(s) = Q(s)[I - G(s)Q(s)]^{-1} \Rightarrow Q(s) \in RH_\infty, \det[I - G(\infty)Q(\infty)] \neq 0$$

Recall from the example in the introduction that one of the reasons for seeking a parametrization of all stabilizing controllers is to recast performance specifications given in terms of closed-loop transfer functions into a form having a simpler dependence on the free parameter. Consider the following block diagram:



We have,  $T_{zw} = F_l[G, F_l(J, Q)] = F_l(T, Q)$ , where

$$T = F_l(G, J) \triangleq \begin{bmatrix} T_{11} & T_{12} \\ T_{21} & T_{22} \end{bmatrix}$$

Under the condition that  $e$  is uncontrollable from  $v$ ,  $T_{22} = 0$ . Thus  $T_{zw}$

$$T_{zw} = T_{11} + T_{12}Q(I - T_{22}Q)^{-1}T_{21} = T_{11} + T_{12}QT_{21}$$

#### *A coprime factorization approach*

The approach allows for a simple derivation of some well known results on the simultaneous stabilization of multiple plants and the related problem of strong stabilization, that is, stabilization with stable controllers.

Two transfer matrices  $M_r$  and  $N_r$  in  $RH_\infty$  are right coprime over  $RH_\infty$  if there exist two matrices  $X_r \in RH_\infty$  and  $Y_r \in RH_\infty$  such that the following Bezout identity holds:

$$X_r M_r + Y_r N_r = I \quad \text{Or} \quad M_l X_l + N_l Y_l = I$$

A similar property holds for left-coprime matrices. Thus coprimeness among elements of the ring of the stable, proper transfer matrices is a generalization of the SISO concept of no common RHP zeros between numerator and denominator. Every proper, real rational transfer matrix  $G(s)$  can be factored as

$$G(s) = N(s)M(s)^{-1} = \tilde{M}(s)^{-1}\tilde{N}(s)$$

Where the  $N$  and  $M$  are right coprime, and  $\tilde{N}$  and  $\tilde{M}$  are left coprime. The following Lemma provides a state-space based algorithm to obtain such factorizations starting from a stabilizable and detectable realization of  $G(s)$ .

$$G(s) \equiv \begin{bmatrix} A & B \\ C & D \end{bmatrix}$$

Be a stabilizable and detectable realization of  $G(s)$  and  $F$  and  $L$  any matrices such that  $A + BF$  and  $A + LC$  are stable. Define

$$\begin{bmatrix} M(s) \\ N(s) \end{bmatrix} \equiv \begin{bmatrix} A + BF & B \\ F & I \\ C + DF & D \end{bmatrix}$$

And

$$\begin{bmatrix} \tilde{N}(s) & \tilde{M}(s) \end{bmatrix} \equiv \begin{bmatrix} A + LC & B + LD & L \\ C & D & I \end{bmatrix}$$

Then define:

$$\begin{bmatrix} X_r(s) & Y_r(s) \end{bmatrix} \equiv \begin{bmatrix} A + LC & -(B + LD) & L \\ F & I & 0 \end{bmatrix}$$

And

$$\begin{bmatrix} Y_l(s) \\ X_l(s) \end{bmatrix} \equiv \begin{bmatrix} A + BF & L \\ F & 0 \\ -(C + DF) & I \end{bmatrix}$$

Then conclude that,

$$\begin{bmatrix} X_r(s) & Y_r(s) \\ -\tilde{N}(s) & \tilde{M}(s) \end{bmatrix} \begin{bmatrix} M(s) & -Y_l(s) \\ N(s) & X_l(s) \end{bmatrix} = \begin{bmatrix} I & 0 \\ 0 & I \end{bmatrix}$$